Delft University of Technology

Graduation Project Report

Improvement of Parameter Selection and Consideration of Constitutive Soil Models for Historical Quay Wall Assessment

Author:

Sjalome Sordam (5202302)

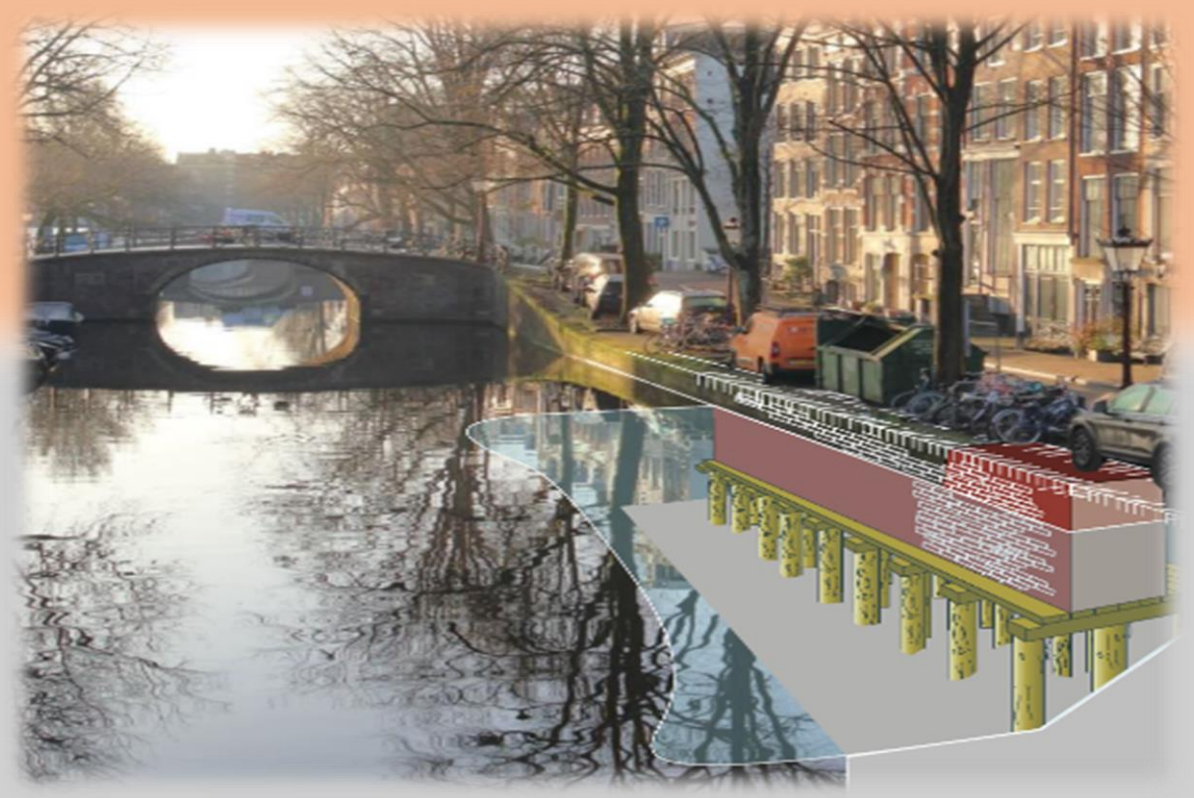

TU Delft Delft University of Technology

Gemeente Amsterdam

The figure on the front page is from Mart-Jan Hemel taken at Reguliersgracht, Amsterdam (23 December 2021)

Improvement of Parameter Selection and Consideration of Constitutive Soil Models for Historical Quay Wall Assessment

by

Sjalome Sordam

born in Paramaribo, Suriname

to obtain the degree of Master of Science

at the Delft University of Technology, Faculty of Civil Engineering,

Track: Geo-engineering,

to be defended publicly on 22 July 2024 at 11:30 A.M.

Graduation Committee:

Chair/Supervisor:

Dr. ir. Mandy Korff (TU Delft / Deltares)

Supervisor:

Dr. ir. Cor Zwanenburg (TU Delft / Deltares)

Company supervisor:

Ing. Aziz Cherkaoui (Ingenieursbureau Gemeente Amsterdam)

Supervisor:

Dr. ing. Mark Voorendt (TU Delft)

Acknowledgements

First, I would like to thank myself and God for giving me the courage to start and persevere in moving without sight in this exciting journey to pursue my master's degree at the Technical University of Delft.

I am incredibly grateful for my lovely partner, my awesome parents, and my siblings for their encouragement and moral support all the way from Suriname, my family who offered me shelter in the Netherlands, and for the valuable relationships I made along this journey.

I am deeply grateful for the geotechnical team at the municipality of Amsterdam for generously opening their doors and providing me with the opportunity to work within their respected organization, especially the company supervisor Ing. Aziz Cherkaoui and assistant supervisor ir. Katerina Rippi for providing insightful perspectives and motivation that immensely enriched the thesis process.

Furthermore, I would like to express my sincere gratitude to my supervisors from TUDelft, Dr. ir. Mandy Korff, Dr. ir. Cor Zwanenburg, and Dr. ing. Mark Voorendt for their invaluable guidance and unwavering support throughout the completion of this thesis.

Sjalome Sordam

July 2024

Abstract

In the center of Amsterdam there are historic quay walls that are more than 100 years old. Over the years, the load-bearing capacity of the quay walls decreased, and it is currently an important topic on how to strengthen these quay walls, but it is important as well to know which quay walls should be given preference for rehabilitation.

The engineering department of the municipality of Amsterdam, in collaboration with other parties, has drawn up a document Toetskader Amsterdamse Kademuren (TAK 3.2), which includes various aspects that contribute to the assessment of historic quay walls. In TAK 3.2, attention has of course been paid to the geotechnical aspects, whereby material model parameters have been determined for the Hardening Soil small strain model and the Soft Soil model. This study examines how the current parameter set in TAK 3.2 can be improved by selection of material model parameters and taking the material models into consideration as well in which the anisotropic Sekiguchi-Ohta model and the anisotropic S-Clay1 model are examined additionally.

Material model parameter sets have been compiled (with expected values) for the most influencing Holocene soil layers, such as Geulopvulling, Hollandveen and Oude zeeklei. These parameter sets have been validated and further optimized with the use of Plaxis SoilTest. The available laboratory results come from isotropically consolidated triaxial tests on Geulopvulling and Oude zeeklei, Direct simple shear (DSS) tests on Hollandveen and oedometer tests. Validation of the anisotropic models has therefore not been entirely possible for Geulopvulling and Oude zeeklei, but in the case of Hollandveen the assumption is made on K0-consolidation in the DSS test simulations, where the anisotropic models yield promising results.

Furthermore, according to the approach of TAK 3.2 in the staged construction of historic quay walls, various simulations are conducted for the assessment of historical quay walls with the Hardening Soil small strain model, Soft Soil model and S-Clay1 model, with different parameter sets. From these simulations, some good prospects are noted, such as the improvement in output results with the optimized parameter set compared to the parameter sets gathered from all laboratory data and TAK 3.2. In simulations in which the S-Clay1 model is considered in combination with the Hardening Soil small strain model and Soft Soil model, a significant decrease was noticed as well in the output results compared to simulations with exclusively the Hardening Soil small strain and/or Soft Soil model.

This study shows that the Hardening Soil small strain model as an isotropic model gives better results and fewer/no difficulties in the finite element method calculations compared to the Soft Soil model. It is further confirmed that calculating the initial phase with the K0-procedure with horizontal soil layers and surface is the best method in the case of the assessment of historic quay walls.

By understanding which differences are observed with different material models and parameter sets, this study contributes to sharpening future research to adequately analyze and assess historic quay walls in the center of Amsterdam.

Keywords: historic quay walls, material models, parameter determination, Holocene soil layers

Table Of Contents

1. Introduction

In this chapter the problem is analyzed, whereafter the objectives and approach for the research are subsequently formulated.

1.1 Research Motivation

Amsterdam has approximately 600 km of quay walls, of which 200 km are masonry works constructed on wooden piles. With the collapse of the Grimburgwal (Figure 1.1) in 2020 it has become increasingly clear that these are vulnerable objects and measures need to be taken. In the meantime, necessary steps have already been taken in the process of renewing approximately 200 kilometers of Amsterdam quay walls. The desire to retain value and work circularly makes lifespan extension preferable to complete renewal (Krabbendam, 2021).

To prevent calamities such as the Grimburgwal, it is essential to test the geotechnical and structural safety of the quays, which is the topic of the present study.

Figure 1.1. Collapsed Grimburgwal 2020 and failure mechanism wooden piles (TUDelft.nl)

1.2 Problem Analysis

The engineering department of the Municipality of Amsterdam (Ingenieursbureau Amsterdam), in collaboration with Engineering companies (known as “samenwerkingsovereenkomst kademuren” SOK-ingenieurs diensten) and research institutes (AMS, TU Delft and Deltares), are in the process of setting up practical guidelines for the assessment of the Structural Safety of Historical Urban Quay Walls, known as Toetskader Amsterdamse Kademuren 3.2 (TAK 3.2).

The Finite Element Method (FEM) Software, Plaxis 2D, is used for the assessment of the historical urban quay walls. Plaxis 2D offers a variety of material models to best represent the soil behavior and the interaction between soil and structural elements. Currently, in TAK 3.2, the Soft Soil model is used for two dominant upper Holocene soil layers (Hollandveen and Oude zeeklei) and Hardening Soil small strain model for the remaining deeper soil layers. The soil parameters are determined based on interpretation and combination of site investigation and laboratory tests that are carried out in the city center of Amsterdam. The soil parameters for the Hardening Soil (small strain) model are from the North-South line (Noord-Zuidlijn) database (Smits, 1999). Due to lack of test results, values have been

given for several soil parameters for the Holocene soil layers based on experience, by engineers of consultancy firm OMEGAM. The Soft Soil model parameters for the dominant Holocene layers proposed in TAK 3.2 are directly obtained from more recent laboratory results, analyzed and delivered by Arcadis Nederland B.V (Verweij, 2023).

Soil Test module (Plaxis 2D) is nowadays widely used for optimizing selected soil parameters. It is not advisable to directly apply the input parameters for material models obtained from laboratory research in Plaxis 2D. Plaxis 2D provides an approximation of reality, therefore, adjustment of some parameters is necessary to best approximate reality. Furthermore, the Hardening Soil model (small strain) and Soft Soil model determine soil behavior in isotropic state, while soil behavior in practice, especially in the case of retaining walls is anisotropic. With assumed isotropic behavior the horizontal soil properties are misjudged, in the sense that greater horizontal stresses are considered in the soil than is the case in practice.

From the above, the problem statement follows that in Plaxis 2D and with the current material model parameter set in TAK 3.2, especially in the case of the assessment of historic quay walls with degraded foundation piles, the quay wall is considered unsafe, while in practice the considered quay wall does not appear to be unsafe.

1.3 Research Questions

Main Question:

How can the current parameter set, as given in Toetskader Amsterdamse Kademuren 3.2, of the most influencing Holocene soil layers for Historical Quay Wall Assessment be improved based on a better selection of parameters and by taking into consideration the applied constitutive soil models?

Sub-Questions:

1. What are the criteria in choosing a suitable constitutive model for geotechnical finite element method analyses?
2. How should laboratory tests be interpreted to derive the appropriate model parameters for the corresponding constitutive soil model?
3. What methods can be employed to validate selected model parameters for different constitutive soil models in geotechnical finite element method analyses?
4. How do the structural forces in the wooden foundation piles differ, with the considered constitutive models, when applying the standard approach for historical quay wall assessment according to Toetskader Amsterdamse Kademuren 3.2 in Plaxis 2D?
5. What is the influence on the result of different ways of modelling the initial situation of an existing retaining wall in Plaxis 2D?

1.4 Research Approach and Report Structure

The steps taken to conduct the research are:

To answer sub question 1:

- From literature summarize features of material models such as the Hardening Soil (small strain) model, Soft Soil model, Sekiguchi-Ohta and the S-Clay1 model, highlighting their specific advantages and disadvantages. (Chapter 2)

To answer sub questions 2 and 3:

- From literature, summarize methods to determine the material model parameters. (chapter 3)
- Determine and validate material model parameters for the considered soil layers in this study with Plaxis soil test (PST). (Chapter 4)
- Use Plaxis soil test to optimize material model parameters from determined parameters from laboratory test results by fitting graphs from simulated data to graphs obtained from laboratory results, for the considered material models. (Chapter 4)

To answer sub question 4 and 5:

- Study the impact of modelling and soil-structure interaction on the shear and normal forces, bending moments, and horizontal deformations of the foundation piles of historic quay walls, and how the different material models and parameter sets affect these results. (Chapter 5).
- Define the initial stress situation for an existing retaining wall by the K_0-procedure and the Gravity loading method and compare the generated field stresses, bending moments, and horizontal deformation in the piles. (Chapter 5).

1.5 Research Scope

This research focuses on the determination and optimization of material model parameters, with the use of Soil Test Plaxis 2D, for the dominant Holocene soil layers, Hollandveen (peat) and Oude Zeeklei (clay) and for a strongly heterogeneous Geulopvulling (mixture of clay, peat, sand, and anthropogenic material) on top of Hollandveen in the center of Amsterdam for conducting safety analyses on historic quay walls constructed on wooden piles. Determining parameters for the Hardening Soil small strain model, Soft Soil model, Sekiguchi-Ohta model and S-Clay1 model are central in this research. The laboratory test results are obtained from isotropic consolidated Triaxial, 1D-compression (Incremental Loading - IL), and Direct Simple Shear (DSS) tests.

Furthermore, the research is limited to the application of finite element method (FEM) calculations for an existing historic quay wall in Plaxis 2D, in which anisotropy is solely considered in Hollandveen with the S-Clay1 material model (reasoning for this choice can be found in Section 5.3).

1.6 Report Structure

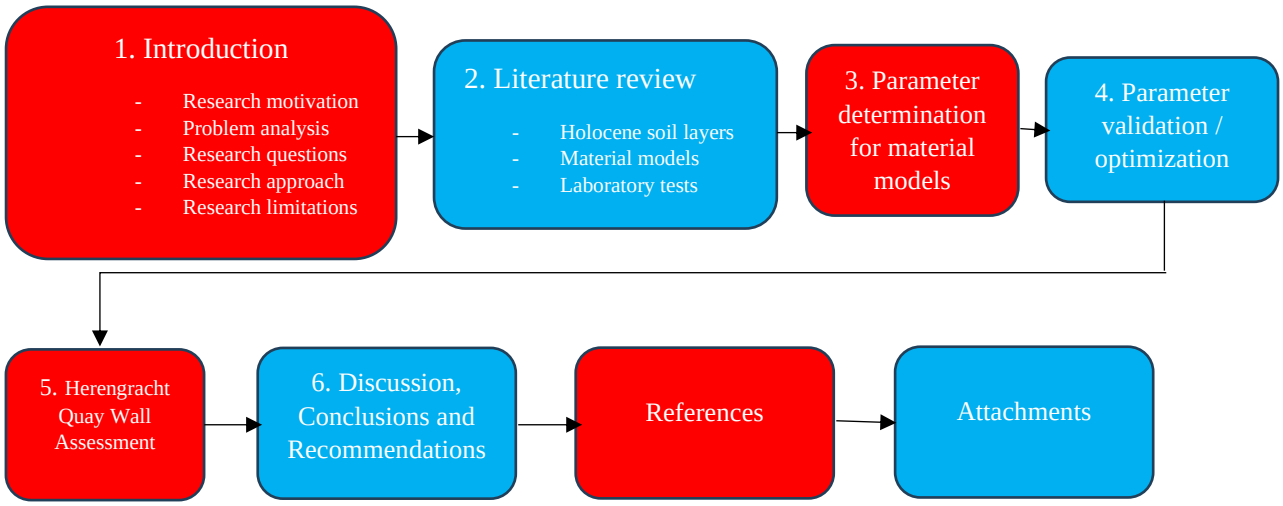

2. Literature Review

This chapter aims to give answer to sub question 1 ”*What are the criteria in choosing a suitable constitutive model for geotechnical finite element method analyses?*”, in particular Section 2.2. In section 2.1, a brief description is given about the soil layers Geulopvulling, Hollandveen and Oude zeeklei to learn more about the general properties of these soil layers for which material model parameters have been determined (Chapter 4) and analysis has been carried out on in the case study (Chapter 5). Further in Section 2.2, features and required material model parameters for the considered constitutive models in Plaxis soil test simulations and Finite Element Method calculations are elaborated on. Lastly, in Section 2.3, features and characteristics of the laboratory tests from which the material model parameters are obtained are summarized.

2.1 Holocene Soil Layers

The occurrence of different soil layers is all related to geological processes. Various periods are classified within geology, of which the Holocene is the most recent period (10.000 years ago till present). During the Holocene, various types of soil material were deposited, of which Figure 2.1 shows a typical subsurface that can be found within Amsterdam. The Holocene deposits of Hollandveen and Oude zeeklei have the greatest influence in determining the safety of old quay walls, because these layers are closest to the surface and are easily influenced by changes at the surface.

For the most part of Amsterdam there is a layer of sand, under which at certain locations a trench fill layer (Geulopvulling) and Hollandveen (peat) lies. Hollandveen is about 2-3 m thick and beneath it an old marine clay layer, Oude zeeklei, is found with a thickness of approximately 1-2 m. The first sand layer formed in the last phase of the Pleistocene is at a depth of 12-13 m NAP. The layers “Wadzand”, “Hydrobiaklei” and “1^{e} zandlaag” are not considered in this study as previously indicated in Section 1.5.

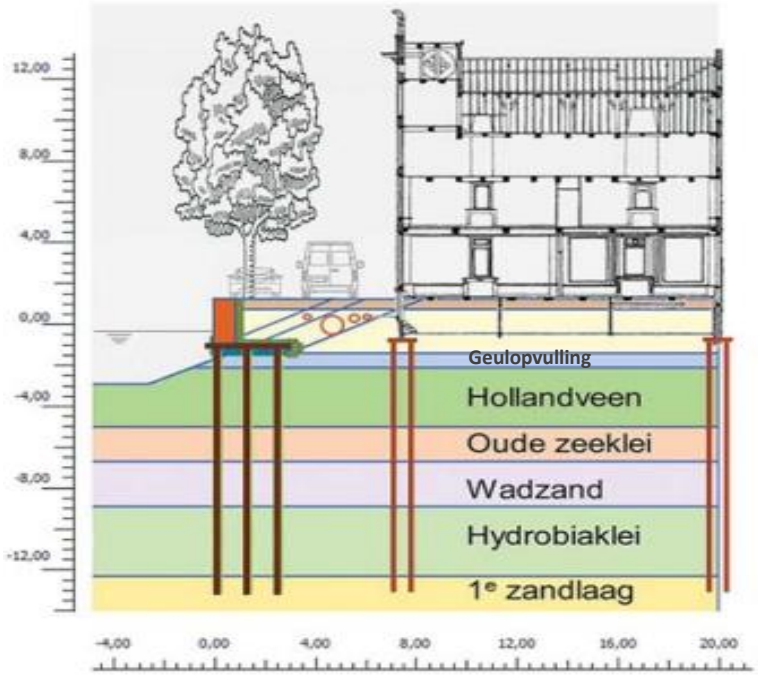

Figure 2.1. Illustration of the subsurface in Amsterdam (TAK 3.2, 2023)

2.1.1 Geulopvulling

This layer is highly heterogeneous in nature. Four different types of Geulopvulling can be found in the subsurface between Central Station and Rokin, namely: humus geulopvulling, Geulopvulling consisting of very soft clay, geulopvulling consisting of clay with sand layers and Geulopvulling consisting of sand with clay layers. In some cases, debris is also found in Geulopvulling. Geulopvulling on which tests have been carried out in this research, can be characterized as a firm, strong organic, weakly calcareous clay layer. Keep in mind that the Geulopvulling is not the same as the Oergeul.

2.1.2 Hollandveen (peat)

Peat predominantly consists of dead plant remains that are mostly horizontally oriented in the material. Peat can have a density that is less than the density of water. Due to the high permeability of peat, it absorbs water quite easily, but at the same time releases water easily when compressed. The strength of peat is very low, but the plant remains, behaving as fibers in the material are very strong. There is a large degree of anisotropy in peat as the tensile strength of the material is greater in horizontal direction and the material has a greater stiffness in vertical direction. Aforementioned makes it complex to characterize peat and the effort required to obtain representative samples from the field as well (Lefebvre, Langlois, Lupien, & Lavallée, 1984). The stress path and loading conditions play a major role in the response of the fibers present in peat. Each fiber is expected to undergo a different degradation in structure depending on the strain path (Muraro & Jommi, 2020).

At high strain levels, deviatoric stress increases almost linearly with deviatoric strain and the stress-strain relationship is dominated by strain hardening behavior (Muraro, 2019). Thus, peat can contain friction angles that are much greater than those of granular material. Furthermore, a well-known problem of peat is determining the cohesion at low stresses.

Hollandveen, on which tests have been carried out in this research, consists of weak, moderately strong to strong peat material and is dark brown in color.

2.1.3 Oude Zeeklei (Clay)

Oude zeeklei is characterized as a clay layer deposited in a lagoon above the basisveen peat and below the Hollandveen peat layers in North Holland. Clay material contains grains with a diameter between 0- and 0.002-mm. Clay has strong swelling and shrinking capabilities, allowing it to absorb and release water. Furthermore, non-reversible deformation also occurs in clay and uneven heave and settlement of clay is often a problem in infrastructure.

Typical for normally consolidated clay in triaxial compression is reaching a peak stress before the material reaches the ultimate state in which softening behavior is observed. This softening response of normally consolidated clays has been discussed recently by Chao et al (2023). Oude zeeklei on which tests have been carried out in this research, consists of strong, inorganic, calcareous clay material and is gray in color.

2.2 Material Models

Material models have been developed to simulate the behavior of soil. Linear elastic material models are insufficient to get a good indication of the behavior of soil. The complex behavior of soil stems from the characteristic of the multi-phase material, such as density, structure, drainage conditions, strain conditions (plane, triaxial), the water content, the loading history, the type of material from which the soil is composed and other factors as well. In this Section the fundamentals, possibilities, and limitations of the Hardening Soil (small strain) model, Soft Soil model, Sekiguchi-Ohta model and S-Clay1 model are discussed.

2.2.1 The Hardening Soil Model

The Hardening Soil (HS) model is based on the foundations of the Duncan-Chang model (Duncan & Chang, 1970) which is again an elaboration on the idea of Robert Kondner (1963) that the stress-strain relationship in a drained triaxial compression test can be described by a hyperbolic function (Duncan & Chang (1970) p.1631).

The HS-model is a double hardening model (shear and compression hardening) which incorporates the stress history (pre-consolidation stress) of the material. The generation of plastic deviatoric strains when the internal friction is mobilized is called shear hardening and when in primary loading it is called compaction hardening. The deviation between the line of the initial stiffness, E_0, and the curve in Figure 2.2 is characterized as the accumulation of plastic strains, which is described as shear hardening. The incorporation of shear hardening and stress-dependent stiffness behavior in the HS-model makes the model suitable for sand and stiff clays. The fact that the HS-model incorporates compaction hardening, makes it suitable for weaker soils such as normally consolidated clays and peat (Brinkgreve R. , z.d.).

Some disadvantages to this model are the fact that there are no peak strength and softening behavior incorporated; the model immediately yields the residual strength of the material. In cyclic loading there is no accumulation of strain or pore pressure within this model, which is the case in realistic cyclic loading soil behavior. Furthermore, this model is not able to reproduce creep nor anisotropy and for very soft soils the ratio $E_{50} / E_{oed} > 2$ becomes problematic as input in Plaxis.

The HS-model uses the theory of plasticity rather than the theory of elasticity, includes soil dilatancy and introduces a yield cap. Aforementioned makes the HS-model a better formulated model than the Duncan-Chang hyperbolic model. The stress dilatancy theory of Rowe (1962, 1971) is used to formulate the flow rule of the HS-model found in (Schanz, Vermeer, & Bonnier, 1999) p.4 and (PLAXIS, Material Models Manual, 2023) p.71. Furthermore, the HS-model involves a more general stress-dependent stiffness behavior based on a power-law formulation given in Equation 2.4 and Equation 2.5.

In Figure 2.2 the hyperbolic relationship is visualized. As can be seen the initial slope of the curve is expressed by the initial Young's modulus stiffness E_0, whereas the tangent stiffness, E_t, can be defined by arbitrary stress states along the curve. For unloading and reloading there is a different stiffness defined E_{ur}.

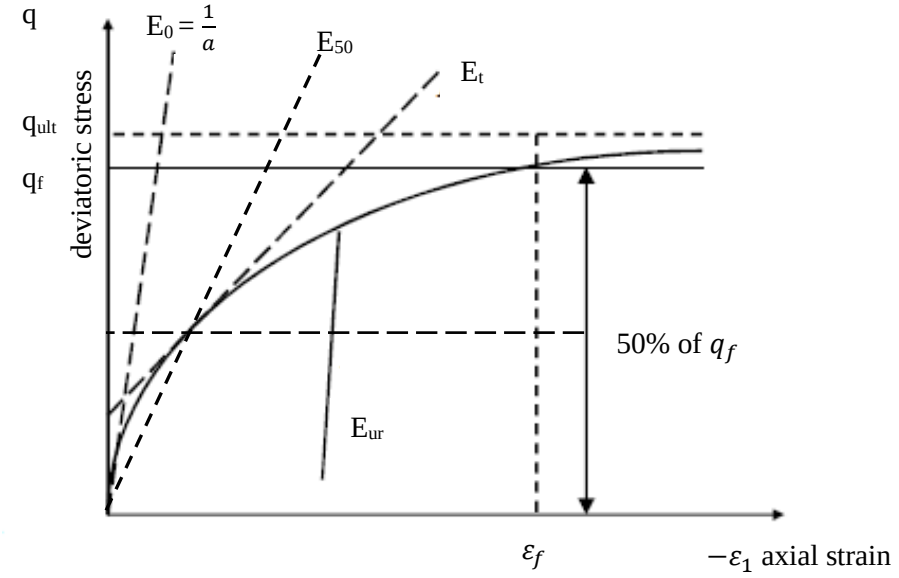

Figure 2.2: Hyperbolic stress strain curve (TU Delft course: behavior of soils and rocks 2021)

The asymptotic value of the ultimate deviatoric stress, q_{ult}, can be related to the deviatoric stress at failure by means of a factor R_f, as follows:

Equation 2.1 $$q_f = R_f\, q_{ult}$$

where:

q_f	deviatoric stress, q, at failure	[kPa]
R_f	failure ratio (0.75 – 1.0)	[-]
q_{ult}	asymptotic value of deviatoric stress, q	[-]

The axial strain at failure can be calculated by:

Equation 2.2 $$-\varepsilon_f = \frac{\frac{q_f}{E_0}}{1-R_f}$$

The maximum principal stress difference at failure, q_f, is related to the Mohr-Coulomb failure criterion by:

Equation 2.3 $$q_f = R_f q_{ult} = \frac{2c'cos\phi' - 2\sigma'_3 sin\phi'}{1-sin\phi'}$$

More information on the formulation of shear hardening can be found in PLAXIS, Material Models Manual (2023 p.69) and Schanz, Vermeer, & Bonnier (1999 p.4.).

As in the Duncan Chang model, there is stress dependent stiffness in the HS-model as well. The stiffness formulations, shown in equations 2.4 and 2.5, look somewhat different than in the hyperbolic model. Furthermore, the secant stiffness, E_{50}, is used instead of the initial, E_0, since E_{50} takes less effort to

obtain from a drained triaxial test (Brinkgreve R. B., 2021). The stiffness modulus, E_{50}^{ref}, is defined for a reference minor principal stress σ'_3 equal to p^{ref}.

Equation 2.4 $$E_{50} = E_{50}^{ref} \left(\frac{c' cos\phi' + \sigma'_3 sin\phi'}{c\, cos\phi' + p^{ref} sin\phi'}\right)^m$$

Equation 2.5 $$E_{ur} = E_{ur}^{ref} \left(\frac{c' cos\phi' + \sigma'_3 sin\phi'}{c\, cos\phi' + p^{ref} sin\phi'}\right)^m$$

As stated before (Equation 2.3), the failure behavior of the HS-model is according to the Mohr-Coulomb failure criterion. By incorporating the plasticity theory, the yield function at failure is formulated as in Equation 2.6 (Brinkgreve R. B., 2021).

Equation 2.6 $$f_f = \frac{1}{2}(\sigma'_3 - \sigma'_1) + \frac{1}{2}(\sigma'_3 + \sigma'_1)\, sin\phi' - c'\, cos\phi'$$

Shear hardening does not incorporate plastic volumetric strain, measured in isotropic compression. Therefore, compaction hardening, or cap hardening is introduced. Without a cap yield surface in the model, illustrated in Figure 2.3, it would not be possible to input the secant stiffness at 50% failure, E_{50}, and the oedometric stiffness, E_{oed} , independently of eachother. To read more on the formulation of compaction hardening see PLAXIS, Material Models Manual (2023 p.79).

The unique measure for deviatoric stress can be formulated in different ways, based on the loading scenario (PLAXIS, Material Models Manual, 2023 p.78).

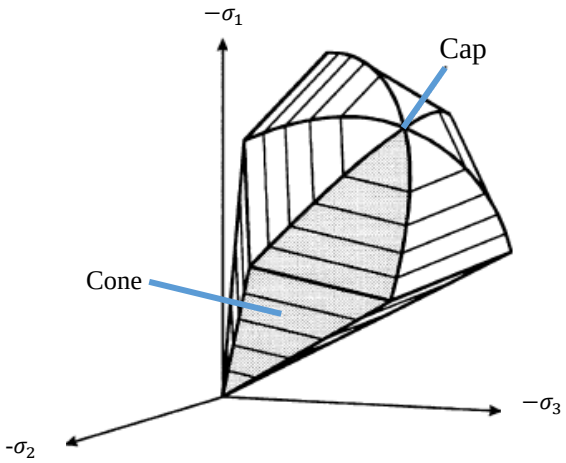

Figure 2.3. Representation of total yield contour of the Hardening-Soil model in principal stress space for cohesionless soil (Schanz, Vermeer, & Bonnier, The Hardening Soil Model: Formulation and verification, 1999).

To determine the oedometer stiffness, Equation 2.7 is used. The reference oedometer stiffness, E_{oed}^{ref}, is a tangent stiffness defined at a vertical stress of $\sigma'_1 = p^{ref}$.

Equation 2.7 $$E_{oed} = E_{oed}^{ref} \left(\frac{c\, cot\phi' + \sigma'_1}{c\, cot\phi' + p^{ref}}\right)^m$$

2.2.2 The Hardening Soil model parameters

The Hardening Soil parameters are shown in Table 2.1. The Mohr-Coulomb parameters are easily obtained from conventional soil testing methods. The basic parameters for soil stiffness and some of the advanced parameters are discussed in previous Sections.

Table 2.1: The HS-model parameters (PLAXIS, Material Models Manual, 2023)

Failure parameters as in Mohr-Coulomb model:		
c'	(effective) Cohesion	[kPa]
ϕ'	(effective) Angle of internal friction	[°]
ψ	Angle of dilatancy	[°]
σ_t	Tension cut-off and tensile strength (see (PLAXIS, Material Models Manual, 2023) p.40)	[kPa]
Basic parameters for soil stiffness:		
E_{50}^{ref}	Secant stiffness in standard drained triaxial test Plastic straining due to primary deviatoric loading	[kPa]
E_{oed}^{ref}	Tangent stiffness for primary oedometer loading Plastic straining due to primary compression	[kPa]
E_{ur}^{ref}	Elastic unloading / reloading stiffness (default $E_{ur}^{ref} = 3\,E_{50}^{ref}$)	[kPa]
m	Stress-level dependency of stiffness according to a power law	[-]
Advanced parameters (it is advised to use the default setting)**:**		
p^{ref}	Reference stress for stiffnesses (default 100 kPa atmospheric)	[kPa]
v_{ur}	Poisson's ratio for unloading-reloading (default 0.2)	[-]
K_0^{NC}	K_0 –value for normal consolidation (default K_0^{nc}= 1 - sin ϕ')	[-]
R_f	Failure ratio (default 0.9) (see (PLAXIS, Material Models Manual, 2023) p.41) and (Obrzud & Truty, 2018) p.106)	[-]
$\sigma_{tension}$	Tensile strength (default 0)	[kPa]
c_{inc}	Increase of cohesion with depth (see (PLAXIS, Material Models Manual, 2023) p.41)	[kN/m^3]
Dilatancy cut -off	See (PLAXIS, Material Models Manual, 2023) p.77	[-]

By default, K_0 is set equal to 1 in Plaxis. K_0^{NC} is an independent parameter for normally consolidated soils and is determined based on Jaky's formula (Jaky, 1948), which gives a very good approximation of the normally consolidated lateral earth pressure coefficient. It is possible that K_0^{nc}- values are rejected by Plaxis depending on parameters such as E_{50}^{ref}, E_{oed}^{ref}, E_{ur}^{ref} and v_{ur}.

In some cases, for soft soils the ratio between E_{50}^{ref} and E_{oed}^{ref} can be as high as 2 or greater, which causes problems in the modelling.

2.2.3 The Hardening Soil Small Strain (HSss) Model

For retaining walls, the typical shear strains lie in the range of small strains as can be seen in figure 2.5, therefore the HSss model is discussed as well. The strain range in which soil material truly exhibits elastic behavior is in fact very small. In addition to the HS model, the HSss model offers the possibility to assess small strain stiffness, and strain-dependency of the stiffness is determined using a modulus reduction curve.

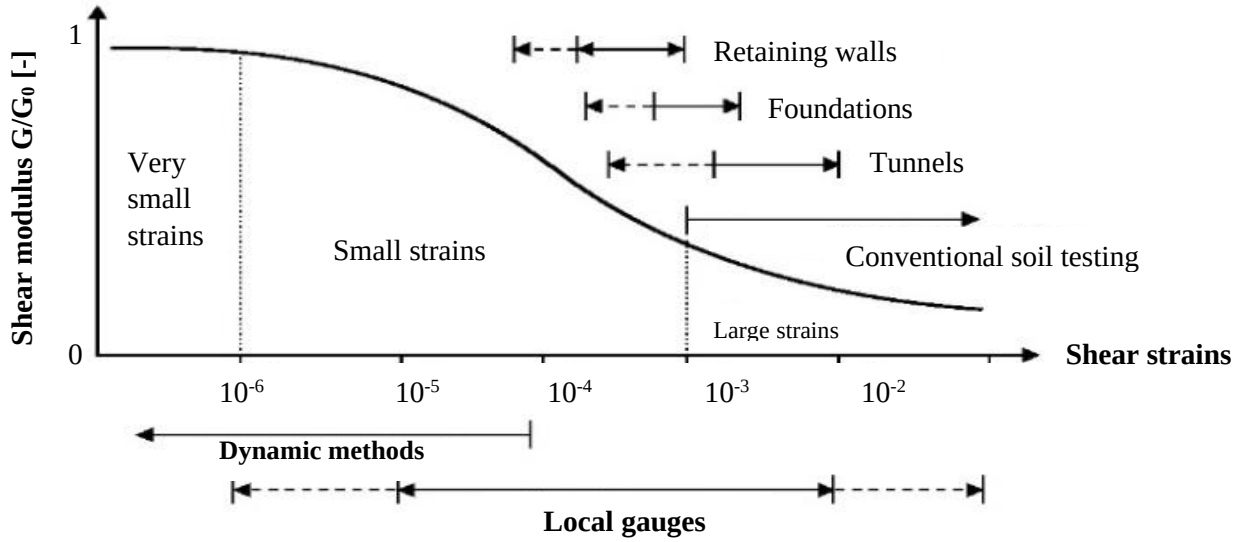

Figure 2.4. Normalized shear modulus vs. shear strain ranges (Atkinson, 1991 and Mair, 1993)

The stress-strain curve for small strains can be simply described by a hyperbolic law given in Equation 2.8 (Hardin & Drnevich, 1972), which is supported by test data.

Equation 2.8 $$\frac{G_s}{G_0} = \frac{1}{1+\left|\frac{\gamma}{\gamma_r}\right|}$$

where

$\gamma_r = \frac{\tau_{max}}{G_0}$ shear strain threshold [-]

where

τ_{max} is the shear stress at failure [kPa]

The stress-strain curve can be better formulated, in the sense that it is less prone to error, as in Equation 2.9, which is proposed in the conference proceedings "Reference threshold shear strain of soil" (Santos & Correia, 2001)). The secant shear modulus, G_s, is reduced with approximately 30% of its initial value to about 70%.

Equation 2.9 $$\frac{G_s}{G_0} = \frac{1}{1+a\left|\frac{\gamma}{\gamma_{0.7}}\right|}$$ *a = 0.385, found from correlation using many tests*

The shear stress at failure is expressed according to the Mohr-Coulomb failure criterion as:

Equation 2.10 $$\tau_{max} = \frac{1}{4}(2c'(1+cos\,2\phi') + (\sigma'_1 + \sigma'_3)sin2\phi')$$

The threshold shear strain, $\gamma_{0.7}$, for normally consolidated soils can be calculated as:

Equation 2.11 $$\gamma_{0.7} = \frac{0.385}{4G_0}(2c'(1 + cos\ 2\phi') + \sigma'_1(1 + K_0^{NC})sin2\phi')$$

The HSss-model uses all previously mentioned parameters of the original HS-model, but with two additional parameters in Table 2.2.

Table 2.2. The HSss-model additional parameters

G_0^{ref}	The initial or very small-strain shear modulus at a reference minor principal stress (-$\sigma'_3 = p^{ref}$)	[kPa]
$\gamma_{0.7}$	Shear strain at which the secant shear modulus G_s is reduced to 70% of G_0 ($G_s = 0.722G_0$)	[-]

Estimates on the void ratio can lead to reasonable estimates of the initial small strain shear stiffness for undisturbed clayey soils (Hardin & Black, 1969) found in (PLAXIS, Material Models Manual, 2023) p. 90:

Equation 2.12 $$G_0^{ref} = 33\frac{(2.97-e)^2}{1+e}\ [Mpa] \qquad for\ p^{ref} = 100\ [kPa]$$

The shear strain at which the secant shear modulus, G_s^{ref}, is decayed to 0.722 G_0^{ref} is defined by the shear strain threshold $\gamma_{0.7}$.

Among the number of factors (Benz, 2006) that influence the small-strain parameters G_0 and $\gamma_{0.7}$, these parameters are most influenced by the material's true state of stress and void ratio, e.

By incorporating a power law, the stress dependency of the shear modulus is ensured in the HSss-model:

Equation 2.13 $$G_0 = G_0^{ref}\left(\frac{c'cos\phi' + \sigma'_3 sin\phi'}{c'cos\phi' + p^{ref}sin\phi'}\right)^m$$

2.2.4 The Soft Soil Model

The Soft Soil (SS) model is suitable for conducting research on soft and highly compressible soil material such as normally consolidated clay, clayey silts, and peat. The SS model is based on the concepts of the Cam-Clay model (Muir Wood, 1990) , however it is not characterized as a critical state model. As in the HS-model, the failure behavior in the SS-model is according to the Mohr-Coulomb failure criterion and the stress history of the material is considered. In the SS model, the stress strain relationship is also represented logarithmically, in which stiffness is linearly dependent on the mean effective stress. There is no issue of shear hardening as in the HS-model, but hardening in primary compression, called cap hardening, is considered. Plastic volumetric strains develop during primary compression, although in unloading and reloading there is elastic strain behavior. Furthermore, parameter M which is based on friction angle in the Cam-Clay theory (see PLAXIS, Material Models Manual (2023) p. 98), is based on the normally consolidated earth pressure coefficient, K_0^{NC}, in primary one-dimensional compression.

The SS model is unsuitable to assess the behavior of stronger soil types such as sand and clay in highly over-consolidated state because no strain softening is allowed and stress states above the Mohr Coulomb failure condition are prohibited (Karstunen & Amavasai, 2017). As is the case in the HS model, there is no distinction between peak strength and residual strength as the SS model directly yields the residual strength. Furthermore, there is no incorporation of creep and anisotropy in this model, and the model is not recommended in the case of pure unloading situations (excavations for example), since the model is based on the advanced feature of compaction hardening.

In primary loading, there is a logarithmic relationship given between the volumetric strain (elastic and plastic) and the mean effective stress, quantified by means of the modified compression index λ^*.

Equation 2.14

$$\varepsilon_v - \varepsilon_{v,0} = \lambda^* ln \frac{p'}{p_0}$$

In unloading and reloading only elastic strain is considered and the relationship between elastic volumetric strains and the mean effective stress is quantified by the modified swelling index κ^*.

Equation 2.15

$$\varepsilon_v^e - \varepsilon_{v,0}^e = \kappa^* ln \frac{p'}{p_0}$$

In Figure 2.5 the logarithmic relationship between mean effective stress and volumetric strain is shown.

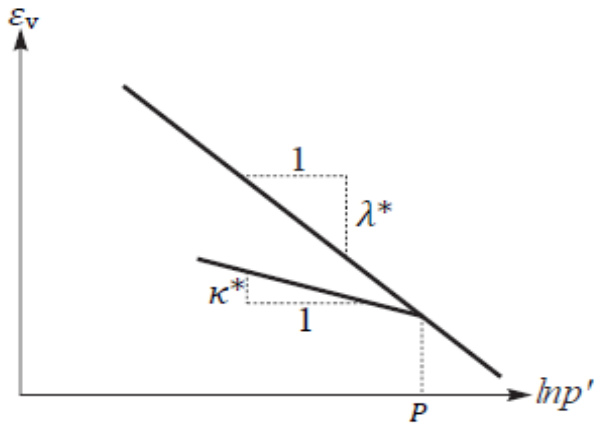

Figure 2.5. Logarithmic relation between volumetric strain and mean stress (PLAXIS, Material Models Manual, 2023)

The yield function and the hardening rule of the SS-model correspond to those of the Modified Cam-Clay model.

Modified Cam-Clay yield function:

Equation 2.16

$$f = \frac{q^2}{M^2} - p'(p' - p_c)$$

The hardening rule differs from the Cam-Clay model by using the plastic volumetric strain rate instead of the void ratio and furthermore using the modified indices.

Hardening Rule:

Equation 2.17

$$d\varepsilon_v^p = (\lambda^* - \kappa^*) \frac{dp_p}{|p_p|}$$

Figure 2.6 illustrates the SS model in the p'- q stress space. Because the parameter M is determined based on K_0^{NC}, the soil strength may be overestimated. By using the MC failure criterion, overestimation of the soil strength is prevented, therefore the SS-model cannot be considered a critical state model. The model contains a small cohesion term, which causes the threshold ellipse to have a minimum size. The threshold ellipse is related to a minimum value for the pre-consolidation stress, which ensures that the model has a minimum strength in the case of a zero-stress state.

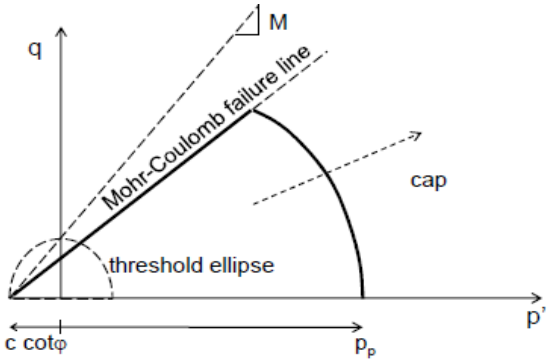

Figure 2.6. The Soft Soil Model illustrated in p'- q stress space.

2.2.5 The Soft Soil Model Parameters

In table 3 are the input parameters for the SS-model in Plaxis. The parameters are divided into basic and advanced parameters.

Table 2.3: The SS-model parameters

Basic parameters for soil stiffness:		
λ^*	Modified compression index	[-]
κ^*	Modified swelling index	[-]
c'	Effective cohesion	[kPa]
ψ	Dilatancy angle	[°]
ϕ'	Friction angle	**[°]**
Advanced parameters:		
v_{ur}	Poisson's ratio for unloading-reloading (default 0.2)	[-]
K_0^{NC}	K_0 –value for normal consolidation (default K_0^{NC}= 1 – sin ϕ')	[-]
σ_t	Tensile strength (default 0)	[kPa]
M	K_0^{NC} -parameter	[-]

The modified parameters ($\lambda^*$and κ^*) can be determined using an isotropic compression test and/or a one-dimensional compression test. These parameters can be related to the parameters of the original Cam-Clay model (λ and κ) (Equation 2.18 and Equation 2.19) and internationally normalized parameters (C_c and C_s) (Equation 2.20 and Equation 2.21).

Equation 2.18 $$\lambda^* = \frac{\lambda}{1+e}$$

Equation 2.19 $$\kappa^* = \frac{\kappa}{1+e}$$

Equation 2.20 $$\lambda^* = \frac{C_c}{2.3(1+e_0)}$$

Equation 2.21 $$\kappa^* \approx \frac{2C_s}{2.3(1+e_0)}$$

Typical ranges for the ratio $\frac{\lambda^*}{\kappa^*}$ $(=\frac{\lambda}{\kappa})$ are between 2.5 and 7 (PLAXIS, Material Models Manual, 2023) p.118.

The parameter K_0^{nc} is better known than parameter M. Therefore parameter K_0^{nc} is used as input in Plaxis and parameter M is automatically converted with Equation 2.22 (Brinkgreve R. B., 1994) p. 42 - 44. The parameter M is influenced by the unloading reloading Poisson's ratio, v_{ur}, and by the ratio between the modified parameters $\frac{\lambda^*}{\kappa^*}$ as well.

Equation 2.22 $$M = \sqrt{\frac{(1-K_0^{nc})^2}{(1+2K_0^{nc})^2} + \frac{(1-K_0^{nc})(1-2v_{ur})(\frac{\lambda^*}{\kappa^*}-1)}{(1-2K_0^{nc})(1-2v_{ur})\frac{\lambda^*}{\kappa^*}-(1-K_0^{nc})(1+v_{ur})}}$$

2.2.6 The Sekiguchi-Ohta model

The Sekiguchi-Ohta (SO) model was developed with the support of Tokyo Geotech. and is suitable for determining the soil behavior of soft soils, in particular normal consolidated clays. The fundamentals of the model lie in the Cam-Clay model (Roscoe, Schofield & Thurairajah, 1963) and the rheological model of Murayama & Shibata (1966) found in PLAXIS Material Models Manual (2023). It is possible for the SO - model to incorporate time dependent (creep) and anisotropic soil behavior of clays, the latter being of interest in this study.

The SO model can be formulated as a time dependent (viscid) and time independent (inviscid) model. Time dependency is not included in this research; thus, the focus is on the inviscid model.

A disadvantage of this model may be that it has been formulated and tested for clay material in Japan and not for clay material in the Netherlands. Furthermore, a failure criterion is used that is very similar to that of Drucker Prager, where it is known that Drucker Prager failure criterion inaccurately predicts earth pressures (Schweiger, 1994) (Alkema, 2018).

The logarithmic relation for the change in volumetric strain is defined similarly as in the soft soil model with Equation 2.14 for primary compression and for unloading reloading with Equation 2.15.

In accordance with the Soft Soil model, there is elastic soil behavior in the Sekiguchi-Ohta model as well during unloading reloading. However, in the SO-model elastic behavior is described by the means of Hooke's law, with linear stress dependency on the tangent bulk modulus as given in Equation 2.23.

Equation 2.23 $$K_{ur} = \frac{E_{ur}}{3(1-2v_{ur})} = \frac{p'}{\kappa^*}$$

The difference between the SS model and the inviscid SO model mainly lies in the formulation of the yield function. The yield function of the SO model in triaxial space is given by:

Equation 2.24 $$f = MD\ ln\ (\frac{p'}{p_p}) + D\frac{\bar{q}}{p'}$$

where

M is the critical state frictional parameter

D is the coefficient of dilatancy

p' is the mean effective stress

p_p is the isotropic hardening stress parameter

$\bar{q}$ is the relative deviatoric stress

The isotropic hardening stress parameter is defined as:

Equation 2.25 $$p_p = p_{p0}\, e^{(\frac{\varepsilon_v^p - \varepsilon_{v,0}^p}{MD})}$$

where

MD is the difference between modified parameters$(\lambda^* - \kappa^*)$

ε_v^p is the plastic volumteric strain

$\varepsilon_{v,0}^p$ is the initial plastic volumteric strain

2.2.7 The inviscid SO-model parameters

In Table 4 the input parameters for the SO-model in Plaxis. The parameters are divided into basic, advanced and alternative parameters.

Table 2.4. The inviscid SO-model parameters

Basic parameters for soil stiffness:		
λ^*	Modified compression index	[-]
κ^*	Modified swelling index	[-]
Advanced parameters:		
v_{ur}	Poisson's ratio for unloading-reloading (0.2)	[-]
K_0^{NC}	K_0 –value for one dimensional normal consolidation	[-]
M	Tangent of the critical state line (CSL) based on the critical state friction angle (ϕ_{cs})	[-]

2.2.8 The S-Clay1 Model

The S-Clay Models are based on an elastoplastic formulation with the possibility to switch features on and off. The S-Clay models can be divided into the S-Clay1 (Wheeler S. , Näätänen, Karstunen, & Lojander, 2003) S-Clay1S and Creep S-Clay1S.

S-Clay1 only the anisotropy feature of the model is included.

S-Clay1S anisotropy, bonding and de-structuration are included as model features.

Creep S-Clay1S all the above features with an additional creep definition.

This document only discusses the S-Clay1 model. Special about this model is the incorporation of a rotational hardening yield locus, in which the inclination of the yield locus can change during plastic deformation because of development or erasure of fabric anisotropy. However, there are some similarities with the Modified Cam-Clay model (Roscoe & Burland, 1968) by means of the yield function, the parameter M is determined by the friction angle, the top of the yield locus coincides with the critical state line (CSL), assumption of isotropic behavior in elastic straining and the hardening rule.

This model may be less suitable in the case of unloading scenarios such as excavations, and situations including cyclic loading, due to the assumption of isotropic elastic behavior.

The yield function of the S-Clay1 model can be expressed in terms of the mean effective stress, p', and deviator stress q (simplified in triaxial space):

Equation 2.26

$$f = (q - \alpha p')^2 - (M^2 - \alpha^2)(p'_m - p')p'$$

where

M	is the inclination of the yield surface or stress ratio η (η = q/p') at critical state	[-]
p'_m	is the maximum pre-consolidation stress, defines the size of the yield locus	[kPa]
α	defines the orientation of the yield locus; measure for plastic anisotropy	[-]

For α = 0, the model is isotropic and corresponds to the Modified Cam Clay model. In Figure 2.7 the yield locus of the S-Clay1 model is illustrated in p'- q stress space and triaxial stress space.

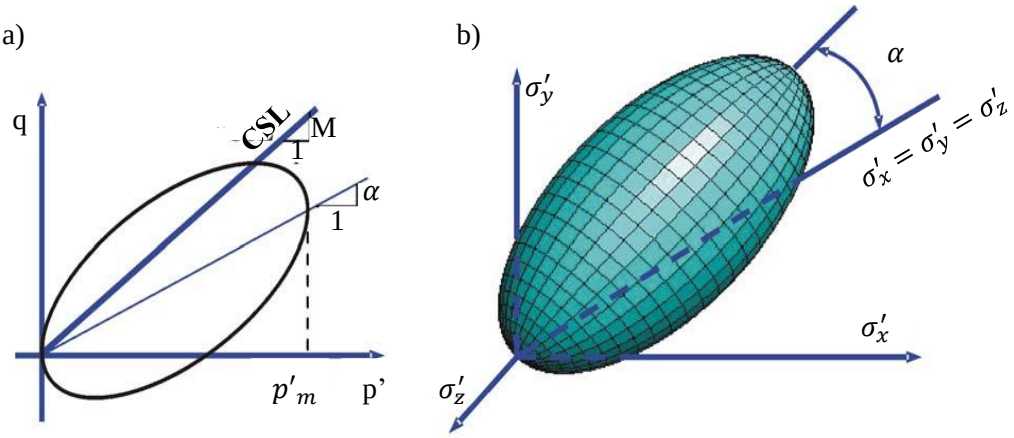

Figure 2.7. Illustration of the S-CLAY1 yield surface a) Triaxial stress space b) 3-D stress space

There are two hardening laws formulated for the S-Clay1 model. Equation 2.27 describes the change of size of the yield curve, related solely to plastic volumetric deformation. Equation 2.28 describes change of the inclination of the yield curve as a result of plastic strain, related to anisotropy. Unfortunately, the rotational hardening law is only based on the occurrence of plastic volume strains, which can lead to incorrect predictions (see Karstunen & Wheeler (2002) (Wheeler, Cudny, Neher, & Wiltafsky, 2003)).

The hardening rule is formulated in terms of the **maximum** pre-consolidation stress p_m:

Equation 2.27
$$d\varepsilon_v^p = \frac{\lambda-\kappa}{v}\frac{dp_m}{|p_m|}$$

where

$d\varepsilon_v^p$ is the plastic volumetric strain increment [-]

v is the specific volume [-]

The **rotational** hardening law is formulated as:

Equation 2.28
$$d\alpha = \omega\left[\left(\frac{3q}{4p'}-\alpha\right)\langle d\varepsilon_v^p\rangle + \omega_d\left(\frac{q}{3p'}-\alpha\right)\left|d\varepsilon_d^p\right|\right]$$

where

$d\varepsilon_d^p$ is the plastic deviatoric strain increment [-]

ω is the control parameter for the absolute rate of rotation of the yield surface towards its current target value of α [-]

ω_d is the relative effective plastic shear strain and plastic volumetric strain parameter [-]

2.2.9 The S-Clay1 model parameters

In Table 2.5: The S-Clay1 model parameters are the input parameters for the S-Clay1 model in Plaxis.

Table 2.5: The S-Clay1 model parameters

User defined parameters:		
λ (λ^*)	(Modified) compression index	[-]
κ (κ*)	(Modified) swelling index	[-]
v	Poisson's ratio (0.2)	[-]
K_0^{NC}	Coefficient of lateral stress in normal consolidation	[-]
M_c	Tangent of the critical state line (CSL) in compression	[-]
M_e	Tangent of the critical state line (CSL) in extension	[-]
α_0	defines the initial orientation of the yield locus	[-]
ω	Controls rate of anisotropy / absolute effectiveness of rotational hardening	[-]
ω_d	Influence of deviatoric plastic strain in rate of anisotropy	[-]
OCR	Over consolidation ratio	[-]

2.3 Laboratory Tests

This Section briefly describes the laboratory tests used to obtain the model parameters for the material models. Thus, giving the reader a better perspective on the laboratory tests used to obtain model parameters in Chapter 3 and 4. The apparatus characteristics are for the laboratory instruments and conditions under which the laboratory tests are performed to obtain model parameters discussed in Chapter 4.

2.3.1 Triaxial test

The triaxial setup (Figure 2.8) is used to determine strength and stiffness parameters of soil using a cylindrical sample. The sample is placed in the center of the triaxial cell and is held together by a rubber membrane. The rubber membrane ensures that the water in the triaxial cell and in the sample remains separated during the test. The sample is compressed or extended via a mechanism underneath the load cell and the corresponding vertical stress is measured by the load cell. The axial displacement of the sample is monitored by the displacement transducer and the difference in pore water pressure is measured by the back pressure. Usually, the cell pressure is kept constant during the test. By using smooth porous discs, shear stresses at the top and bottom boundaries of the sample are prevented, which would incorrectly influence the test results. Furthermore, it is assumed that the stresses are equally distributed in the sample, which is in fact incorrect, since the sample is not homogeneous.

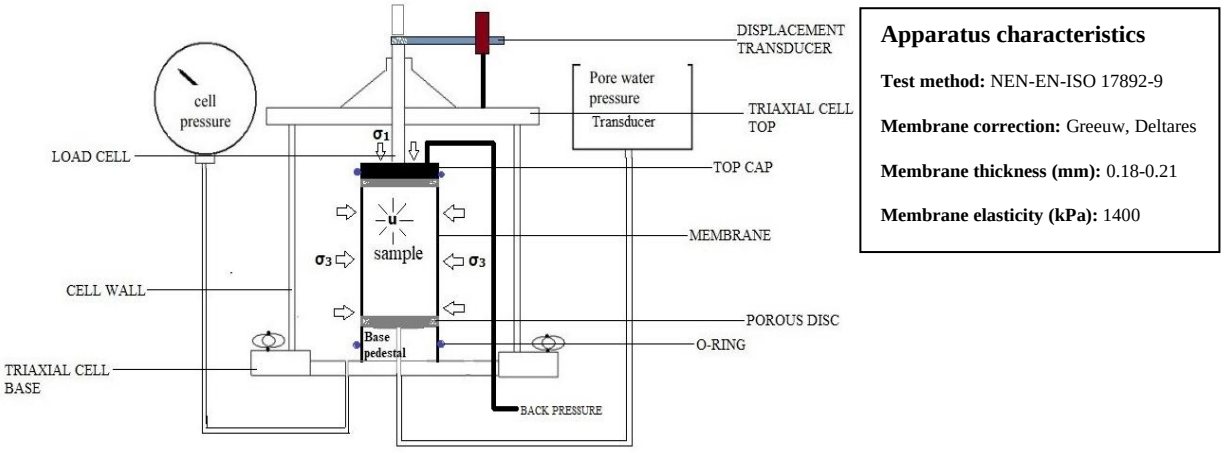

Figure 2.8. Triaxial test setup

In general, a triaxial test can be performed consolidated undrained, consolidated drained and unconsolidated undrained, either isotropic or anisotropic, compression or extension. The test results in this document come from single stage consolidated isotropic undrained compression (CIUc) tests, which are strain controlled. Usually for clay material the test is carried out undrained, due to the low permeability and therefore it would take a great amount of time to carry out a drained triaxial test. Undrained parameters can be converted into drained parameters by measuring the excess pore water pressure and subtracting it from the total stress values.

Consolidated Undrained (CU): Open valve during consolidation stage but closed during shearing. During the shearing stage, the pore pressure is measured. The CU triaxial test is the most common. The soil sample is not allowed to drain and measures both the pore water pressure and the excess pore water pressure change of the soil sample during the shearing stage.

Using laboratory results from triaxial tests, the cohesion and friction angle of the material can be determined. Three tests on the same material at different cell pressures are conducted in practice. The

results from triaxial tests are not limited to determining strength parameters of soil, but stiffness parameters can be obtained as well by plotting the deviatoric stress vs. the axial strain.

2.3.2 Direct Simple Shear (DSS) test

Advanced to the DSS test is the fact that deformations are prevented from being centered in the apparatus by use of rotating side walls. Figure 2.9 shows a sketch of the DSS test setup. A vertical weight is placed on the top plate before the test is started. The DSS test can be performed in two ways: drained or undrained, where the vertical load is constant and the volume of the sample changes in a drained execution of the test and in an undrained execution the vertical load is varied, and the volume of the sample is kept constant. The top plate and the base can move horizontally relative to each other, in which an external force is applied on the base resulting in shear forces in the sample. The shear forces increase until failure is reached, whereafter the shear forces may slightly increase further and then decrease. The internal horizontal forces (both directions) are unknown during shearing, making it unclear at which point of the Mohr circle the critical state has been reached.

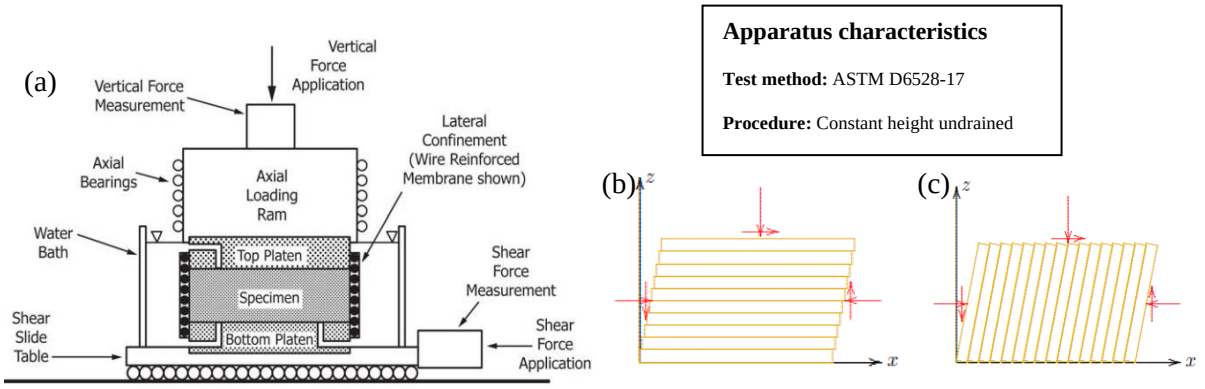

Figure 2.9. (a) DSS test components (ASTM D6528-17) (b) sliding on horizontal planes (c) sliding on vertical planes (Verruijt, 2012)

Many studies have shown that lower values are found for the shear strength with the DSS test compared to the triaxial test. The occurrence of a wide range of results for the same type of soil material in different DSS tests brings the reproducibility of the results in question. The shear stresses that occur can differ for each test and there is great uncertainty in whether the stresses are indeed the true critical stresses. Aforementioned gives the DSS test a great disadvantage, especially when compared to triaxial test where the stresses are well known in a three-dimensional space.

The DSS test is one of the few laboratory tests available in which shear stresses are applied to the sample and the conditions appearing along a potential sliding plane are fulfilled.

As is the case with triaxial tests, multiple DSS tests can be used to determine strength parameters by plotting the shear stress vs. the applied vertical stress. The results from DSS tests are not limited to determining strength parameters of soil, but stiffness parameters (shear modulus G) can be obtained as well by plotting shear stress vs. shear strain.

2.3.3 One Dimensional Compression

Classic Oedometer test

The classic oedometer test (Figure 2.10) is used in this research to determine the oedometer stiffness, used as input in the HSss model. The oedometer test is used to determine many other parameters such as consolidation parameters, permeability, pre-consolidation stress and creep. The load on the sample is increased in stages and is referred to as incremental loading (IL). Seven stages are used when performing the test, which include loading, unloading, and reloading.

The reference oedometer stiffness is determined by plotting the vertical stress against the axial strain shown in Figure 3.4. Where the tangent line coincides with the graph for a vertical stress, σ'_1, equal to p^{ref}, is chosen as the reference oedometer stiffness E_{oed}^{ref}. The oedometer stiffness, E_{oed}, is determined by equation 2.9 (Section 2.2.1). Measuring the resulting horizontal stress is not possible for a classic oedometer test, which is seen as a disadvantage. The development of horizontal stresses in relation to the imposed vertical stress provides important information about the stresses that might occur in reality.

(a)

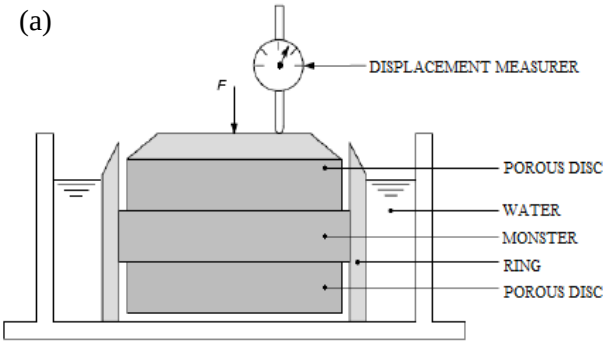

Apparatus characteristics

Test method: NEN-EN-ISO 17892:5

Procedure: 7 stages (1-4 Load, 5 Unload, 6 Reload, 7 Load)

Circumstances: wet

Temperature: 20 ° C

Figure 2.10. (a) Sketch of oedometer test (Backhausen & van der Stoel, 2014)

2.4 Concluding Remarks

From the above sections it is known that the material models have similar and different features and therefore similar and different material model parameters as well. Corresponding features between material models include non-linear stress dependent stiffness, different stiffnesses for loading/unloading, stress history effect and volumetric hardening. Differences are in features such as the flow rules (associated/non-associated), where the associated flow rule for the Soft Soil model and the Hardening Soil small strain model is defined as CAP hardening and the non-associated flow rule as the Mohr-Coulomb failure surface. Deviatoric hardening is not considered in the Soft Soil and Sekiguchi-Otha model but is considered in the HSss model and S-Clay1 model. In total 19 material model parameters must be determined separately for the considered soil layers, such as: c', ϕ', ψ, E_{50}^{ref}, E_{oed}^{ref}, E_{ur}^{ref}, m, p^{ref}, v_{ur}, K_0^{NC}, R_f, λ^*, κ^*, M_c, M_e, α_0, ω, ω_d and OCR.

Furthermore, the characteristics of the laboratory tests (triaxial, DSS and oedometer), used to determine material model parameters in this study and the method of execution are known. The shortcomings of the laboratory tests, such as the rather long duration to perform consolidated drained triaxial tests on clay material and the unknown horizontal stresses that arise in the DSS and oedometer apparatus. The advantages are mentioned as well, such as the possibility of controlling the stress/strain during the performance of the tests. The stiffness parameters can simply be determined with the oedometer test for all considered material models in this study.

3. Material Models Parameter Determination

In the previous chapter all the required material model parameters are listed, of which in this chapter answer is given to sub question 2 "*How should laboratory tests be interpreted to derive the appropriate model parameters for the corresponding constitutive soil model?*", in which it is made clear how the material model parameters, are determined for the material models and how, despite the lack of necessary laboratory results, assumptions and approximations can be made to arrive at realistic estimates for model parameters.

3.1 Mohr-Coulomb parameters (cohesion, Friction angle and Dilatancy angle)

The Mohr-Coulomb parameters are common model parameters and are obtained from Triaxial and DSS test results. In the case of soft clay material, the dilation angle is assumed to be zero (Karstunen & Amavasai, 2017), since dilation angles are extremely low for soft soils and therefore negligible.

The cohesion and internal friction angle from different laboratory results for a given soil type are related in such a way that one set of strength parameters is obtained. The strength parameters adapted from regression are determined according to the method described in (van Duinen, 2014) p.34 as can be seen in Figure 3.1. The strength parameters obtained from regression are further used to determine other constitutive model parameters. Assessment of a quay wall concerns an actual momentary state, thereby the stiffness of soil in combination with effective (drained) peak strengths is assumed (Toetskader Amsterdamse Kademuren TAK 3.2) specifically (Verweij, 2023) (Attachment E, p.9 in TAK 3.2).

By converting the slope of the critical state line (tan α (= t/s' = 0.62)) through the peaks of the graphs, the internal friction angle (38.3 °) can be obtained by the relation tan α = sin ϕ'. This conversion from α to ϕ' is necessary because in the triaxial tests the peak points of the stress paths are equal to the top of the Mohr circles. These points do not coincide with the tangent points of the failure envelope of the Mohr circles (van Duinen, 2014) p. 32. The effective cohesion (c') in this case is equal to 5.5 kPa.

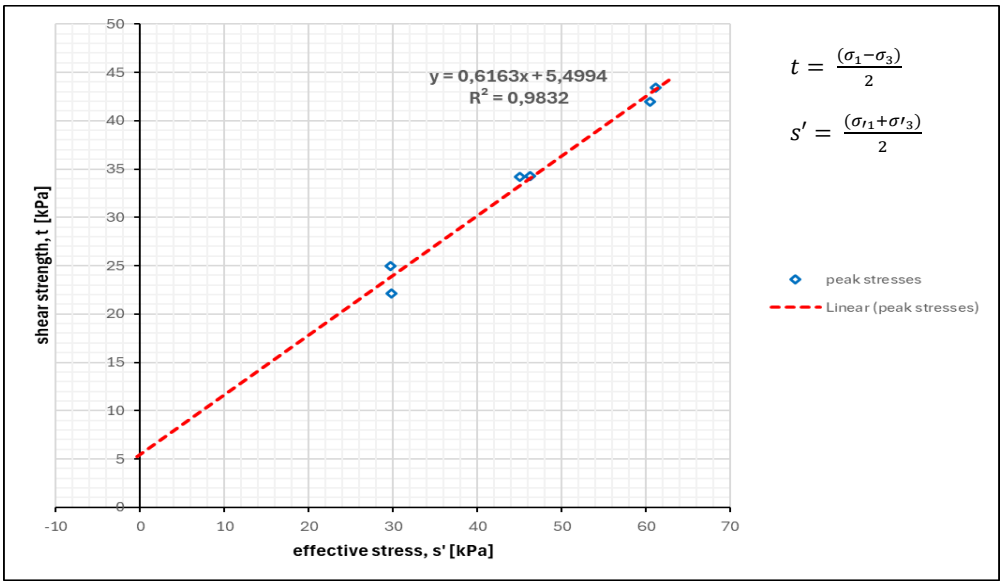

Figure 3.1. Deviator stress, t, and mean effective stress, s', with critical state line from Triaxial test results on Geulopvulling

For the DSS laboratory results on Hollandveen (Figure 3.2) the line through the measured values of shear stress is assumed the critical state line. The internal friction angle (°) is calculated with the slope of the critical state line, α, where tan α = sin ϕ' = 0.61. In the case of DSS test results the assumption is made that the points on the stress path are equal to the top points of the Mohr circles. The stress state in a DSS test is not fully known, therefore other assumptions are possible as well (van Duinen, 2014). The effective cohesion (c') is equal to 1.58 kPa.

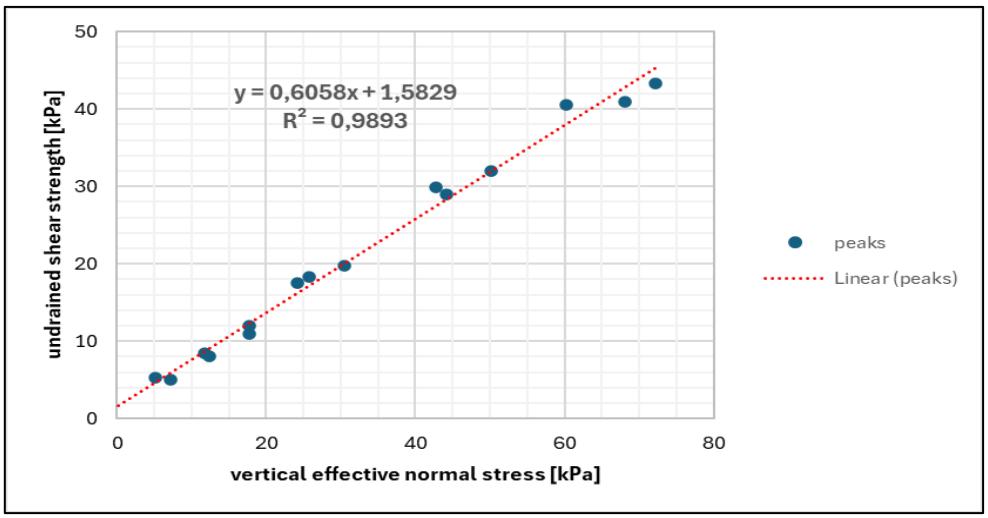

Figure 3.2. DSS test results on Hollandveen in shear stress versus total effective vertical stress graph

3.2 Unloading-Reloading Poisson's ratio (v_{ur}, v)

Poisson's ratio is an elastic soil material property, which determines the ratio between the axial and radial direction under axial loading. Poisson's ratio for soil materials is generally between 0.1 and 0.4. In case the material hardly changes in the lateral direction under uniaxial loading, the value of Poisson's ratio approaches 0. The value of Poisson's ratio is equal to 0.5 when no volume change occurs under uniaxial loading. For low normalized mobilized stress ratios of $\frac{q}{q_{max}}$, up to approximately 0.3, most soils have a Poisson's ratio between 0.1 and 0.2 shown in Figure 3.3. Therefore, v_{ur} is set equal to 0.2 for most soils and is used in this study as well.

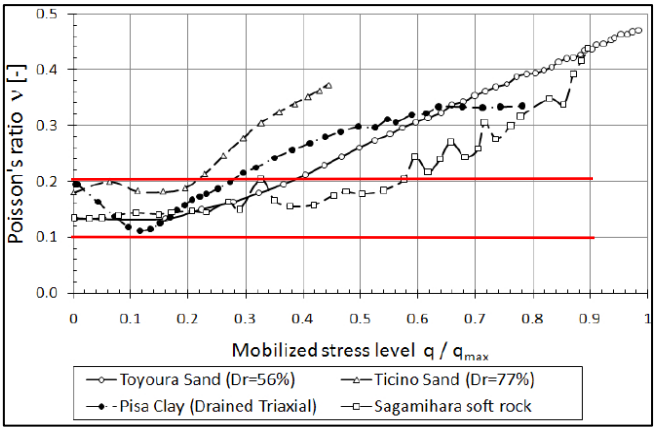

Figure 3.3. Poisson's ratio vs. mobilized stress level derived from local strain measurements on different soils (Mayne, Coop, Springman, Huang, & Zornberg, 2009)

3.3 Coefficient of earth pressure at rest (K_0^{NC})

The coefficient of earth pressure "at rest" and for normally consolidated conditions, gives the ratio between the horizontal stress and vertical stress in one dimensional consolidation and is often related to the internal friction angle of the soil material. Jaky's (1947) often used relation (3.1) to approximate K_0^{NC} is used in this study.

Equation 3.1 $$K_0^{NC} \cong 1 - \sin \phi'$$

Formulation 3.1 is a simplified formulation from the original given in equation 3.2.

Equation 3.2 $$K_0^{NC} = \frac{1 - \sin \phi\prime}{(1+ \sin \phi\prime)(1+\frac{2}{3}\sin \phi')}$$

3.4 Stiffness Moduli (E_{oed}, E_{50}, E_{ur}) for HSss model & stress level dependency (m)

Oedometric modulus:

The oedometer stiffness, E_{oed}, is determined from results of the IL oedometer test. First, the reference oedometer stiffness, E_{oed}^{ref}, is obtained at a reference stress for stiffness, p^{ref}, of 100 kPa from a vertical stress vs. vertical strain plot. Afterwards E_{oed} is determined using Equation 2.7 previously mentioned in Section 2.2.1.

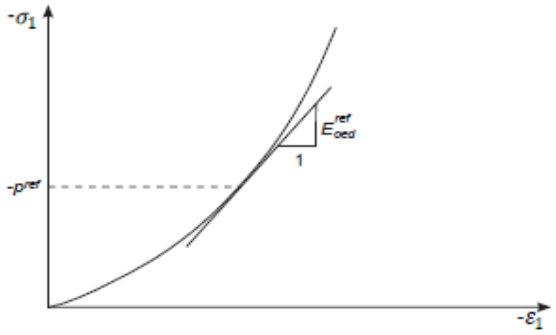

Figure 3.4. Oedometer test results (PLAXIS, Material Models Manual, 2023)

Secant and unloading reloading moduli:

The secant stiffness, E_{50}, and unloading reloading stiffness, E_{ur}, are obtained from Triaxial test results. First reference stiffnesses, E_{50}^{ref} and E_{ur}^{ref}, are determined for cell pressure, σ'_3, equal to the reference stress (p^{ref} = 100 kPa). Afterwards E_{50} and E_{ur} are determined with Equation 2.4 and Equation 2.5. In the absence of laboratory results to directly determine E_{ur}^{ref}, the relationship can be assumed to be (Obrzud & Truty, 2018):

Equation 3.3 $$\frac{E_{ur}^{ref}}{E_{50}^{ref}} = 2 \; to \; 6$$

Stiffness stress dependency parameter, m:

Parameter m is found by performing three triaxial tests, for which three values of $E_{50}^{(i)}$ are obtained corresponding to three values of cell pressure $\sigma'^{(i)}_3$. Afterwards a trend line is formed in a coordinate system where the y-axis contains the values of ln $E_{50}^{(i)}$ and the x-axis values for ln $\left(\frac{c'cos\phi' + \sigma'_3 sin\phi'}{c'cos\phi' + p^{ref} sin\phi'}\right)$ as shown in Figure 3.5. The slope of the trendline is the parameter m.

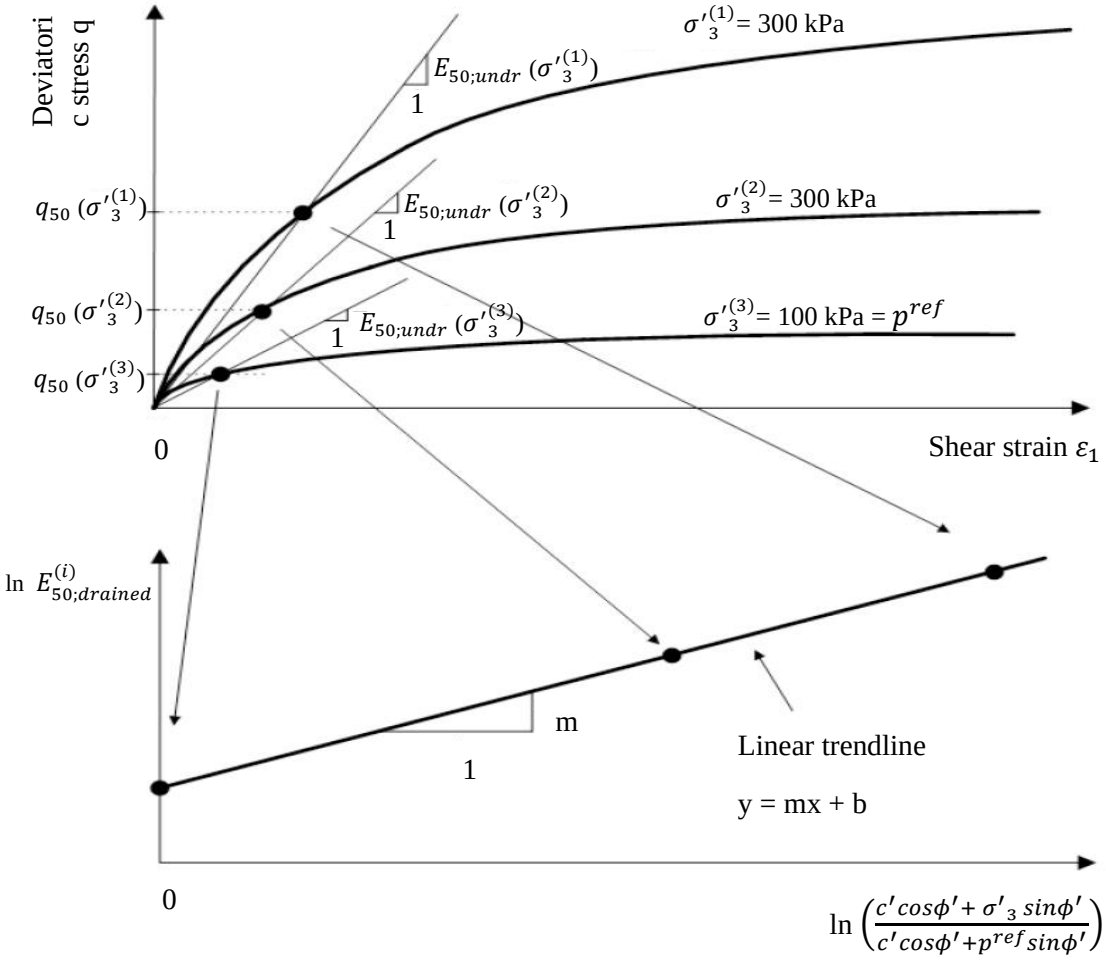

Figure 3.5. Determination of the stiffness stress dependency parameter m from three triaxial compression test results (Obrzud & Truty, 2018)

Because the results come from CIUc triaxial tests, undrained parameters are obtained. The obtained undrained parameters are converted to drained parameters based on assumptions and linear elastic relations through Hooke's law.

The relation between undrained stiffness, E_{undr} , and drained stiffness, E_{dr}, in the case of elastic behavior is:

Equation 3.4 $$E_{dr} = \frac{2(1+\nu')}{3} E_{undr}$$

For ν' = 0.2, results in $E_{dr} = 0.8\, E_{undr}$.

However, it is a gross approach to use Equation 3.4, as it concerns elastic stiffness parameters, while there is dealt with elastoplastic parameters in this case.

Since there are only undrained triaxial tests available (no drained triaxial tests available) Plaxis soil test is used to adjust stiffness parameters, to ensure that the test results available yield reasonable outcomes of simulations before implementing in finite element method (FEM) analyses.

3.5 Small strain shear modulus (G_0) and $\gamma_{0.7}$ for HSss model

The shear modulus can be determined directly by conducting geophysical field tests. Due to the lack of geophysical test results from the field, approximations are made based on given formulas from correlations of many tests conducted by researchers such as B. Hardin and W. Black soils (1969), and T. Kim and M. Novak. The initial small strain shear modulus, G_0, can be determined using Equation 2.13, after G_0^{ref} is determined at a reference stress of $\sigma'_3 = p^{ref} = 100\ kPa$. The small shear strain threshold, $\gamma_{0.7}$, is determined with Equation 2.11. In this study Equation 2.13 is used to determine G_0^{ref} in the case of Oude zeeklei and for Geulopvulling and Hollandveen an initial assumption was made that G_0^{ref} is equal to E_{ur}^{ref}, since Equation 2.13 resulted in quite low values for G_0^{ref}.

3.6 Stiffness parameters of the Soft Soil, Sekiguchi-Otha and S-Clay1 model

The stiffness parameters of the soft soil, Sekiguchi-Otha and S-Clay1S model are defined by the modified compression index λ^* and the modified swelling index κ^*. By plotting oedometer results in a stress-strain logarithmic curve, Bjerrum one-dimensional consolidation parameters for primary compression C_c and swelling C_s are obtained. Bjerrum consolidation parameters are converted to $\lambda^*$and κ^* with Equation 2.20 and Equation 2.21. In Figure 3.6 the results of an IL oedometer test are plotted by void ratio vs. the logarithmic value of the vertical effective stress, for which the stiffness parameters and Bjerrum consolidation parameters are derived.

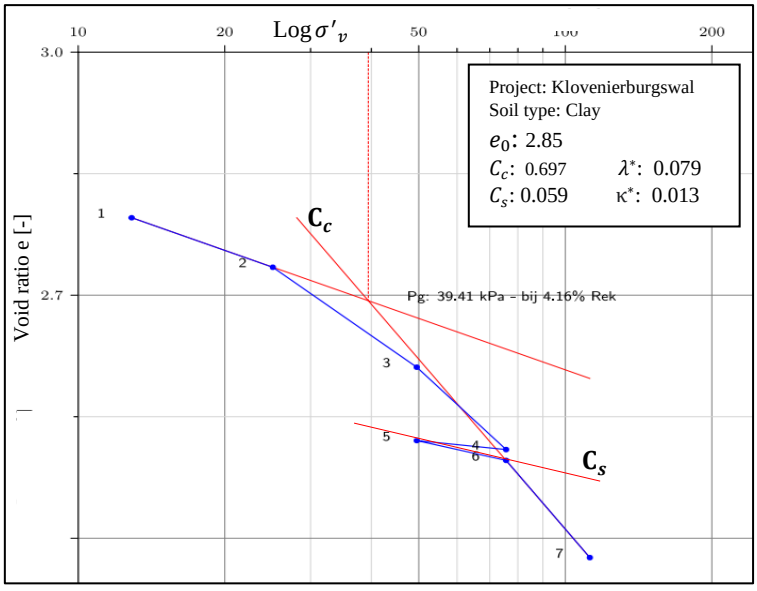

Figure 3.6. Determination of the stiffness parameters from oedometer test results

3.7 Parameters relating to anisotropy of the S-Clay1 model

Measure for plastic anisotropy α

In the case of normally or slightly over-consolidated soil, an estimate of α can be found by deriving an estimate of the normally consolidated coefficient of earth pressure, K_0^{NC} Wheeler et al. (2003). In this study, K_0^{NC} is estimated by Jaky's formulation given in Equation 3.1. The stress ratio of η_{K_0} (= $\frac{3(1-K_0^{NC})}{(1+2K_0^{NC})}$) corresponding to the stress level at which K_0^{NC} is determined is then used to obtain α ($\alpha = \alpha_{K_0}$) as shown in Equation 3.5. parameter M_c (= $\frac{6\,sin\phi'}{3-sin\phi'}$) and M_e (= $\frac{6\,sin\phi'}{3+sin\phi'}$) are related to the critical state friction angle, ϕ'_{cs}.

Equation 3.5

$$\alpha_0 = \alpha_{K_0} = \frac{{\eta_{K_0}}^2 + 3\eta_{K_0} - M^2}{3}$$

Plastic volumetric strain parameter

The relative effective plastic shear strain and plastic volumetric strain parameter, ω_d, is related to the critical state friction angle through parameter M and the stress ratio, η_{K_0} as given below:

Equation 3.6

$$\omega_d = \frac{3(4M^2 - 4{\eta_{K_0}}^2 - 3\eta_{K_0})}{8({\eta_{K_0}}^2 + 2\eta_{K_0} - M^2)}$$

Control parameter

The control parameter, ω, for the absolute rate of rotation of the normal consolidation yield surface towards its current target value of α, is not so straightforward calculated. A convenient estimate of ω is given by Leoni et al. (2008) below, with the assumption that erasure of anisotropy takes place when α decreases to 1/10th of its initial value, meaning $\frac{\alpha_0}{\alpha} = 10$.

Equation 3.7

$$\omega = \frac{1}{\lambda^*}\, ln \frac{10M^2 - 2\alpha_0\omega_d}{M^2 - 2\alpha_0\omega_d}$$

4. Validation of model parameters

Following the procedures in Chapter 3, this chapter answers sub question 3 *"What methods can be employed to validate selected model parameters for different constitutive soil models in geotechnical finite element method analyses?"*, in which material model parameters for Geulopvulling, Hollandveen and Oude zeeklei have been determined from laboratory results. The model parameters are derived from laboratory results from location Kloveniersburgwal (historic quay wall) in Amsterdam.

In section 4.1 the material model parameters and general information (4.1.1) is provided, which are used to obtain graphs from Plaxis Soil Test simulations. For each soil layer, model parameters have been determined over the entire set of laboratory results and subsequently model parameters are determined based only on the selected representative test in Section 4.1.2 to 4.1.4. Furthermore, model parameters for the set of all laboratory results are optimized (optimized parameters) with the use of Plaxis Soil Test, in which resulting graphs from Plaxis Soil Test are fitted to the graphs from measured laboratory data as best as possible. In Section 4.2 comparison is made between the resulting Plaxis Soil Test graphs of the considered material models, including resulting graphs obtained from model parameters in TAK 3.2. In Section 4.3 the sensitivity of the anisotropy parameters in the S-Clay1 model is analyzed, followed by a discussion and conclusions on this chapter in Section 4.4.

It is time-consuming and almost impossible to separately do simulations for each laboratory result, which is why a representative test is selected to validate the model parameters. Validation is done by plotting the graphs from Plaxis Soil Test together with graphs obtained from measurement data of the representative laboratory test and analyze how well these graphs correspond.

4.1 Model parameters for Geulopvulling, Hollandveen and Oude zeeklei

4.1.1 General Remarks for Validation and Optimization of Model Parameters

Following are some general points to keep in mind that apply to all soil layers and material models in this study:

- The analysis is performed for model parameters at the peak undrained shear strength.
- For Geulopvulling the axial strains are between 8 % and 15 % when the maximum undrained shear strength is reached.
- For Oude zeeklei the axial strains are between 1.5 % and 8 % when the maximum undrained shear strength is reached.
- For Hollandveen the shear strains are between 18 % and 25 % when the maximum undrained shear strength is reached.
- No analysis has been conducted for values of axial strain at exactly 2% and 5%. Axial strains of 2% and 5% (triaxial test) are used within the Dutch consultancy practice for the design of new earth retaining structures.
- The dilation angle, ψ, unloading-reloading Poisson's ratio, v_{ur}, the normally consolidated earth pressure coefficient, K_0^{NC}, the reference unloading-reloading Young's modulus, E_{ur}^{ref}, the reference shearing modulus, G_0^{ref}, the small shear strain threshold, $\gamma_{0.7}$, are not directly derived from laboratory results, therefore estimated.
- The effective (drained) secant stiffness at 50% of the maximum deviatoric stress, $E_{50;drained}^{ref}$, is roughly estimated with the undrained secant stiffness at 50%, $E_{50;undrained}^{ref}$, via Hooke's relation.

- Due to the lack of laboratory results containing of unloading-reloading phase, for Geulopvulling and Hollandveen E_{ur}^{ref} is 3.5 * E_{50}^{ref} and for Oude zeeklei E_{ur}^{ref} is 2.7 * E_{50}^{ref}, inspired from TAK 3.2 parameter set.
- For G_0^{ref}, Equation 2.12 gives an underestimated value for Geulopvulling and Hollandveen, compared to values usually found for G_0^{ref}. Therefore, G_0^{ref} is set equal to E_{ur}^{ref} for these soil materials, as done in TAK 3.2. For Oude Zeeklei, G_0^{ref} is obtained by Equation 2.12 (Hardin & Black, 1969). The void ratios of Oude zeeklei correspond more closely to the void ratios of the material on which this equation was developed.
- Over consolidation ratio (OCR) is obtained from oedometer (IL) laboratory results.
- E_{50}^{ref} for Oude zeeklei, obtained from samples on land, rather than both from samples on land and water, because then an extremely high value of 35968 kPa is obtained.
- $\gamma_{0.7}$, estimated with Equation 2.11 from (PLAXIS, Material Models Manual, 2023).
- K_0^{NC} estimated with jaky's relation.
- For the user defined model Creep-SClay1S it is not able to set the modified creep index (μ*) equal to zero to arrive at the S-Clay1 model, therefore the modified creep index is set equal to 1/20th of the modified compression index (λ^*) for all layers.
- The initial anisotropy, α_0, for the S-Clay1 model is set equal to zero in the case of Geulopvulling and Oude zeeklei, because tests on these samples are performed in isotropic consolidated fashion.

The overall sequence used to optimize the model parameters is as follows:

Note that the focus is on fitting the maximum deviatoric stress, which is reached at large strains, therefore the small strain parameters are not or slightly changed. The measured laboratory data for the highest consolidation stress is used, with the underlying idea that the soil sample with the highest consolidation stress develops greater stresses and strains before proceeding to the shearing stage and the highest maximum value of the deviatoric stress is reached as well. There is more certainty that the material experiences a higher axial stress than the determined pre-consolidation stress. When the pre-consolidation stress is surpassed, there is a greater chance that soil material will restructure itself and end up in the failure state (peak deviatoric stress) after some time.

Hardening Soil small strain model

- Often, E_{oed}^{ref} is required to be increased, to satisfy Plaxis 2D input requirement $E_{50} / E_{oed} < 2$.
- First the stiffness parameter E_{ur}^{ref} is optimized because it is obtained from rough estimations.
- The stiffness dependent parameter, m, is increased to decrease the steepness of the slope in the q - ε graph.
- Afterwards c' and/or ϕ' are enhanced to further improve the fitting of the graph.
- It is desirable to retain model parameters obtained from laboratory research, so it was decided not to adjust E_{50}^{ref}, because this parameter is obtained from a relation to the maximum deviatoric stress, q, in the q - ε graph from measured laboratory data.

Soft Soil model

- First the unloading/reloading parameter, κ*, is enhanced, since there is no unloading/reloading taking place in the current situation of the historic quay walls. Same as for the Sekiguchi-Ohta model and S-Clay1 model.
- Afterwards c' and/or ϕ' are enhanced to further improve the fitting of the graph.
- Virgin compression parameter, λ^*, is not enhanced to retain model parameters obtained from laboratory research. The stiffness parameters would have to be significantly adjusted to get a good fit, which is why c' and/or ϕ' are chosen for adjustments.

Sekiguchi-Ohta model

- First the unloading/reloading parameter, κ^*, is enhanced, whereafter K_0^{NC} is enhanced, not in relation to ϕ' with Jacky's equation, because a too low value of ϕ' would be required.

S-Clay1

- First the unloading/reloading parameter, κ^*, is enhanced, which decreases the slope of the graph and the maximum deviatoric stress in the q - ε_{yy} space.
- Afterwards K_0^{NC}, M_c and M_e are enhanced.
- The anisotropy parameter alpha is set equal to zero in the case of Geulopvulling and Oude zeeklei.

Table 4.1 shows the common parameters used, for all models per soil type. The initial void ratio is chosen from the representative triaxial test for Geulopvulling and Oude zeeklei, and from the representative oedometer test used for stiffness parameters for Hollandveen. The unit weight is the average value for a total of 9, 36 (triaxial) and 5 (DSS) laboratory test results, for respectively Geulopvulling, Oude zeeklei and Hollandveen. The OCR is the average value for a total of 3, 6 and 5 Oedometer test results, for respectively Geulopvulling, Oude zeeklei and Hollandveen. The consolidation stress is the same value used in the laboratory test and the pre-consolidation stress is chosen from the sample coming out of the same bore hole as the representative triaxial and DSS test samples.

Table 4.1 Common initial stress state parameters

Description	Geulopvulling	Hollandveen	Oude zeeklei	
Initial void ratio, e_0	min - used - max 2.10 - 2.10 - 5.68	min - used - max 5.77 - 6.60 - 11.32	min used max 1.20 - 1.52 - 1.88	[-]
Unit weight, γ	min - used - max 11.27 - 12.0 - 13.83	min - used - max 10.20 - 10.50 - 11.20	min - used - max 15.01 - 16.5 - 17.18	[kN/m^3]
Over consolidation in situ, OCR	min - used - max 1.01 - 1.07 - 1.14	min - used - max 1.0 - 1.62 - 2.04	min - used - max 1.04 - 1.36 - 1.80	[-]
Consolidation stress	29, 59, 88	29, 59, 88	38, 76, 113	[kPa]
Pre-consolidation stress	39	53	58	[kPa]

In Figure 4.1 the settings used in PST for simulations of triaxial test and DSS test are shown.

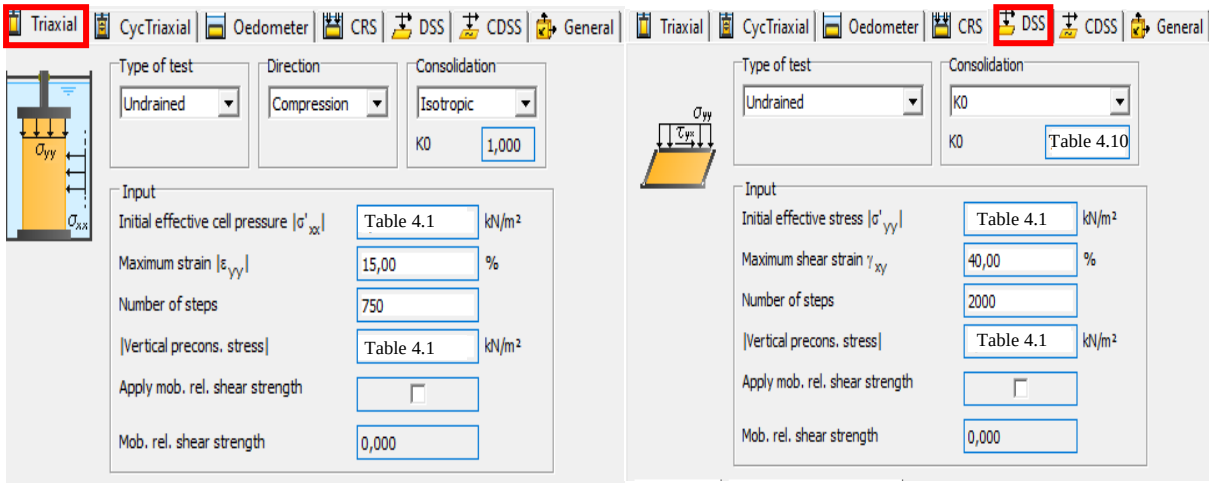

Figure 4.1. Settings used in PST for triaxial test and DSS test simulations

4.1.2 Geulopvulling model parameters

As indicated earlier, 3 sets of model parameters have been compiled for each material model namely All laboratory results, Representative test and optimized. All laboratory results consist of 6 triaxial test results in the case of Geulopvulling. The representative test results (3 triaxial tests) (m004-b1, m004-b2, m005-a2) are chosen based on the course of the graph in the axial strain vs. deviatoric stress space (see Attachment figure A.1, blue lines), but as well that the strength parameters (c', ϕ') obtained from linear regression on all laboratory results are approximately equal to the strength parameters from the representative test obtained by the tangent to the three resulting Mohr circles. The modified stiffness parameters (Attachment table A.3) for all laboratory results are obtained from a total of three oedometer tests and the representative test parameters come from sample M004-a3.

In Table 4.2 to Table 4.5 the model parameters on the Geulopvulling are shown. Expected values (mean) are used for the strength and stiffness parameters.

Hardening Soil Small Strain model

From Table 4.2 it is concluded that there is a small difference between the 3 sets of model parameters. The reference oedometer stiffness is increased to satisfy PST input requirements for the ratios between stiffness parameters.

Table 4.2. Hardening Soil small strain model parameters Geulopvulling.

Hardening Soil Small Strain											
	c' [kPa]	ψ [°]	ϕ' [°]	K_0^{NC} [-]	E_{50}^{ref} [kPa]	E_{oed}^{ref} [kPa]	E_{ur}^{ref} [kPa]	$\gamma_{0.7}$ 10^{-4}[-]	G_0^{ref} [kPa]	m [-]	v_{ur} [-]
All laboratory results	8	0	36.9	0.40	6242	1009→3500	22000	5.4	22000	0.64	0.2
Representative test	10.4	0	33.5	0.45	5730	1100→2500	20000	7.0	20000	0.60	0.2
Optimized	6	0	32.5	0.46	6242	3500	25000	5.4	22000	0.9	0.2

Laboratory result → PST requirement

In Figure 4.2 the graphs obtained from soil test (Hardening Soil small strain) and measured laboratory data are shown. The graphs for the optimized parameters are shown and discussed in Section 4.2.

In the ε_{yy} vs. q and p' vs. q space the PST graphs for all laboratory data and the representative test both overestimate and underestimate the peak deviator stress compared to the graphs from measured laboratory data for the different consolidation stresses, but the difference between the simulated graphs is minimal. The peak excess pore water pressures are fairly well estimated for the two lowest consolidation stresses by the PST graphs of all laboratory data, and with the representative test data giving a small overestimation, compared to measured laboratory data. In general, the resulting graphs from PST are quite similar. With the optimized parameter set, the best fit is achieved for the highest consolidation stress, where the maximum deviatoric stress corresponds well with the maximum deviatoric stress from measured laboratory results and the stiffness (steepness graph) is reduced in the q - ε_{yy} space. The stiffness dependent parameter, m, has a great influence on the steepness of the graph.

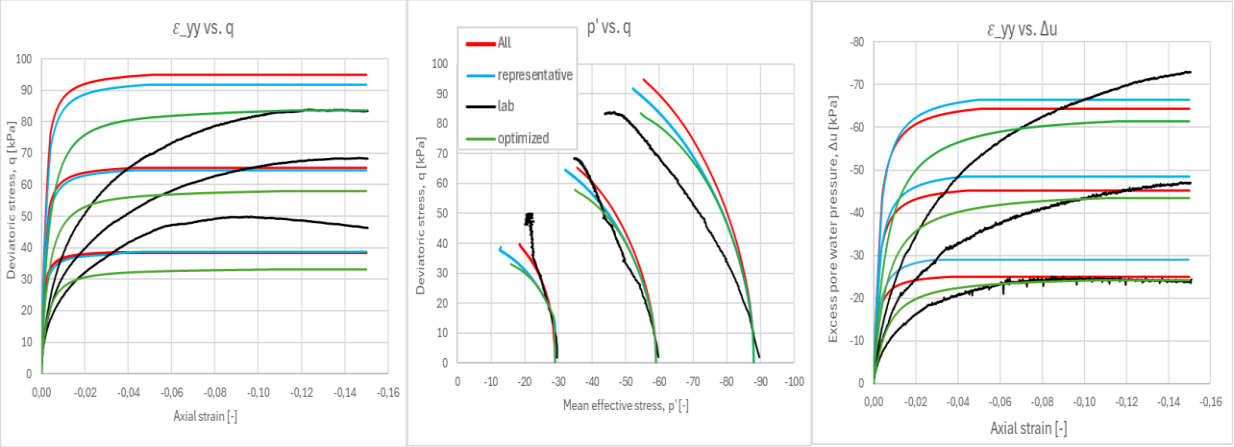

Figure 4.2. PST simulation and laboratory resulting graphs for HSss on Geulopvulling (all = all laboratory results; representative = representative test; lab data = measured in laboratory)

Soft Soil model

In Table 4.3 there is a small difference between the sets of all laboratory results and representative test. For the optimized parameters the cohesion and internal friction angle are reduced, and a much higher unloading reloading stiffness is given.

Table 4.3. Soft Soil model parameters Geulopvulling.

Soft Soil							
	c' [kPa]	ψ [°]	ϕ' [°]	K_0^{nc} [-]	λ^* [-]	κ^* [-]	ν_{ur} [-]
All laboratory results	8	0	36.9	0.40	0.088	0.0175	0.2
Representative test	10.4	0	33.5	0.45	0.11	0.02	0.2
Optimized	6	0	29	0.52	0.088	0.035	0.2

In Figure 4.3 the graphs obtained from PST (Soft Soil) and measured laboratory data are shown. In the ε_{yy} vs. q and p' vs. q space the PST graphs from all laboratory data and the representative test both overestimate and underestimate the peak deviator stress in comparison with the measured laboratory data for the different consolidation stresses, only for the second consolidation stress the peak deviatoric stress is well estimated. The maximum excess pore water pressures are only quite well estimated for the second consolidation stress by both simulated graphs compared to measured laboratory data. In general, the resulting simulated graphs from PST are quite similar. The optimized parameter set yields the best fit for the highest consolidation stress, where the maximum deviatoric stress corresponds well with the maximum deviatoric stress from measured laboratory results and the stiffness (steepness of graph graph) is reduced. The unloading-reloading stiffness parameter, κ^*, affects the steepness of the graph.

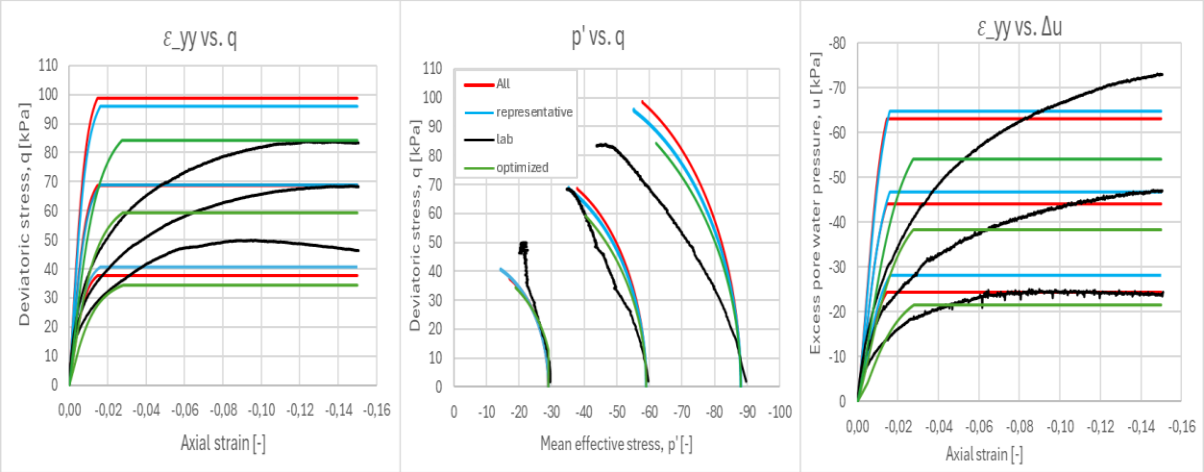

Figure 4.3. PST simulation and laboratory resulting graphs for SS on Geulopvulling (all = all laboratory results; representative = representative test; lab data = measured in laboratory)

Sekiguchi-Ohta model

In Table 4.4 the coefficient of lateral earth pressure for the optimized parameters has a quite high value and is not related to the internal friction angle (Jaky).

Table 4.4. Sekiguchi-Otha model parameters Geulopvulling.

Sekiguchi-Ohta					
	K_0^{NC} [-]	λ^* [-]	κ^* [-]	v_{ur} [-]	M_{CSL} [-]
All laboratory results	0.40	0.088	0.0175	0.2	1.50
Representative test	0.45	0.11	0.02	0.2	1.35
Optimized	0.77*	0.088	0.025	0.2	1.50

*Not related to ϕ' by Jaky's formulation; freely chosen in PST

In Figure 4.4 the simulated PST graphs (Sekiguchi-Ohta) and graphs from measured laboratory data are shown. In the ε_{yy} vs. q and p' vs. q space the resulting simulation graphs from the Sekiguchi-Ohta model give highly deviating results compared to the measured laboratory data, showing very high peak deviatoric stresses and suggesting over-consolidated behavior in the p'-q and Δu - ε_{yy} space. The deviating simulated graphs may be the result of the model parameters coming from isotropic consolidated soil material, whereas the Sekiguchi-Ohta model has been pioneered and tested for anisotropic consolidated material, and/or from the fact that this model is aimed at Japanese clayey soil, which differs in composition and soil properties from Dutch clayey soils.

By maintaining a high K_0^{NC} and increasing κ^* in the optimized parameter set, there is a strong improvement in the progression of the graphs. The maximum deviatoric stress corresponds to that of measured laboratory data, the stiffness of the material is reduced, and normal consolidated behavior is observed in the graphs.

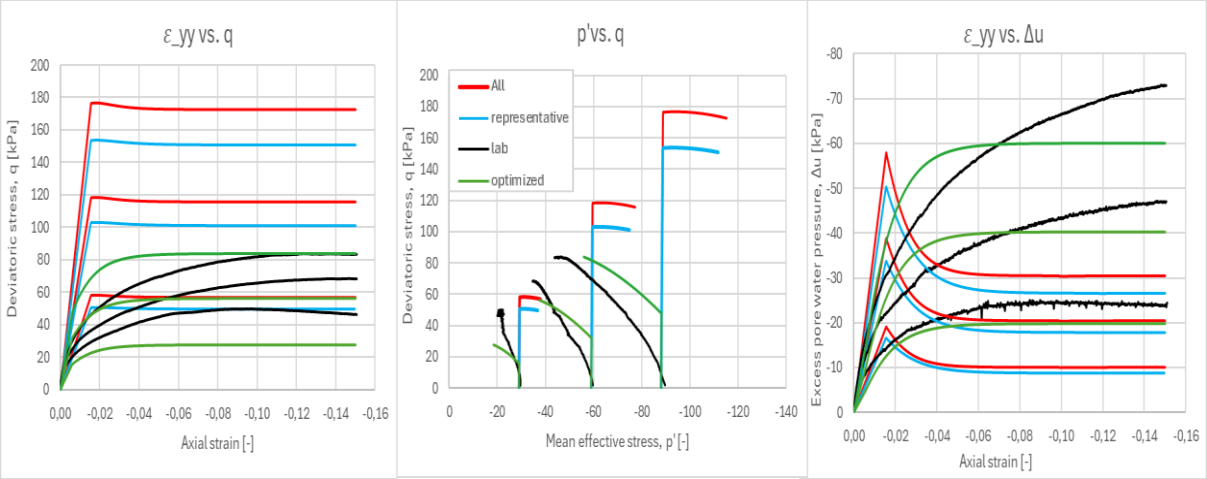

Figure 4.4. PST simulation and laboratory resulting graphs for SO on Geulopvulling (all = all laboratory results; representative = representative test; lab data = measured in laboratory)

S-Clay1 model

In Table 4.5 there is a small difference in the stiffness and in the anisotropy parameters as well between model parameters obtained from all laboratory results and the representative test.

Table 4.5. S-Clay1 model parameters Geulopvulling.

S-Clay1									
	λ^* [-]	κ^* [-]	K_0^{NC} [-]	M_c [-]	M_e [-]	v [-]	α_0 [-]	ω [-]	ω_d [-]
All laboratory results	0.088	0.0175	0.40	1.50	1.07	0.2	0.0	22	1.0
Representative test	0.11	0.02	0.45	1.35	0.93	0.2	0.0	22	0.91
Optimized	0.088	0.0175	0.60*	1.20*	0.70*	0.2	0.0	22	1.0

$*$ M_c, M_e, and K_0^{NC} **NOT** based on ϕ'; $\mu^* = \lambda^*/20$

In Figure 4.5 the simulated graphs obtained from PST (S-Clay1) and measured laboratory data are shown. In the ε_{yy} vs. q and p' vs. q space both simulated graphs have difficulty to correctly estimate the peak deviatoric stress for all three consolidation stresses. Depending on the consolidation stress the simulated graphs either underestimate or overestimate the maximum deviatoric stress. Only for the second consolidation stress, the simulated graphs from all laboratory data correspond to measured laboratory data for the maximum deviatoric stress. The excess pore water pressure is underestimated by both simulated graphs from all laboratory results and the representative test data compared to measured laboratory results. Furthermore, over-consolidated behavior is predicted with this model as well.

The optimized parameter set only improves the q - ε_{yy} graph for the highest consolidation stress. The over-consolidated behavior depends heavily on the value for the initial anisotropy, α_0, which is now set to zero.

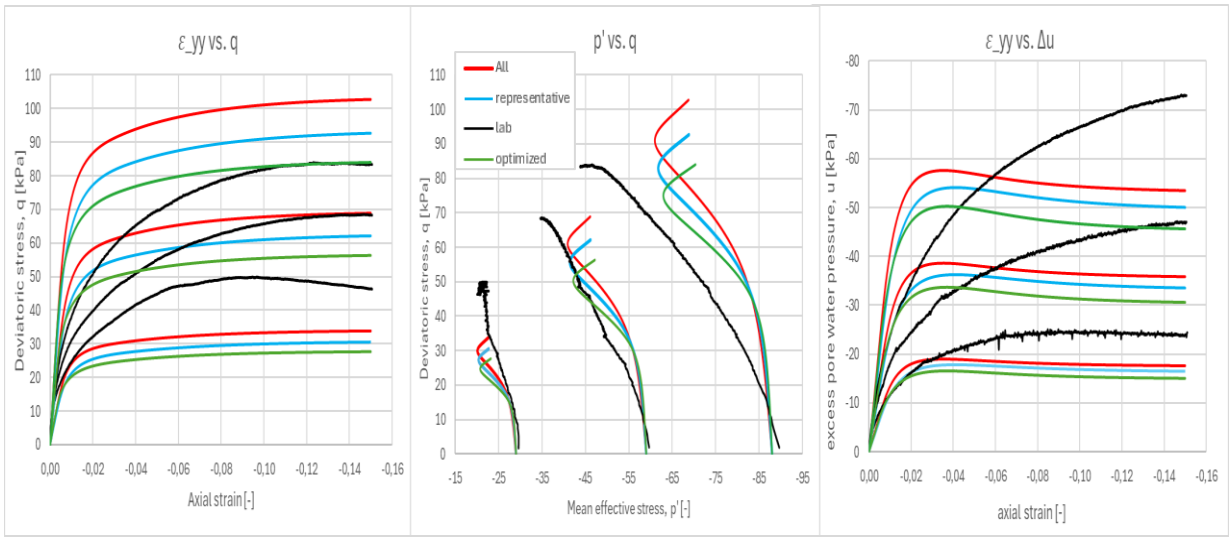

Figure 4.5. PST simulation and laboratory resulting graphs for S-Clay1 on Geulopvulling (all = all laboratory results; representative = representative test; lab data = measured in laboratory)

Figure 4.6 illustrates the behavior of the material according to PST when there is no incorporation of the rotational yield curve and plastic anisotropy by setting ω equal to zero. The S-Clay1 model is identical to the Modified Cam-Clay model in this state. The S-Clay1 model with anisotropy completely switched off is not further discussed as another isotropic model is not the purpose of this study. Normally consolidated behavior is observed instead of over-consolidated behavior.

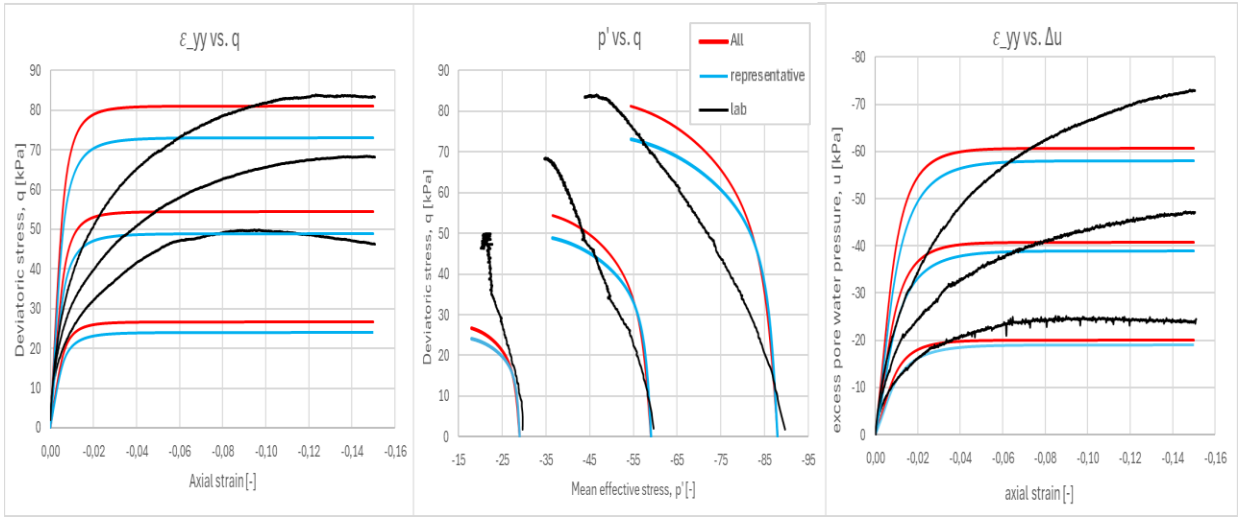

Figure 4.6. PST simulation and laboratory resulting graphs for S-Clay1 on Geulopvulling with complete isotropic behavior

All the material models have difficulty in providing consistent predictions for the Geulopvulling on the course of the graphs for all three consolidation stresses. It should be considered that the heterogeneity of Geulopvulling leads to variability in laboratory test results for different consolidation stresses. Furthermore, it is difficult as well to get good fits in both the q - ε_{yy} space and Δu - ε_{yy} space with the same parameter set.

4.1.3 Oude zeeklei model parameters

For Oude zeeklei all laboratory results consist of 24 triaxial tests. The representative test results (3 triaxial tests; 1 sample) (m009-a2, m009-a3, m009-a4) are chosen based on the course of the graph in the axial strain vs. deviatoric stress space (see Attachment figure B.1, yellow lines), but as well that the strength parameters (c', ϕ') obtained through linear regression on all laboratory results are approximately equal to the strength parameters from the representative test obtained by the tangent to the three Mohr circles.

The modified stiffness parameters (Attachment table B.3) for all laboratory results are obtained from a total of six oedometer tests and the representative test parameters come from sample M009-a1.

In Table 4.6 to Table 4.9 the model parameters on Oude zeeklei are shown. Expected values (mean) are used for the strength and stiffness parameters.

Hardening Soil Small Strain model

In Table 4.6 the stiffness parameters for the representative test are much higher than the stiffness parameters obtained from all laboratory results. Despite this large difference in parameter values, the PST graphs look similar. The reference oedometer stiffness has been strongly increased to meet the input requirement of PST, as a result of which this model parameter does not correspond to the laboratory results.

Table 4.6. Hardening Soil small strain model parameters Oude zeeklei.

Hardening Soil Small Strain											
	c' [kPa]	ψ [°]	ϕ' [°]	K_0^{nc} [-]	E_{50}^{ref} [kPa]	E_{oed}^{ref} [kPa]	E_{ur}^{ref} [kPa]	$\gamma_{0.7}$ 10^{-4}[-]	G_0^{ref} [kPa]	m [-]	v_{ur} [-]
All laboratory results (24)	1.6	0	34.8	0.43	14721	1467→6700	39747	4.5	27800	0.71	0.2
Representative test (3)	4	0	33	0.46	41000	1000→17000	111000	5.0	47000	1.0	0.2
Optimized	2.0	0	30	0.52	14721	6700	32000	4.5	27800	0.9	0.2

Laboratory result → PST requirement

In Figure 4.7 the graphs obtained from soil test (Hardening Soil small strain) and measured laboratory data are shown.

In the ε_{yy} vs. q and p' vs. q space the simulated graphs of all laboratory data and the representative test both overestimate and underestimate the peak deviatoric stress in comparison with the measured laboratory data for the different consolidation stresses, but the difference between the simulated graphs is minimal. The peak excess pore water pressures are underestimated for all consolidation stresses by both the simulated graphs of all laboratory data, and the representative test compared to measured laboratory data. In general, the resulting graphs from PST are similar.

With the optimized parameter set, the best fit is achieved for the two highest consolidation stresses, where the maximum deviatoric stress corresponds well with the maximum deviatoric stress from measured laboratory results and the stiffness (steepness graph) is reduced in the q - ε_{yy} space. The stiffness dependent parameter, m, has a great influence on the steepness of the graph.

The maximum excess pore water pressures are further reduced with the optimized parameter set.

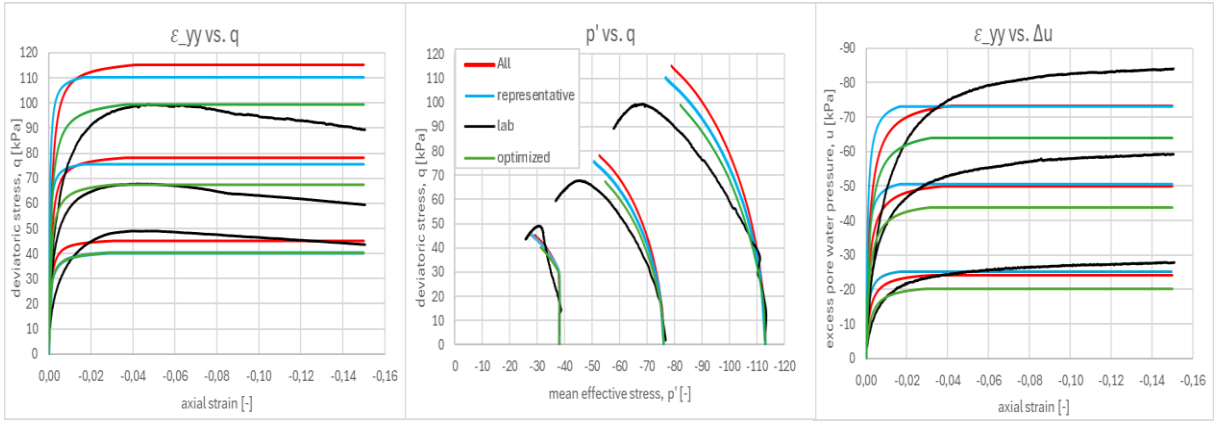

Figure 4.7. PST simulation and laboratory resulting graphs for HSss on Oude zeeklei (all = all laboratory results; representative = representative test; lab data = measured in laboratory)

Soft Soil model

In Table 4.7 there is almost no difference in the parameter values between all laboratory results and the representative test.

Table 4.7. Soft Soil model parameters Oude zeeklei.

Soft Soil							
	c' [kPa]	ψ [°]	ϕ' [°]	K_0^{nc} [-]	λ^* [-]	κ* [-]	ν_{ur} [-]
All laboratory results	1.6	0	34.8	0.43	0.073	0.005	0.2
Representative test	4.0	0	33	0.46	0.087	0.005	0.2
Optimized	2.0	0	30.5	0.49	0.073	0.015	0.2

From Figure 4.8, the maximum deviatoric stresses are slightly overestimated and the peak excess pore water pressures are underestimated. The optimized parameter set yields the best fit for the two highest consolidation stresses, where the maximum deviatoric stress corresponds well with the maximum deviatoric stress from measured laboratory results and the stiffness (steepness of graph graph) is reduced. The unloading-reloading stiffness parameter, κ^*, affects the steepness of the graph.

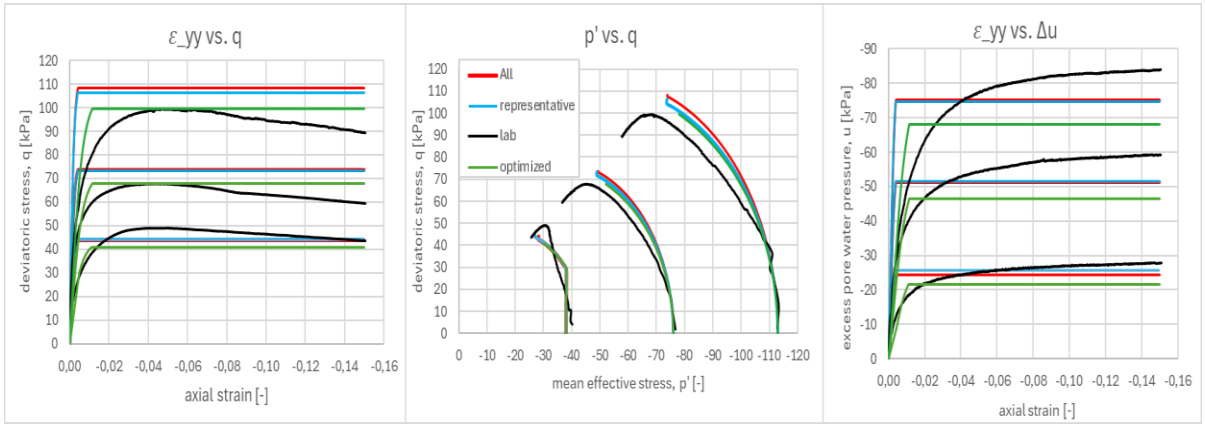

Figure 4.8. PST simulation and laboratory resulting graphs for SS on Oude zeeklei (all = all laboratory results; representative = representative test; lab data = measured in laboratory)

Sekiguchi-Ohta model

Similar to the Geulopvulling, the coefficient of lateral earth pressure for the optimized parameters in Table 4.8 is much higher and not related to the internal friction angle (Jaky).

Table 4.8. Sekiguchi Otha model parameters Oude zeeklei.

Sekiguchi-Ohta					
	K_0^{NC} [-]	λ^* [-]	κ^* [-]	v_{ur} [-]	M_{CSL} [-]
All laboratory results	0.43	0.073	0.005	0.2	1.41
Representative test	0.46	0.087	0.005	0.2	1.33
Optimized	0.77*	0.073	0.018	0.2	1.41

*Not related to ϕ' by Jaky's formulation

In the case of Oude zeeklei, the Sekiguchi-Ohta model gives a large overestimation of the deviatoric stress, over-consolidated behavior takes place, which is noticeable in the excess pore water pressure development as well. By maintaining a high K_0^{NC} and increasing κ^* in the optimized parameter set, there is a strong improvement in the progression of the graphs. The maximum deviatoric stress corresponds to that of measured laboratory data, the stiffness of the material is reduced, and normal consolidated behavior is observed in the graphs.

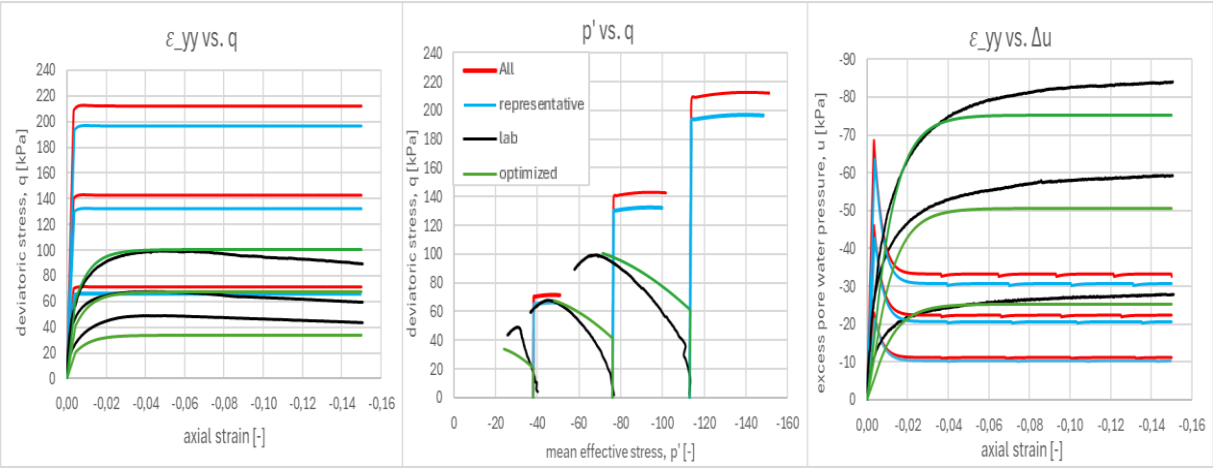

Figure 4.9. PST simulation and laboratory resulting graphs for SO on Oude zeeklei (all = all laboratory results; representative = representative test; lab data = measured in laboratory)

S-Clay1 model

In Table 4.9, there is a small difference in the model parameters obtained from all laboratory results and the representative test.

Table 4.9. S-Clay1 model parameters Oude zeeklei.

S-Clay1									
	λ^* [-]	κ^* [-]	K_0^{NC} [-]	M_c [-]	M_e [-]	v [-]	α_0 [-]	ω [-]	ω_d [-]
All laboratory results	0.073	0.005	0.43	1.41	0.96	0.2	0.0	37.5	0.62
Representative test	0.087	0.005	0.46	1.33	0.92	0.2	0.0	34	0.89
Optimized	0.073	0.015	0.65	0.80	0.70	0.2	0.0	37.5	1.0

∗ M_c, M_e, and K_0^{nc} **NOT** based on ϕ'; μ* = λ*/20

In the ε_{yy} vs. q and p' vs. q space (Figure 4.10) both simulated graphs overestimate the measured laboratory maximum deviatoric stress by far for the two highest consolidation stresses. For the lowest consolidation stress the simulated graphs give a good estimation of the maximum deviatoric stress in relation to the measured laboratory results. The excess pore water pressures are underestimated by both simulated graphs from all laboratory results and the representative test data compared to measured laboratory results. Furthermore, over-consolidated behavior is predicted with this model just as is the case for Geulopvulling.

The optimized parameter set only improves the q - ε_{yy} graphs for the two highest consolidation stresses. Overconsolidated behavior is still predicted with the optimized parameter set. The over-consolidated behavior depends heavily on the value for α_0 which is now set to zero (isotropic).

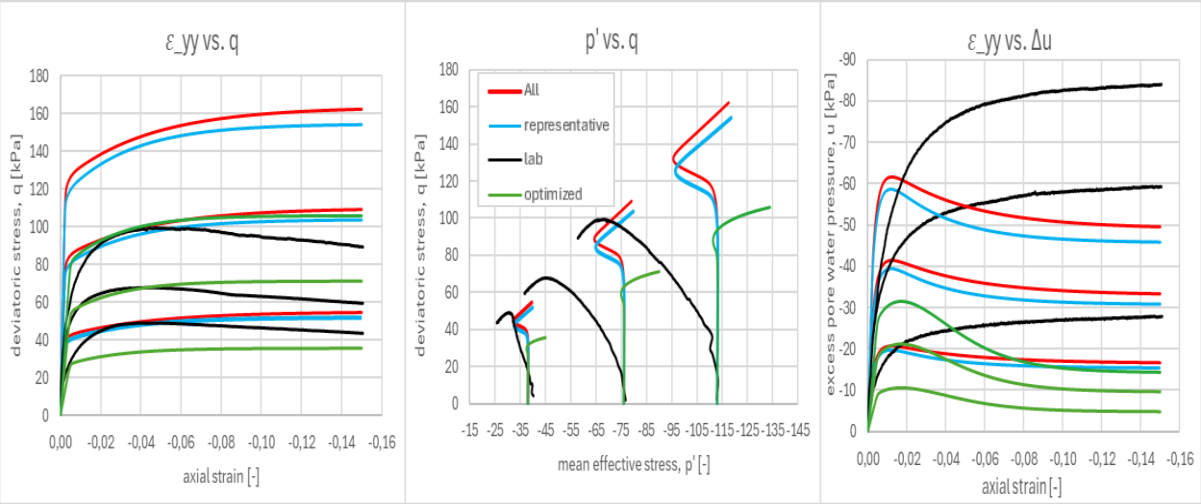

Figure 4.10. PST simulation and laboratory resulting graphs for S-Clay1 on Oude zeeklei (all = all laboratory results; representative = representative test; lab data = measured in laboratory)

4.1.4 Hollandveen model parameters

All laboratory results consist of 15 DSS tests. The representative test results (3 DSS tests) are samples M005-a1, M005-a2 and M005-a3 in Attachment table C.3. The modified stiffness parameters for all results are obtained from a total of 5 oedometer test results in Attachment table C.2, of which sample M005-a1 is used as representative test.

In the case of Hollandveen K_0 - consolidation is assumed in PST for the Sekiguchi-Ohta and the S-Clay1 model (Table 4.10). Horizontal stresses are not measured in the laboratory during the consolidation phase in a DSS-test, therefore K_0 - consolidation is assumed. K_0 – consolidation is enhanced in PST until a satisfying fit to the measured laboratory data is achieved. An improvement is observed in the graphs with this assumption for these models. However, the K_0 – consolidation value for the Sekiguchi-Ohta model is rather high for soft soils.

Table 4.10. K_0 – consolidation values Hollandveen

	K_0 – consolidation [-]
All laboratory results Sekiguchi-Ohta	0.76
All laboratory results S-Clay1	0.55
Representative test Sekiguchi-Ohta	0.85
Representative test S-Clay1	0.55

Hardening Soil small strain model

In Table 4.11 the E_{ur}^{ref} from the representative test is adjusted to a lower value to obtain a higher maximum for the deviatoric stress and E_{oed}^{ref} is increased.

Table 4.11. Hardening Soil small strain model parameters Hollandveen.

Hardening Soil Small Strain											
	c' [kPa]	ψ [°]	ϕ' [°]	K_0^{NC} [-]	E_{50}^{ref} [kPa]	E_{oed}^{ref} [kPa]	E_{ur}^{ref} [kPa]	$\gamma_{0.7}$ 10^{-4}[-]	G_0^{ref} [kPa]	m [-]	ν_{ur} [-]
All laboratory results	2	0	37.3	0.39	1693	565	5900	8.1	5900	0.83	0.2
Representative test	3.3	0	31.2	0.48	2000	545→800	7100→4000	9.0	4000	1.0	0.2
Optimized	3.5	0	37.3	0.39	1500	750	3000	8.1	3000	0.90	0.2

In the shear strain vs. shear stress space and the total effective stress vs. shear stress space the PST graphs from all laboratory data give a better prediction for the maximum deviatoric stress, as well as the maximum excess pore water pressures. With the optimized parameter set, the graphs from measured lab data are approximated very nicely with the simulated graphs for all three consolidation stresses, except for the excess pore water pressures.

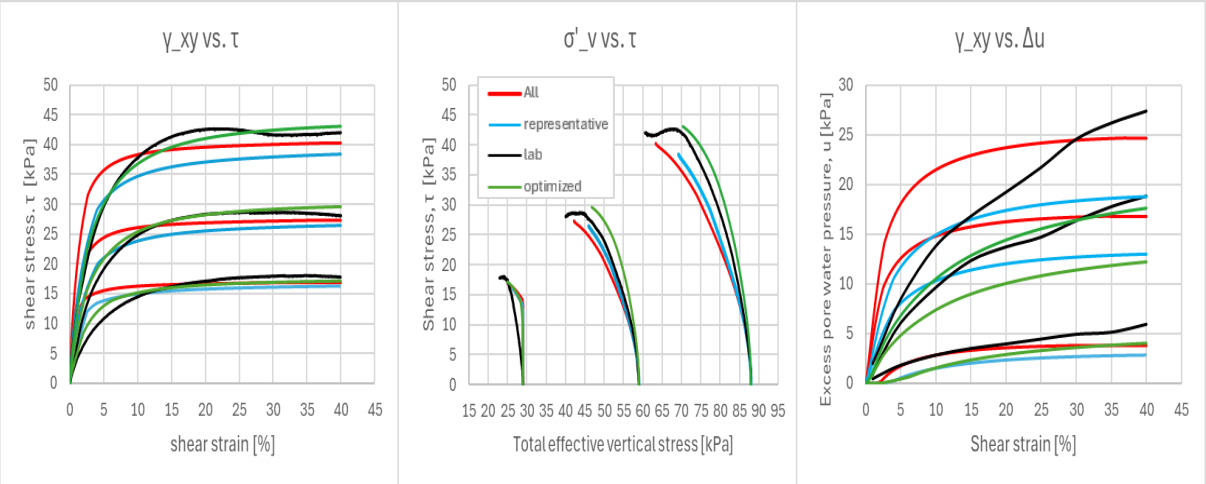

Figure 4.11. PST simulation and laboratory resulting graphs for HSss on Hollandveen (all = all laboratory results; representative = representative test; lab data = measured in laboratory)

Soft Soil model

In Table 4.12 the Soft Soil model parameters for Hollandveen are given. A rather high value for the effective internal friction angle is found from linear regression over all laboratory results.

Table 4.12. Soft Soil model parameters Hollandveen.

Soft Soil							
	c' [kPa]	ψ [°]	ϕ' [°]	K_0^{NC} [-]	λ^* [-]	κ* [-]	ν_{ur} [-]
All laboratory results	2	0	37.3	0.39	0.1758	0.021	0.2
Representative test	3.3	0	31.2	0.48	0.21	0.042	0.2
Optimized	2	0	35	0.43	0.20	0.070	0.2

The PST graphs for all laboratory results give accurate predictions for the maximum deviatoric stresses for the three consolidation stresses. The representative test underestimates the maximum deviatoric stresses, except for the lowest consolidation stress. The excess pore water pressures are underestimated by all three PST graphs of all laboratory data, the representative test and optimized parameter set. With the optimized parameter set improvements have mainly been made in the stiffness of the material.

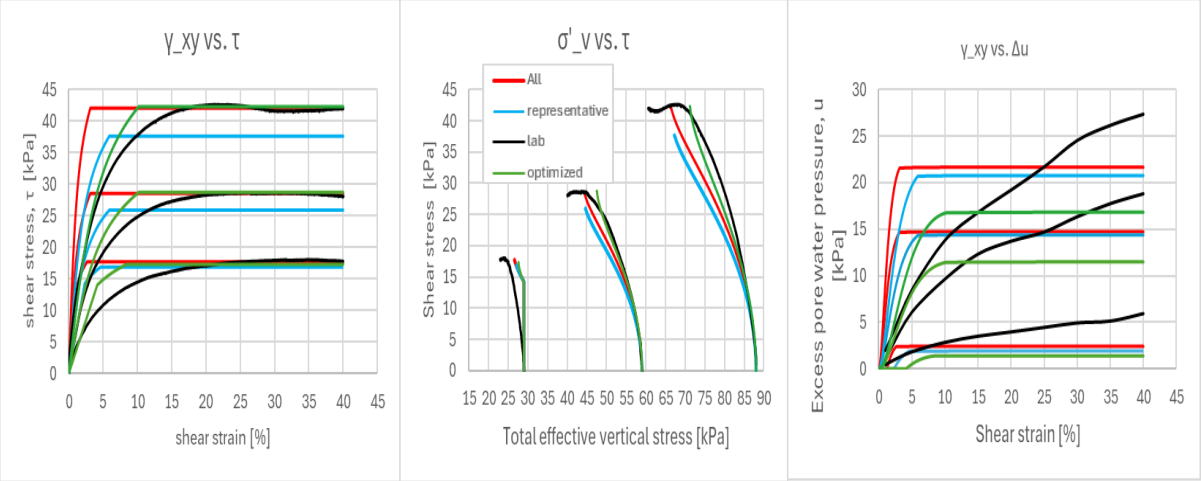

Figure 4.12. PST simulation and laboratory resulting graphs for SS on Hollandveen (all = all laboratory results; representative = representative test; lab data = measured in laboratory)

Sekiguchi-Ohta model

In Table 4.13 the K_0^{NC} value does not become as high as is the case for Geulopvulling and Oude zeeklei for the optimized parameters, with the incorporation of K_0 – consolidation.

Table 4.13. Sekiguchi Otha model parameters Hollandveen.

Sekiguchi-Ohta					
	K_0^{NC} [-]	λ^* [-]	κ^* [-]	v_{ur} [-]	M_{CSL} [-]
All laboratory results	0.39	0.1758	0.021	0.2	1.62
Representative test	0.48	0.21	0.042	0.2	1.25
Optimized Plaxis	0.45*	0.21	0.055	0.2	1.62

*Not related to ϕ' by Jaky's formulation

From a K_0 – consolidation value greater than 0.85, over-consolidated behavior occurs in PST simulation with the representative model parameters. Therefore, the maximum deviatoric stress for the representative test is lower than the maximum of the measured laboratory data for all three consolidation stresses (Figure 4.13). The maximum excess pore water pressures are greatly underestimated by both the representative test and all laboratory data. The PST graphs for all laboratory data give a good estimate of the maximum deviatoric stress for the two highest consolidation stresses.

Over-consolidated behavior is not observed with this model in case of K0-consolidation and a lower value for K_0^{NC} can be used in the optimized parameter set. The stiffness parameters are slightly enhanced for a better progression of stiffness in the simulated graphs.

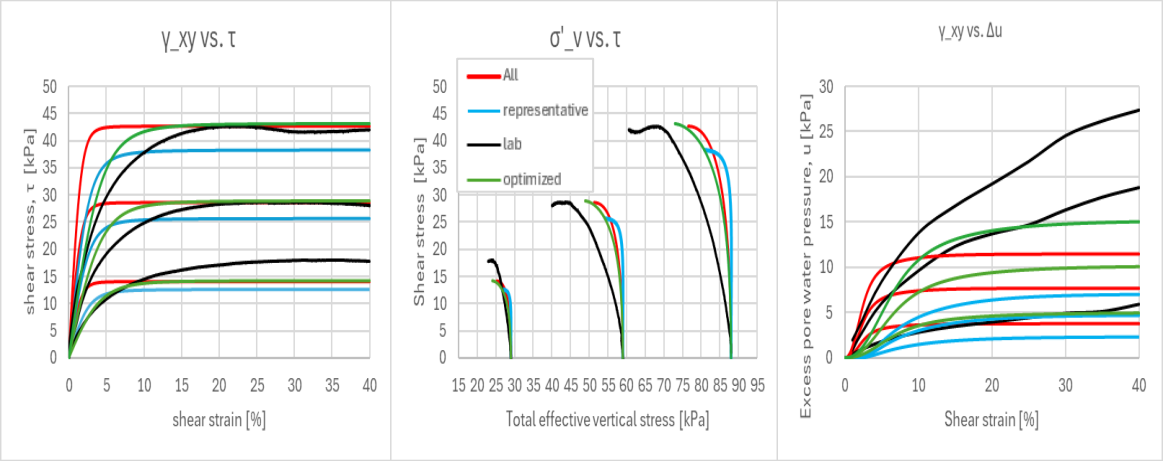

Figure 4.13. Soil test simulation and laboratory resulting graphs for S-O on Hollandveen (all = all laboratory results; representative = representative test; lab data = measured in laboratory)

S-Clay1 model

In Table 4.14 the S-Clay1 model parameters for Hollandveen are given.

Table 4.14. S-Clay1 model parameters Hollandveen.

S-Clay1									
	λ^* [-]	κ^* [-]	K_0^{NC} [-]	M_c [-]	M_e [-]	ν [-]	α_0 [-]	ω [-]	ω_d [-]
All laboratory results	0.1758	0.021	0.39	1.62	1.02	0.2	0.59	17	1.0
Representative test	0.21	0.042	0.48	1.25	0.88	0.2	0.48	17	0.82
Optimized	0.1758	0.06	0.52*	1.20	0.87	0.2	0.59	17	1.0

$*$ M_c, M_e, and K_0^{NC} based on ϕ'= 31.0°; $\mu^* = \lambda^*/20$

In Figure 4.14 both the PST graphs from all laboratory data and the representative test give good predictions of the peak deviatoric stresses, but in the total effective stress vs. shear stress space the graphs from all laboratory data yield a better progression. The excess pore water pressures are better approximated by the PST graphs for all laboratory data. Over-consolidated behavior is not observed with this model as well in the case of K0-consolidation, with anisotropy parameter, α_0, related to K_0^{NC}.

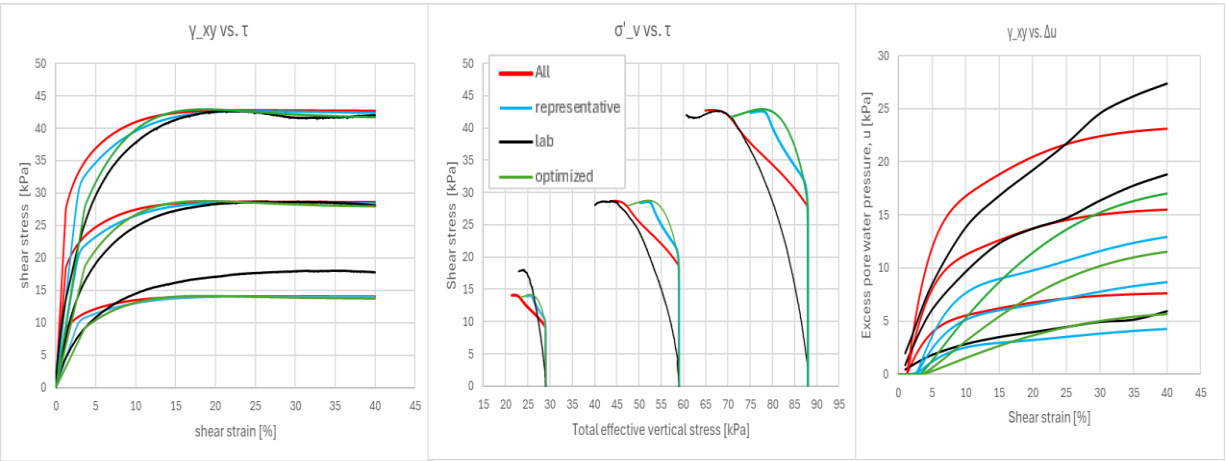

Figure 4.14. PST simulation and laboratory resulting graphs for S-Clay1 on Hollandveen (all = all laboratory results; representative = representative test; lab data = measured in laboratory)

4.2 Comparison of PST simulated Graphs for all Material Models

In this Section resulting PST graphs of all material models are compared and examined with regard to the measured laboratory data. The resulting PST graphs with HSss and SS model parameters from TAK 3.2 are included as well.

In Table 4.15 and Table 4.16 the TAK 3.2 model parameters are given, which are used for simulations as well, to make a comparison between the model parameters gathered in this study for the HSss and SS model. It is unknown at what strain levels the Hardening Soil small strain parameters in TAK 3.2 have been determined. The Soft Soil parameters in TAK 3.2 are determined at maximum strengths.

Table 4.15. TAK 3.2 Hardening Soil Small Strain model characteristic parameters for Plaxis 2D (2% axial strain Triaxial test; 8% shear strain DSS-test)

Soil layer	γ_{wet} [kN/m^3]	γ_{dry} [kN/m^3]	c' [kPa]	ψ [°]	ϕ' [°]	E_{50}^{ref} [kPa]	E_{oed}^{ref} [kPa]	E_{ur}^{ref} [kPa]	$\gamma_{0.7}$ 10^{-4}[-]	G_0^{ref} [kPa]	m [-]
GO	13.9	13.9	7.1	0	20	4284	2200	15000	2.0	15000	0.8
HV	10.5	10.5	3.6	0	18	2000	1085	7000	2.0	7000	0.8
OZ	16.5	16.5	5.0	0	26	7500	3780	20000	2.0	47000	0.8

The strength parameters in Table 4.16 are not dependent on the model and can be used for the Hardening Soil small strain model as well (Neijzing, Cherkaoui, Pijpers, & Wesstein, 2023).

Table 4.16. TAK 3.2 Soft Soil model characteristic parameters for Plaxis 2D

Soil layer	γ_{wet} [kN/m^3]	γ_{dry} [kN/m^3]	c' [kPa]	ϕ' [°]	λ^* [-]	κ^* [-]
HV	10.4	10.4	3.1	32.8	0.256	0.081
OZ	16.6	16.6	1.6	35.5	0.121	0.023

4.2.1 Simulations Geulopvulling

Figure 4.15 shows the PST and measured laboratory resulting graphs for the highest consolidation stress. As previously noted, the Sekiguchi- Otha model gives deviating results. The S-Clay1, the HSss and SS model give an overestimation of the maximum deviatoric stress. The model parameters for the HSss model from TAK 3.2 underestimate the maximum deviatoric stress from measured laboratory results. In the p' vs. q space the S-Clay1 and Sekiguchi-Ohta model predict over-consolidated behavior, with the S-Clay1 model having a better progression.

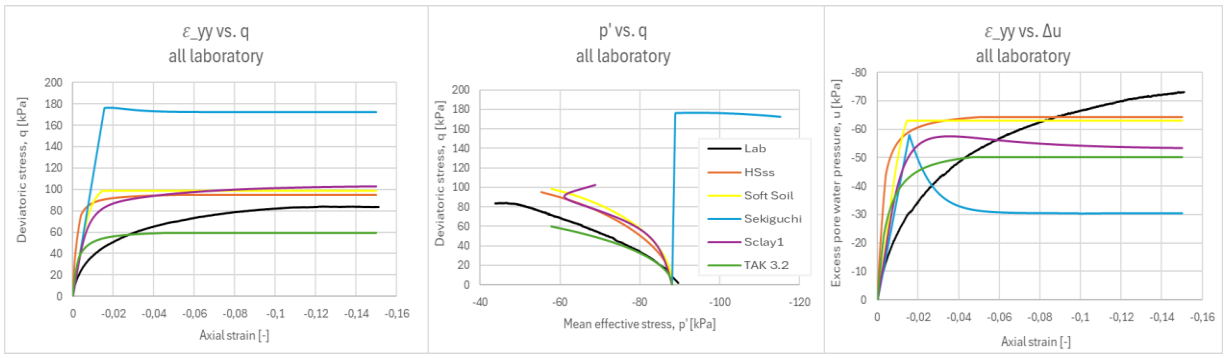

Figure 4.15. All laboratory data model parameters resulting PST and measured laboratory graphs Geulopvulling

With the optimized parameters there is a good estimate of the maximum deviatoric stress and the Sekiguchi- Otha model has been greatly improved (Figure 4.16). It is difficult to get both good estimates with PST on the maximum deviatoric stress and maximum excess pore water pressure with one set of model parameters. The maximum excess pore water pressures are best approximated with the Sekiguchi-Ohta and HSss model.

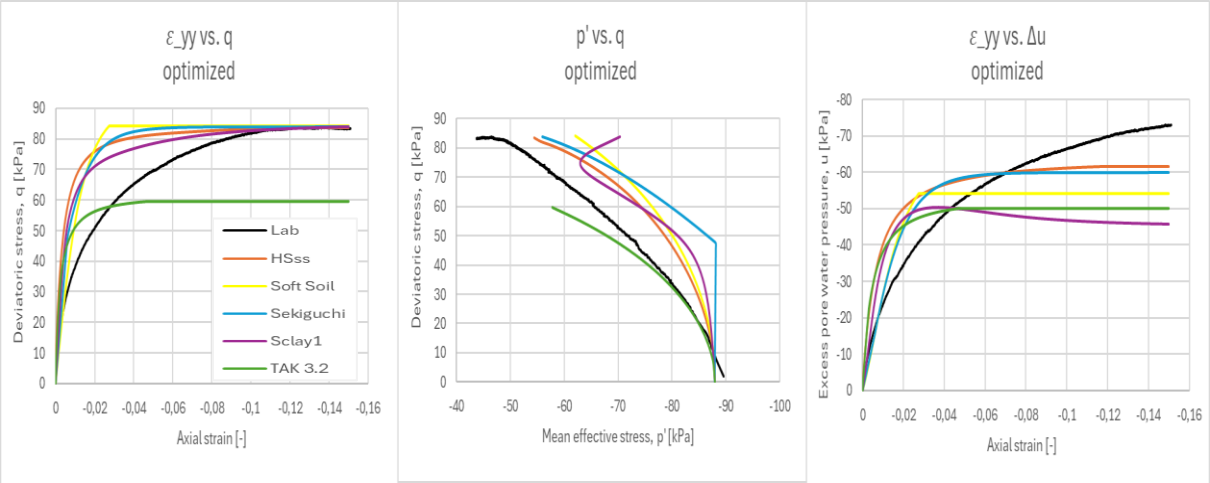

Figure 4.16. Optimized model parameters resulting PST and measured laboratory graphs Geulopvulling

4.2.2 Simulations Oude zeeklei

Figure 4.17 shows the PST and measured laboratory resulting graphs. In the case of Oude zeeklei it is noticeable as well that the Sekiguchi-Ohta model gives deviating predictions as well as the S-Clay1 model. With the model parameters from TAK 3.2 a good prediction is obtained on the progression of the graphs with an overestimation of the maximum deviatoric stress for TAK 3.2 HSss model. The model parameter set found in this study for the Soft Soil model and the parameter set for this model in TAK 3.2 differ from each other but yield approximately identical maximum deviatoric stresses with some difference noticeable in the stiffness of the graphs.

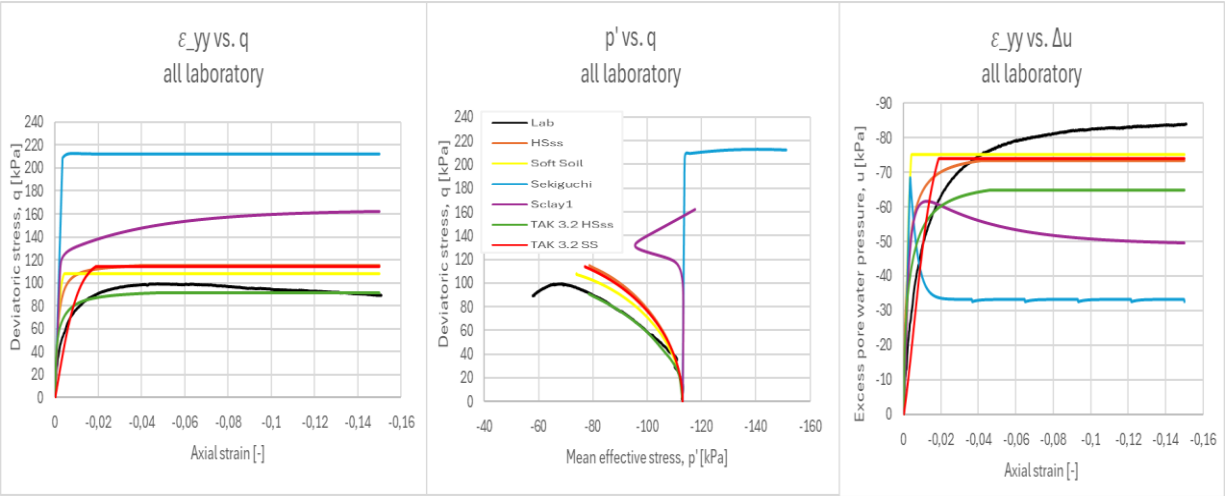

Figure 4.17. All laboratory data model parameters resulting PST and measured laboratory graphs Oude zeeklei

With the optimized parameters a good fit is found for the Sekiguchi-Ohta model, but at the cost of a rather high K_0^{NC}. The Sekiguchi-Ohta model gives the best approximation for both the maximum deviatoric stress and the maximum excess pore water pressure. The S-Clay1 model continues to predict over-consolidated behavior with the optimized parameter set.

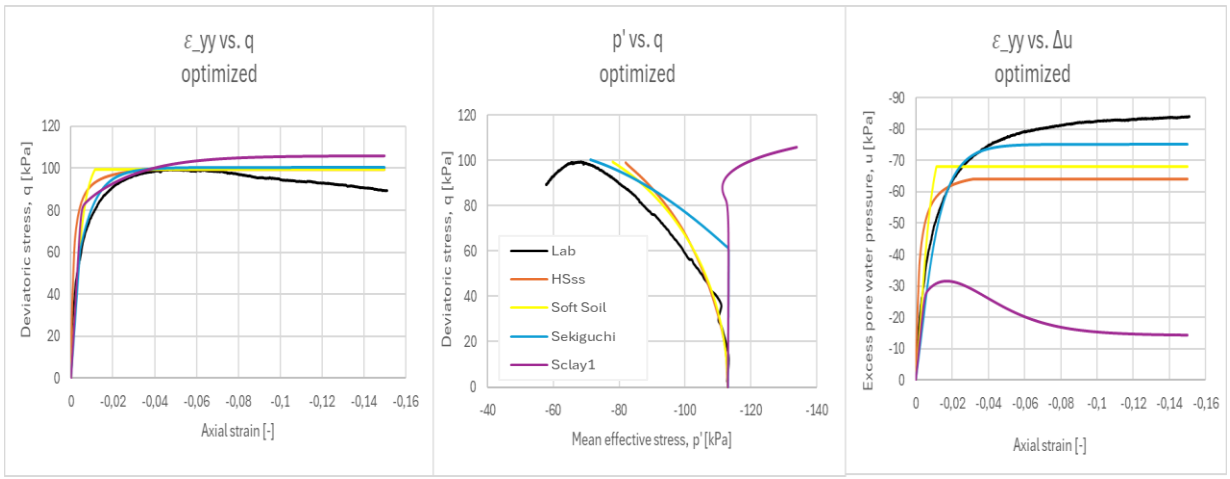

Figure 4.18. Optimized model parameters resulting PST and measured laboratory graphs Oude Zeeklei

4.2.3 Simulations Hollandveen

As previously noted, taking K_0 – consolidation into account for the DSS tests, a well fitted PST graph was obtained for the anisotropic material models, which can be seen in Figure 4.19. The isotropic models also provide a good fit to the graph from measured laboratory data, with the Soft Soil model giving the best prediction of the maximum deviatoric stress and the HSss model the best prediction for the maximum excess pore water pressure. The progress of the excess pore water pressure from measured laboratory data is quite deviating. The model parameters from TAK 3.2 for the SS model make a fairly good prediction of the course of the graph.

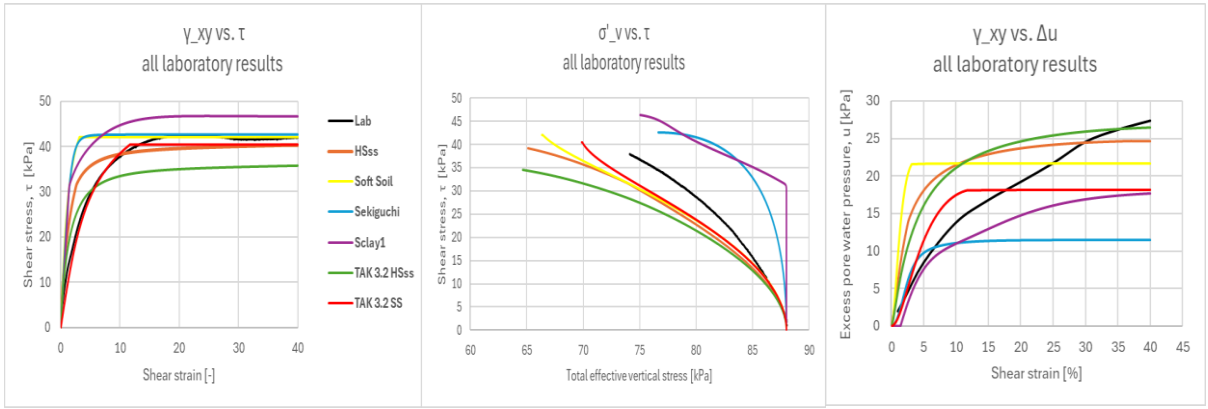

Figure 4.19. All laboratory data model parameters resulting PST and measured laboratory graphs Hollandveen

From Figure 4.20, with the optimized parameters a very nice fit is obtained in the shear strain vs. shear stress space and a slightly less good fit in the total effective stress vs. shear stress space. The maximum excess pore water pressure measured in the laboratory is far underestimated by all material models.

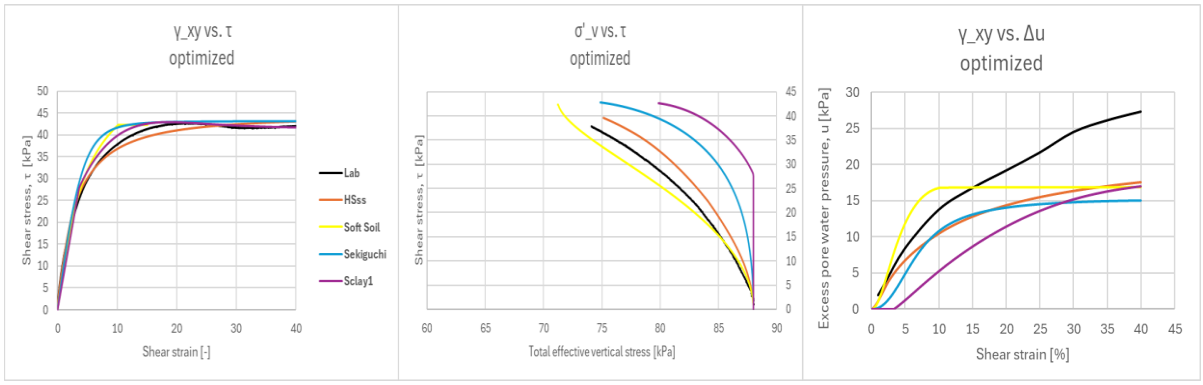

Figure 4.20. Optimized model parameters resulting PST and measured laboratory graphs Hollandveen

4.3 Sensitivity analysis on anisotropy parameters S-Clay1 model

Since there are no available anisotropically consolidated triaxial laboratory results and the S-Clay1 model with isotropic behavior ($\alpha_0 = 0$) gives undesirable predictions, it is examined how α_0 influences the results that the model gives.

The considered equations (Equation 3.5, Equation 3.6, and Equation 3.7) to estimate values for anisotropy parameters of the S-Clay1 model are all related to the normally consolidated earth pressure coefficient, K_0^{NC}, which again is approximated on the basis of the internal friction angle (Jaky's formulation). Therefore, the internal friction angle is the independent parameter and the measure for plastic anisotropy, α_0, and K_0^{NC} are dependent parameters. Parameter α_0 is considered, because it has the most influence on the angle of the yield contour in the p'- q space. Furthermore, α_0 is decisive in whether the model predicts normally consolidated or over-consolidated behavior, which is made clear in the following analysis as well.

Figure 4.21 shows how α_0 and K_0^{NC} change as the (critical state) internal friction angle, ϕ'_{cs}, is changed. Between ϕ'_{cs} and K_0^{NC} there is a negative correlation, whereas there is a positive correlation between ϕ'_{cs} and α_0.

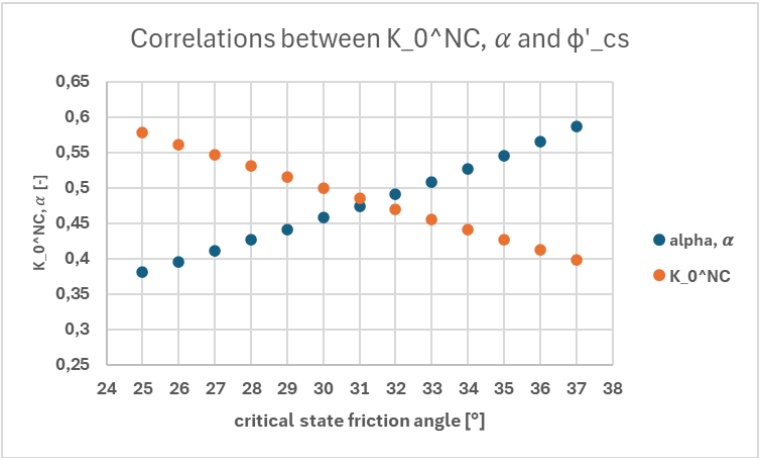

Figure 4.21. Visual representation of the relationship between K_0^{NC}, α_0 and ϕ'_{cs}

In Table 4.17 the anisotropy parameters that are changed for the sensitivity analysis are given. In the case where α_0 = 0, the material model yields isotropic behavior. The sensitivity in the maximum deviatoric stress and the excess pore water pressures is related to the critical state internal friction angle. ϕ'_{cs} is the input parameter and the maximum deviatoric stress and excess pore water pressure are the output parameters. Except where α_0 is changed from 0.586 to 0.0, α_0 is taken as the input parameter as it is not related to ϕ'_{cs} in that case.

The equation used for the sensitivity is the percentage change in output divided by the percentage change in input. ϕ'_{cs} is increased with 3 degrees for each step. The values of sensitivity for q_{max} are between 0.23 and 0.34 meaning that a percentage change between 0.23 and 0.34 in ϕ'_{cs} will result in a percentage change between 0.23 and 0.34 for q_{max}.

Table 4.17. S-Clay1 anisotropy parameter values for sensitivity analysis

ϕ'_{cs} [°]	K_0^{NC} [-]	M_c [-]	α_0 [-]	ω [-]	ω_d [-]	$\lvert q_{max} \rvert$ [kPa]	$\lvert \Delta u \rvert$ [kPa]	Sensitivity $\lvert q_{max} \rvert$	Sensitivity $\lvert \Delta u \rvert$	
25	0.577	0.98	0.381	37.64	0.488	128	63	0.26	0.13	
28	0.531	1.11	0.426	39.12	0.655	124	64	0.23	0.29	
31	0.485	1.24	0.473	40.20	0.807	121	66	0.34	0.16	
34	0.441	1.37	0.527	40.80	0.928	117	67	0.29	0.17	
37	0.398	1.51	0.586	40.81	1.0	114	68	0.32	0.21	
37	0.398	1.51	0.0	40.81	1.0	150	54	0.32	0.21	Isotropic

Figure 4.22 is the visual representation of what follows from the parameters of Table 4.17. For decreasing K_0^{NC} and increasing α_0, q_{max} decreases and the Δu increases. As α_0 decreases, over-consolidated behavior begins to occur.

From anisotropic behavior (purple graph) to isotropic behavior (green graph) there is a significant increase of almost 36 kPa in the maximum deviatoric stress and a decrease of 14 kPa in the maximum excess pore water pressure. Furthermore, there is a change from normal consolidated behavior to over-consolidated behavior.

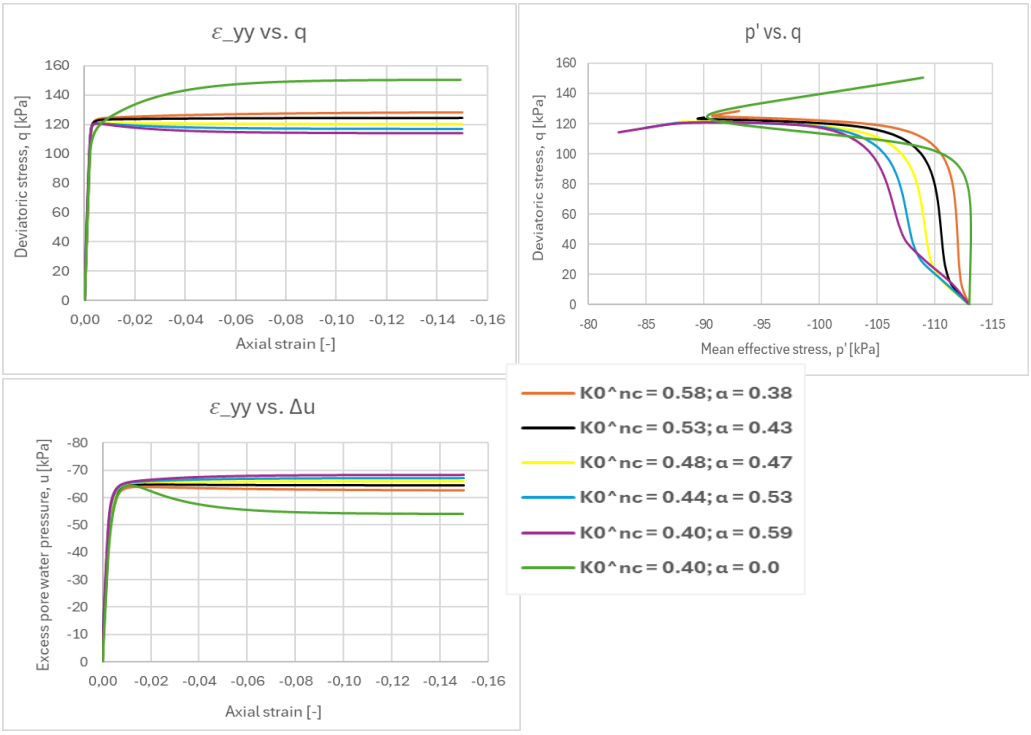

Figure 4.22. PST graphs S-Clay1 model for varying parameters in Table 4.17

4.4 Discussion and Conclusions on chapter 4

Discussion

There are some points of discussion to be raised regarding the model parameters and results, especially for the Hardening Soil small strain model. The unloading-reloading reference stiffness, E_{ur}^{ref}, is not directly obtained from laboratory data and is empirically approximated by multiplication with the secant stiffness, E_{50}^{ref}. However, varying the E_{ur}^{ref} parameter in PST has a significant influence on the maximum values of the deviatoric stress and the excess pore pressures and therefore it is interesting to find out to what extent E_{ur}^{ref} obtained from measured laboratory data leads to a good fit of the simulated graph to the graph from measured laboratory data. Furthermore, the oedometer stiffness, E_{oed}^{ref}, is initially obtained from measured laboratory data and yet strongly adjusted (increased) to meet the required ratio between the stiffness parameters in Plaxis 2D. Although it is not a 1-D settlement issue, this adjustment in E_{oed}^{ref} has influence on the deviatoric stress and can therefore lead to wrong impressions.

In the case of isotropically consolidated triaxial tests, the S-Clay1 model can be implemented by setting the initial yield surface, α_0, equal to zero. However, with an α_0 value determined with Equation 3.5, a much better fit is obtained for the parameter set of all laboratory data, the representative test and optimized, as can be seen in attachement E (E.4 and E.8) compared with Figure 4.5 and Figure 4.10, where α_0 is equal to zero. By setting the anisotropy rotational yield surface parameter (ω) equal to zero as well, overconsolidated behavior seen for Geulopvulling and Oude zeeklei changes into normally consolidated behavior in the p'-q space and in the excess pore water pressures vs axial strain graph. However, the S-Clay1 model is now turned into an isotropic model.

Finally, it is known that the samplers have been hammered, and it is known for samplers that are hammered into the subsurface can lead to sample disturbance and could influence the laboratory results (could be an explanation for the low stiffness behavior of the test results from the laboratory).

Conclusions

The Hardening Soil small strain and the Soft Soil model yield approximately identical graphs in PST, with the Hardening Soil small strain model giving a more realistic gradient (rounding) towards the maximum deviatoric stress in the q - ε_{yy} space.

Although no significant differences can be observed in general in the PST graphs for model parameter set with all laboratory data and the representative test, the parameter set of all laboratory data (all material models) is used for further analysis. The parameter set from all laboratory results is used because it is determined from multiple laboratory test results. Furthermore, the parameter set of the optimized parameters is considered as well for further analysis.

Due to the deviations from both the Sekiguchi-Ohta model and S-Clay1 model in the case of Geulopvulling and Oude zeeklei results, these models are not considered for these soil layers. The HSss and the SS model are considered for Geulopvulling and Oude zeeklei.

The Sekiguchi-Ohta model is not considered for Hollandveen either, because a quite high K0-consolidation value is required to deliver satisfying results. Thus, the S-Clay1 model is considered for Hollandveen in case of inclusion of anisotropy.

5. FEM-Calculations of Historic Quay Wall Herengracht

In this chapter sub-question 4 "*How do the structural forces in the wooden foundation piles differ, with the considered constitutive models, when applying the standard approach for historical quay wall assessment according to Toetskader Amsterdamse Kademuren 3.2 in Plaxis 2D?*" and sub-question 5 "*What is the influence of different ways of modelling the initial situation of an existing retaining wall in Plaxis 2D?"* are answered. First, background (technical) information is provided about the historic quay wall and the part of the quay wall chosen for this case study. Afterwards, only the phases from TAK 3.2 in the calculation of a historic quay wall in Plaxis 2D, considered in this research are explained. Furthermore, the structural forces on the wooden pile foundation are examined when using the considered material models, except for the Sekiguchi-Ohta model. To answer sub-question 5, a comparison between results in case of an initial situation according to the K_0-procedure or Gravity loading method is considered. Finally, a sensitivity analysis is carried out to gain more insights into the anisotropy behavior of the S-Clay1 model.

5.1 Description of The Historic Quay Wall Herengracht

The age of the quay wall is estimated at around 120 years. The quay wall (Figure 5.1) is located in the center of Amsterdam along the Herengracht and has a total length of 240 m. The quay is subdivided into 5 parts, of which part C is analyzed in this study.

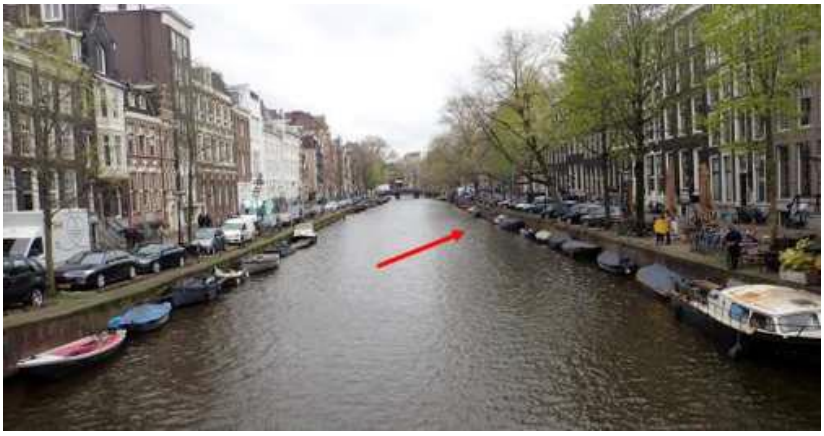

Figure 5.1. Historic Quay Wall located at the Herengracht, Amsterdam (Toetsing Amsterdamse Kademuren; Rapportage Technisch Advies Kademuur HEG0201, 2023)

The technical dimensions of the quay wall in Plaxis 2D are in accordance with Figure 5.2. Part C of the quay wall has a length of approximately 16 m and is constructed by a masonry wall above and under the waterline. From the top of the capstone to the waterline, the masonry wall has a height of 140 cm and extends another 54 cm below the waterline to a 20x7 cm (h x w) side wood (schuifhout).

The front side of the sliding beam extends 31 cm in front of the masonry and behind the sliding beam, a wooden floor (vloerhout) is constructed with a measurement of 5x25 cm (h x w). This whole of masonry wall, sliding beam and wooden floor rests on 18x22 cm (h x w) headstock (kesp) which extend 31 cm in front of the sliding beam. The headstock is founded on wooden foundation piles of 18 cm in diameter.

The first row of piles is 35 cm in front of the masonry and the second row of piles is 100 cm center to center in relation to the first row of piles. There is no wooden sheet pile screen (onderloopsheidscherm) constructed underneath the structure. The initial ground level lies 45 cm below the bottom of the pile cap and the bottom of the construction is located 129 cm below NAP.

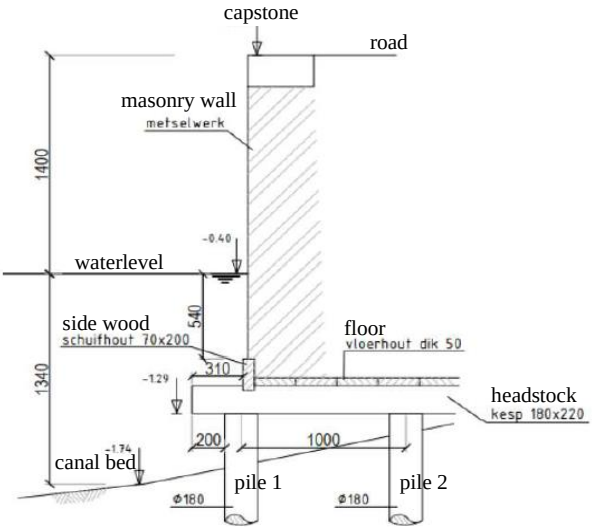

Figure 5.2. Typical cross-section of quay wall (Toetsing Amsterdamse Kademuren; Rapportage Technisch Advies Kademuur HEG0201, 2023)

5.2 TAK 3.2 Approach for Historic Quay Wall Assessment

Convenient about Plaxis 2D is the possibility to include multiple phases in the assessment of a quay wall. There are 36 phases in total (see attachment F), of which phase 0 to phase 10 are included in this study.

Phase 0: The initial phase in which the horizontal soil layers are still present and there is no quay wall and waterway yet. The initial phase can be applied with different methods (explained in Section 5.5), of which the K0-procedure is used to do calculations in Sections 5.3 and 5.4. Figure 5.3 (left) illustrates the situation in the initial phase.

Phase 1: As shown in Figure 5.3 (right), excavation of the canal takes place and elastoplastic drained analysis is considered, without inclusion of consolidation. After this phase displacements and small strain are resetted to zero.

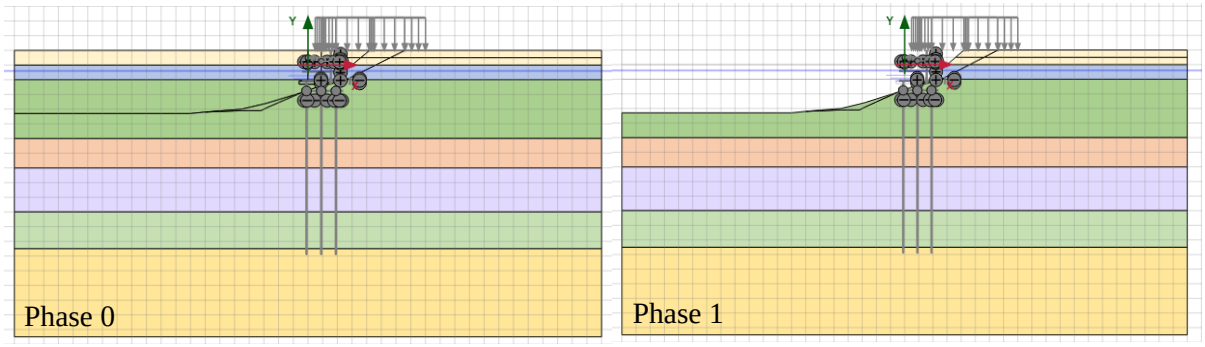

Figure 5.3. Phase 1 "initial phase" and phase 2 "excavation of canal" in FEM-calculation for the assessment of historic quay walls

Phase 2 and 3: In phase 2 drying of the construction pit near the quay wall up to approximately 0.5 m below the wooden floor takes place (Figure 5.4 left), whereafter the construction pit is further excavated in phase 3 (Figure 5.4 right).

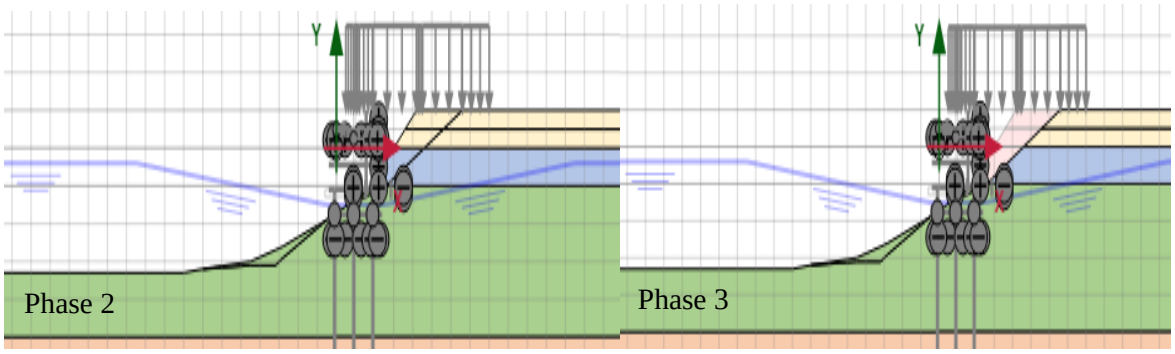

Figure 5.4. Phase 2 and phase 3 working on the construction pit near the quay wall

Phase 4 and 5: In phase 4 the wooden foundation piles are installed, with pile tips in the first sand layer (Figure 5.5 left) and in phase 5 construction of the other parts of the quay wall as explained in the cross-section of Figure 5.2 takes place (Figure 5.5 right).

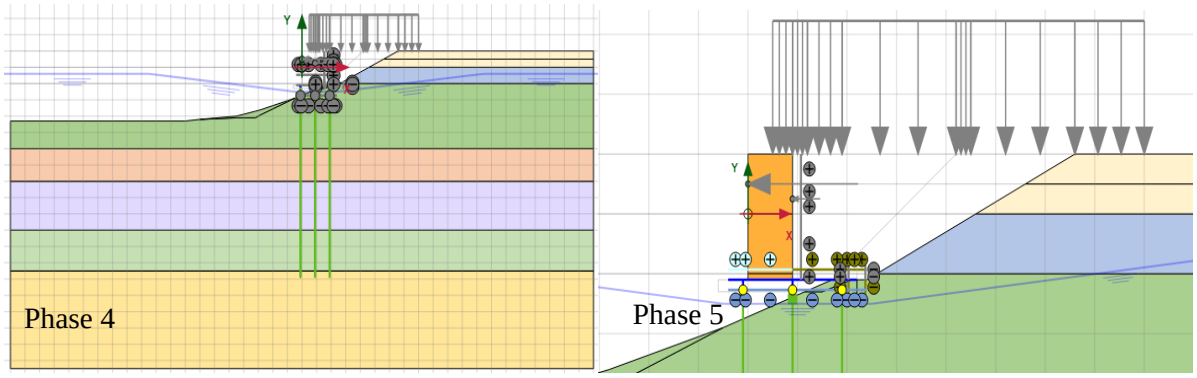

Figure 5.5. Phase 4 and phase 5 construction of the quay wall and load-bearing construction parts

Phase 6 and 7: In phase 6 the excavation behind the quay wall is backfilled with sand and a paving layer is applied. In phase 7 the water level is brought back to its initial level (Figure 5.6).

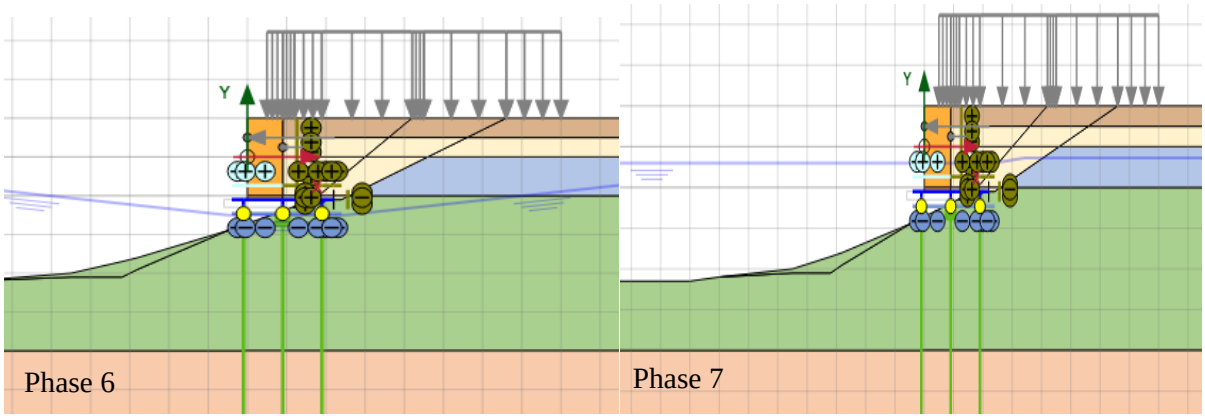

Figure 5.6. Phase 6 and phase 7 final phases of the construction of the quay wall

Phase 8: wood undergoes degradation over the years due to deterioration and other influences. In phase 8, the wooden foundation piles are degraded to the current situation and a residual lifetime of 1 year.

Phase 9: permanent loads (load combination 1 (traffic)) is applied to the construction. up to the 9th phase, all phases are performed with elastoplastic drained analysis.

Phase 10: plastic undrained analysis in the serviceability limit state (SLS1) with a residual lifetime of 1 year and load combination 1 as shown in Figure 5.7.

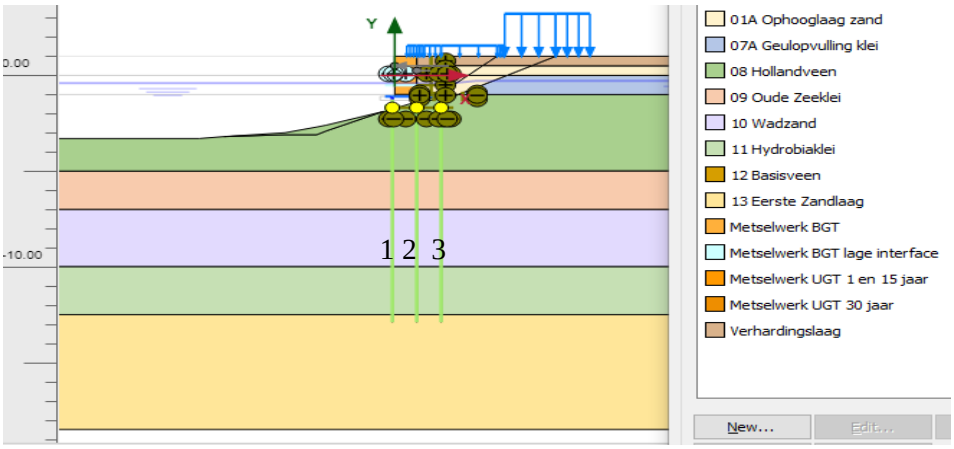

Figure 5.7. Plaxis 2D snippet historic quay wall with Load combination 1 – (Traffic) and legend for soil layers

5.3 Calculation of Forces, Bending Moments, and Deformations in the Piles according to TAK 3.2 approach

5.3.1 Output Results of Simulations 1-4

In this section shear and normal forces, bending moments, and horizontal deformations in the wooden piles are analyzed for various FEM-calculations performed with the HSss and S-Clay1 material models and the parameter sets discussed in Chapter 4.

Table 5.1 shows which material model and parameter set is used for each soil layer during the FEM calculation in Plaxis 2D. To make a clear comparison analysis on the results of the simulation, the Hardening Soil small strain model is used for the three considered soil layers in this research. In simulation 4 anisotropy is assumed with the S-Clay1 model in Hollandveen, because the DSS laboratory tests on Hollandveen were K0-consolidated explained before in section 4.1.4. In simulation 4 the Hardening Soil small strain parameters for Geulopvulling and Oude zeeklei are from parameter set Study. In all simulations the remaining soil layers under Oude zeeklei and above Geulopvulling are modeled with the Hardening Soil small strain model and parameters from TAK 3.2 (see attachment H).

Table 5.1. Material models and parameter sets, used for each soil layer during the FEM-calculation; simulations 1 - 4

	Geulopvulling	Hollandveen	Oude zeeklei	Legend
Simulation 1	Hardening Soil ss	Hardening Soil ss	Hardening Soil ss	TAK 3.2 (characteristic values)
Simulation 2	Hardening Soil ss	Hardening Soil ss	Hardening Soil ss	Study (all laboratory results)
Simulation 3	Hardening Soil ss	Hardening Soil ss	Hardening Soil ss	Optimized
Simulation 4	Hardening Soil ss	S-Clay1	Hardening Soil ss	Anisotropy HV

Shear Forces

In Figure 5.8 the shear forces are plotted against the depth of the piles in the subsurface. At the head of the piles at approximately -1.25 m NAP, the shear forces in all three piles in descending order are from parameter sets TAK 3.2, Study, Optimized and Anisotropy HV.

Reflecting on Chapter 4 Figure 4.15 in the deviatoric stress vs. axial strain graph it shows that in descending order for maximum deviatoric stress, q, follows for parameter set Study, Optimized and TAK 3.2. For Hollandveen and Oude zeeklei the same order as in the Geulopvulling is noticed, whereas in Hollandveen the anisotropic model gives the highest maximum (Figure 4.19) value of deviatoric stress, q. It is expected that for a lower maximum value of deviatoric stress, higher shear forces must be absorbed by the piles. Therefore, it is expected that the highest shear forces in the piles should be observed with the parameter set from TAK 3.2 and the lowest shear forces with the parameter set Study for the isotropic models. The parameter set Optimized would be expected to lie between the two aforementioned parameter sets, but what is striking is that the parameter sets of TAK 3.2 and Study alternately reach approximately the same maximum shear forces.

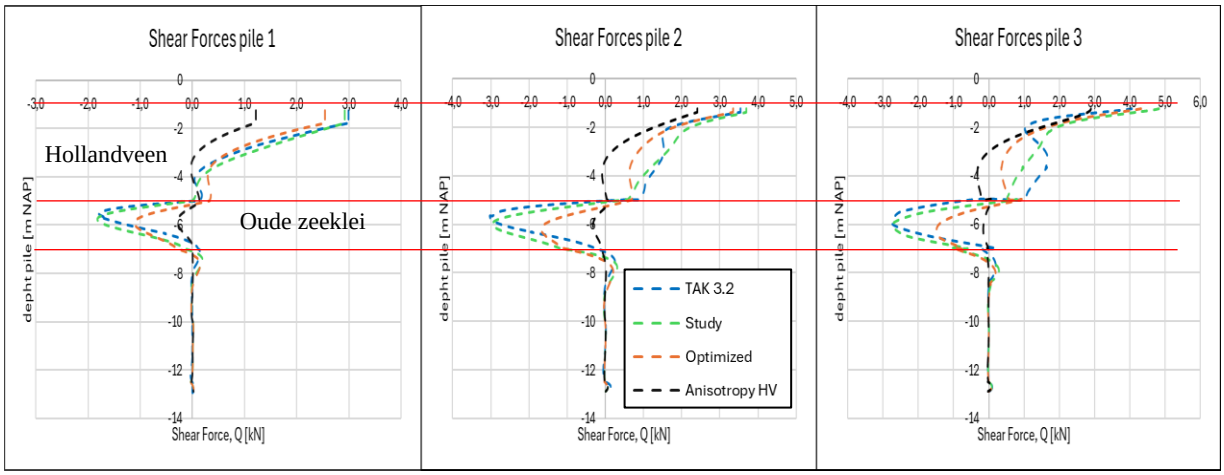

Figure 5.8. Shear force development in the piles Hardening Soil small strain model and S-Clay1 model

Normal Forces

In Figure 5.9 the normal forces are plotted against the depth of the piles in the subsurface. The largest normal forces are noticed in pile 2 and for the different model parameters there is no significant difference in the normal forces developed in the pile. In piles 1 and 3, a difference is noticed in the normal forces between the different sets of model parameters, whereby the simulation with anisotropic behavior in Hollandveen in particular produces a larger and smaller normal force respectively.

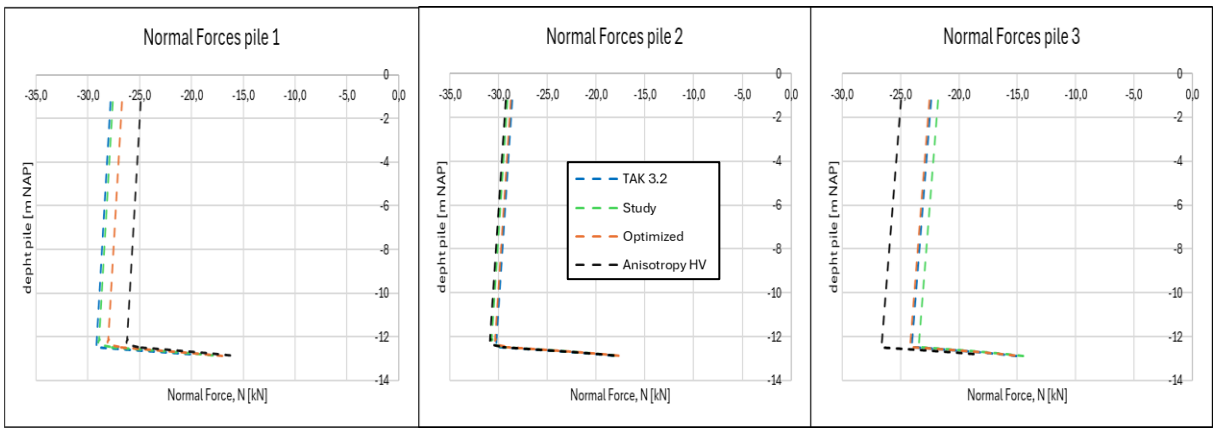

Figure 5.9. Normal force development in the piles Hardening Soil small strain model and S-Clay1 model

Bending Moments

Similar to the shear force development in the piles, the bending moments (Figure 5.10) decrease when anisotropy is considered in Hollandveen. The decrease in shear forces and bending moments is expected, because with assumed isotropic behavior in Hollandveen (peat) the horizontal soil properties in Hollandveen are misjudged, in the sense that greater horizontal forces/stresses are considered in the soil and therefore, greater horizontal forces and bending moments are developed in the piles. In Hollandveen a significant difference is observed between the development of bending moments in all 4 simulations. Increasing with depth in Oude zeeklei the graphs of simulations 1, 2 and 3 converge. There is a large reduction in maximum bending moments of the piles in simulation 4 compared to simulations 1 to 3, in percentages this is approximately between 75% and 87%.

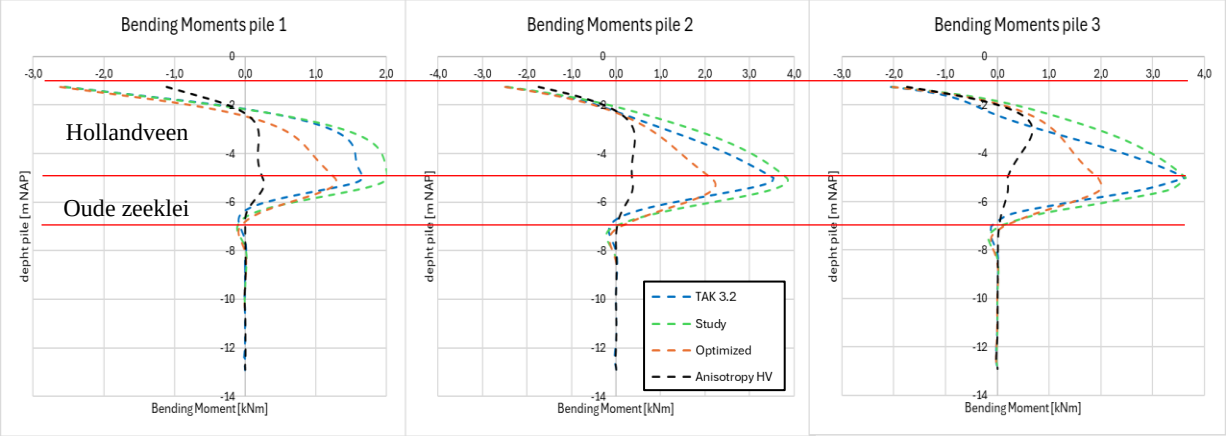

Figure 5.10. Bending moment development in the piles Hardening Soil small strain model and S-Clay1 model

Horizontal Deformation

The largest horizontal deformation (Figure 5.11) is observed at the head of the pile in Hollandveen towards the canal, with almost no deformation in Oude zeeklei. The largest deformations are noticed for simulation 2 with (Study), followed by simulation 1 (TAK 3.2), simulation 3 (Optimized) and the smallest deformations with simulation 4 (Anisotropy HV). The horizontal deformations are similar in all three piles for each simulation. As is the case with the bending moments, the reduction in maximum horizontal deformation of the piles in simulation 4 is quite large compared to simulations 1 to 3, in percentages this is approximately between 78% and 88%.

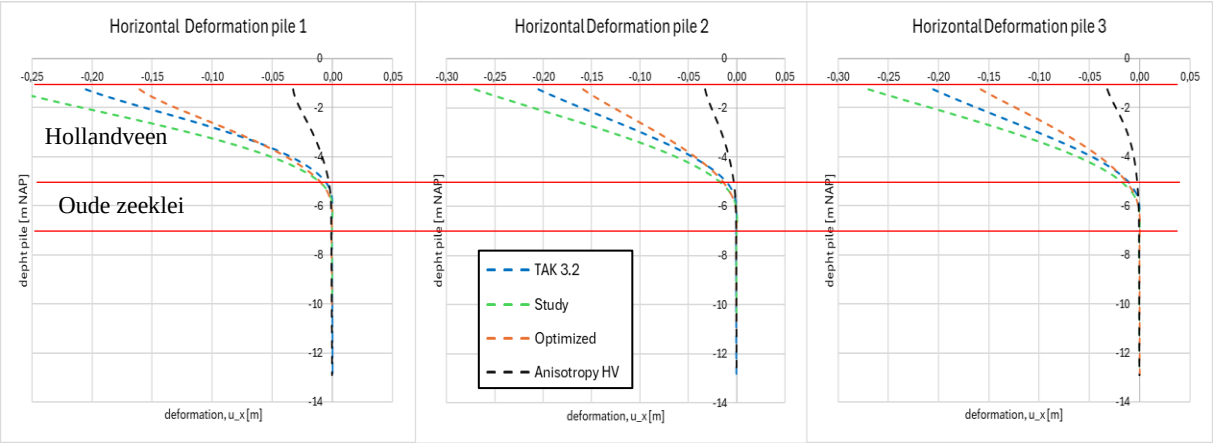

Figure 5.11. Horizontal deformation in the piles Hardening Soil small strain model and S-Clay1 model

The optimized parameter set compared to the parameter set Study in the case of the Hardening Soil small strain model in Hollandveen is decreased in stiffnesses, E_{50}^{ref} (11%) and E_{ur}^{ref} (49%) and increased

in E_{oed}^{ref} (32%) and c' (75%) see Table 4.11. The combination of an increase in c' and E_{oed}^{ref} outweighs the reduction in E_{50}^{ref} and E_{ur}^{ref} , as the soil reacts more strongly and the forces and horizontal deformation in the piles decrease.

5.3.2 Line cross-section analysis in Hollandveen and Oude zeeklei (simulations 1-4)

To provide more insight into the differences in structural forces in the wooden piles, the effective stress distribution in mainly Hollandveen and Oude zeeklei are observed. A line cross section (Figure 5.12) is drawn to the right of the foundation piles at a distance of x is 4 m from the frontside of the quay wall and between y = -1 mNAP and y = -7 mNAP.

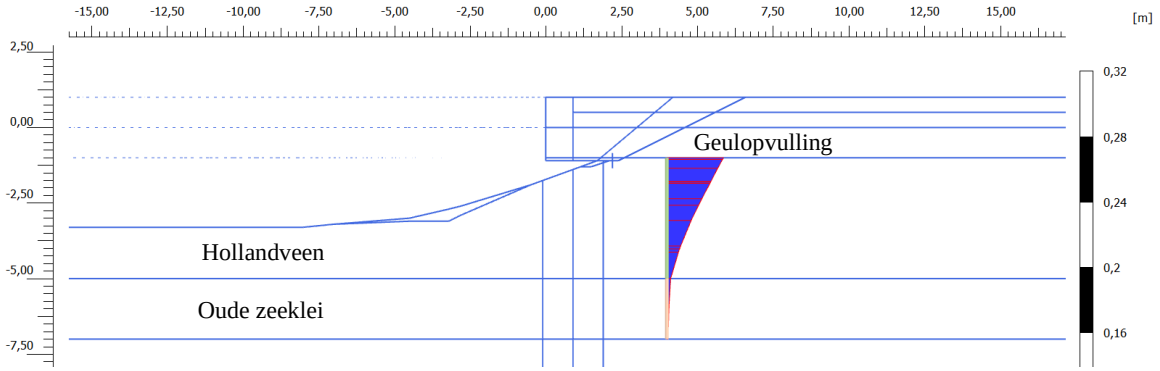

Figure 5.12. Line cross section through Hollandveen and Oude zeeklei

Figure 5.13 shows the effective principal stress directions versus depth at the line cross-section. For soil layers with a horizontal surface and in a triaxial test, the effective major (σ_1') and minor (σ_3') principal stress directions (0° rotation) are identical to the vertical and horizontal stress, respectively. Since the line cross-section is located near the slope of the quay wall, the principal stress directions are rotated, with principal stress in direction 2, σ_2', remaining horizontal and perpendicular to the plane of the cross-section, since plane strain conditions have been assumed. The rotation of the effective major and effective minor principal stresses increases with depth until a depth of approximately 5 m is reached, after which the rotation decreases.

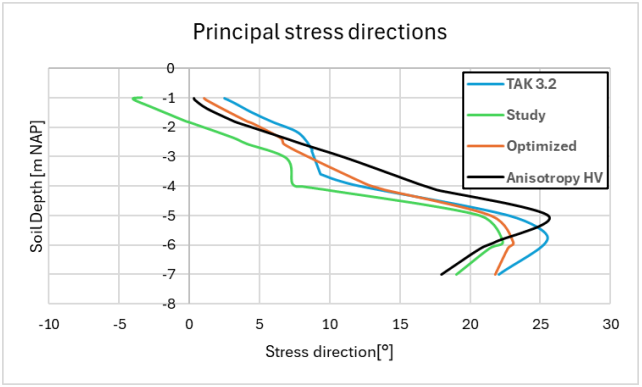

Figure 5.13. Effective principal stress paths in soil body at x = 4 m and y = -1 m to -7 m; simulations 1-4; SLS1 phase

Figure 5.14 shows the effective principal stress paths along the line cross-section. First a comparison is made between simulations with parameter set Study and Anisotropy HV, because there is only a difference in Hollandveen in terms of considered material model (HSss and S-Clay1). The differences in the stress paths are mainly noticed in Hollandveen, where the difference in material models lies. The

effective principal stress in direction 1 (σ_1') is smaller in the anisotropic model and clearly influences the stress path in Oude zeeklei, where the HSss model (same model parameters) was used in both simulations. The S-Clay1 model in Hollandveen has minimal influence on the effective principal stress path in directions 2 and 3 (σ_2' and σ_3') in Oude zeeklei.

Overall simulation 4 with the S-Clay1 model for Hollandveen (**Anisotropy HV**) develops slightly lower major principal effective stresses (σ_1') in the soil body compared to simulations 1-3 where all three soil layers are considered with the HSss model, and σ_2' and σ_3' are approximately identical for all simulations. Although there is a small difference in σ_3' of approximately a maximum of 15% in the line cross-section of the soil body, quite large differences are observed in maximum bending moments and maximum horizontal deformation.

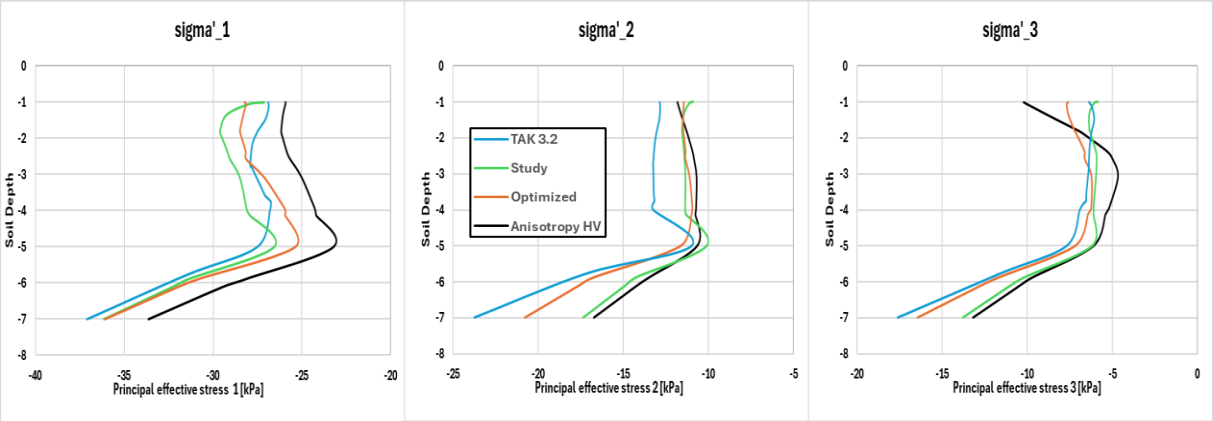

Figure 5.14. Effective principal stress paths in soil body at x = 4 m and y = -1 m to -7 m; simulations 1-4; SLS1 phase

5.3.3 Plaxis 2D horizontal deformation output results (simulations 2 and 4)

Figure 5.15 shows the horizontal deformation and the direction of the horizontal deformation in the soil layers from simulation 4. The direction of the horizontal deformation changes around x = 3 m and x = 4 m, from a deformation towards the canal to a deformation inland in Geulopvulling, Hollandveen and Oude zeeklei. Distance of x starts from the frontside of the quay wall at 0 m.

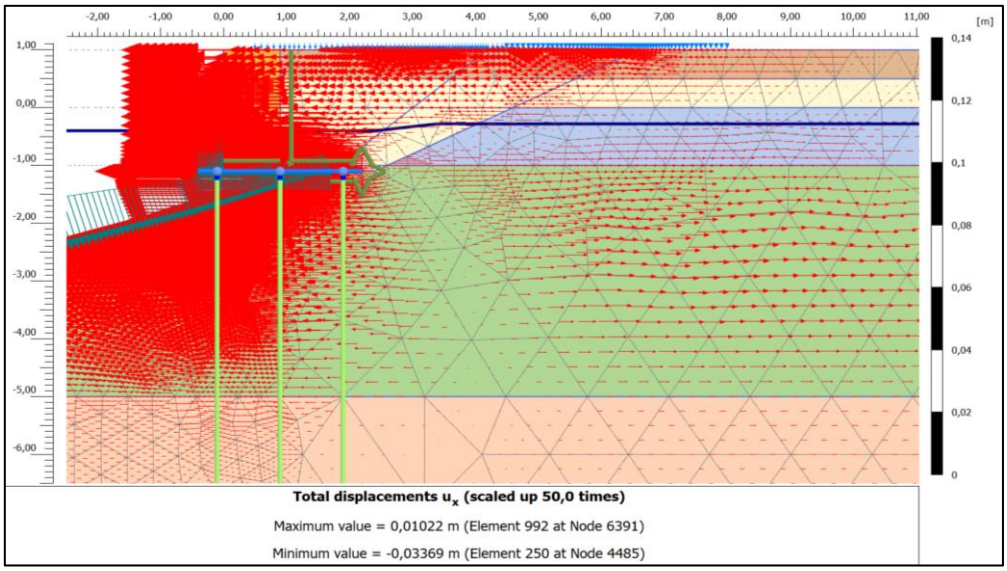

Figure 5.15. Horizontal deformation directions simulation 4 (geulopvulling HSss; Hollandveen SClay1; Oude zeeklei HSss)

Figure 5.16 shows the contour plot of simulation 4 for the horizontal deformations. In the case of a stability problem with a slope, the failure plane is expected to occur as a wedge sliding plane, which is not visible in this case. Furthermore, it is found as well that there is a small amount of horizontal deformation in the soil layers towards the canal and that the largest horizontal deformation takes place in the quay wall and just behind the quay wall.

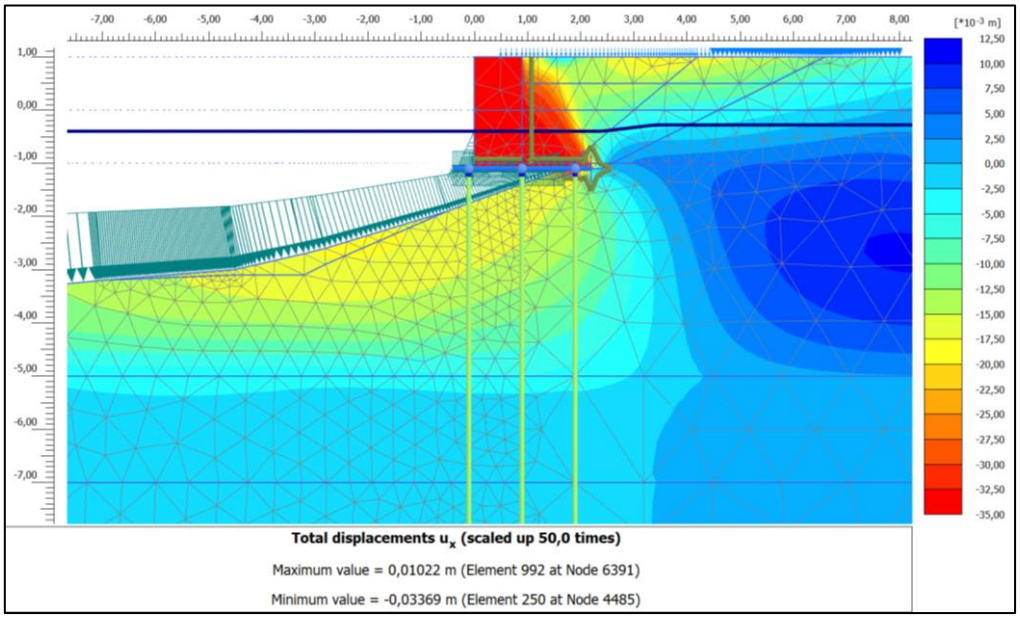

Figure 5.16. Horizontal deformations contour plot of Simulation 4 (Geulopvulling HSss; Hollandveen S-Clay1; Oude zeeklei HSss)

Figure 5.24 shows the horizontal deformation and the direction of the horizontal deformation in the soil layers from simulation 2. The direction of the horizontal deformation changes around x = 6 m and x = 7 m in Hollandveen and Oude zeeklei, from a deformation towards the canal to a deformation inland. In Geulopvulling the change of direction is at approximately x = 10 m. From the density and size of the arrows it can be seen that a larger horizontal deformation takes place in this case compared to simulation 4 (Figure 5.15).

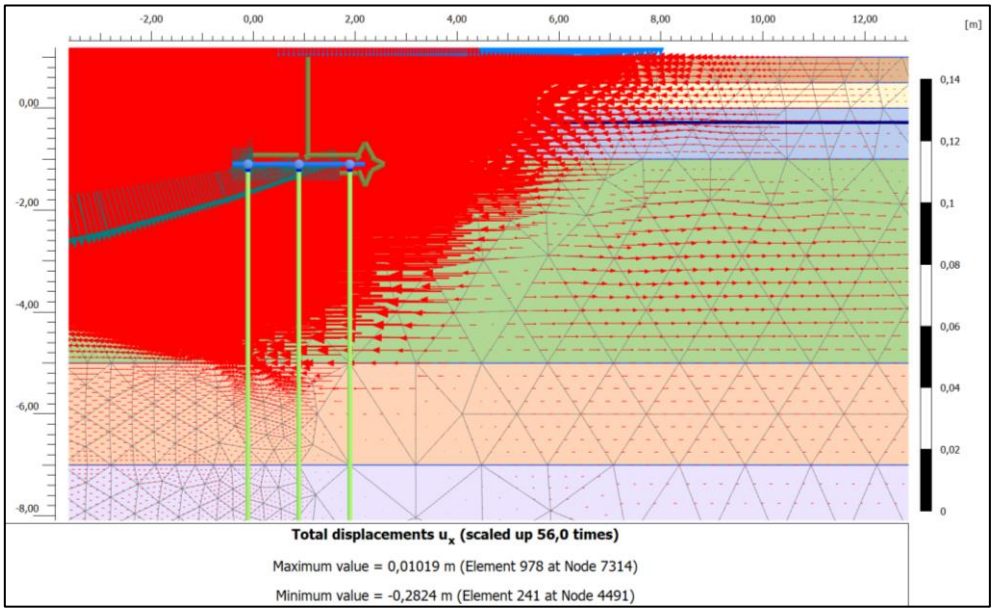

Figure 5.17. Horizontal deformations directions of Simulation 2 (Geulopvulling HSss; Hollandveen HSss; Oude zeeklei HSss)

Figure 5.18 shows the contour plot of simulation 2 for the horizontal deformations. In this case the expected failure plane is occurring as a wedge sliding plane, which is clearly visible. Furthermore, it is found as well that there is a greater amount of horizontal deformation in the soil layers right under the quay wall towards the canal and that the largest horizontal deformation takes place in the quay wall and just behind the quay wall.

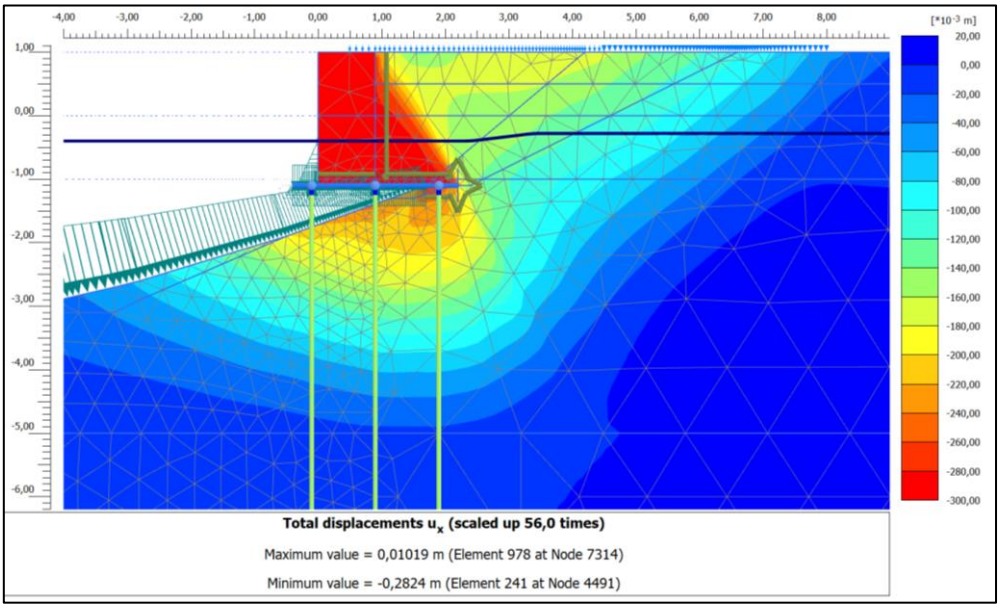

Figure 5.18. Horizontal deformations contour plot of Simulation 2 (Geulopvulling HSss; Hollandveen HSss; Oude zeeklei HSss)

5.3.4 Additional simulations with the HSss and S-Clay1 model

Due to some deviation in the results of simulation 4 in terms of the strong reduction of the maximum field bending moments, maximum horizontal deformation and the graphical output representation, it was investigated whether the transition from the HSss model to the S-Clay1 model between the considered soil layers is of any influence.

Two additional simulations have been performed to observe the change in output results. Additional simulation one, the S-Clay1 model is considered for all 3 soil layers, and in additional simulation two the HSss model is replaced with the S-Clay1 model in Geulopvulling and Oude zeeklei and the S-Clay1 model in Hollandveen changed for the HSss model. The parameter set obtained from all laboratory data is used, from Table 4.5, Table 4.9, Table 4.11 and Table 4.14.

Figure 5.19 and Figure 5.20 display the development of the maximum bending moments and maximum horizontal deformations in the foundation piles.

The simulation (All SClay1) in which the S-Clay1 (isotropic and anisotropic) model is considered in Geulopvulling, Hollandveen and Oude zeeklei results in a small (neglectable) increase in the bending moments and horizontal deformations. The sliding plane is similar to the sliding plane observed in Figure 5.16.

The simulation (GO&OZ SClay1; HV HSss) in which the S-Clay1 (isotropic) model is considered in Geulopvulling and Oude zeeklei, and the HSss model in Hollandveen, an increase in maximum bending moments (approx. 55%) and maximum horizontal deformation (approx. 60%) is observed.

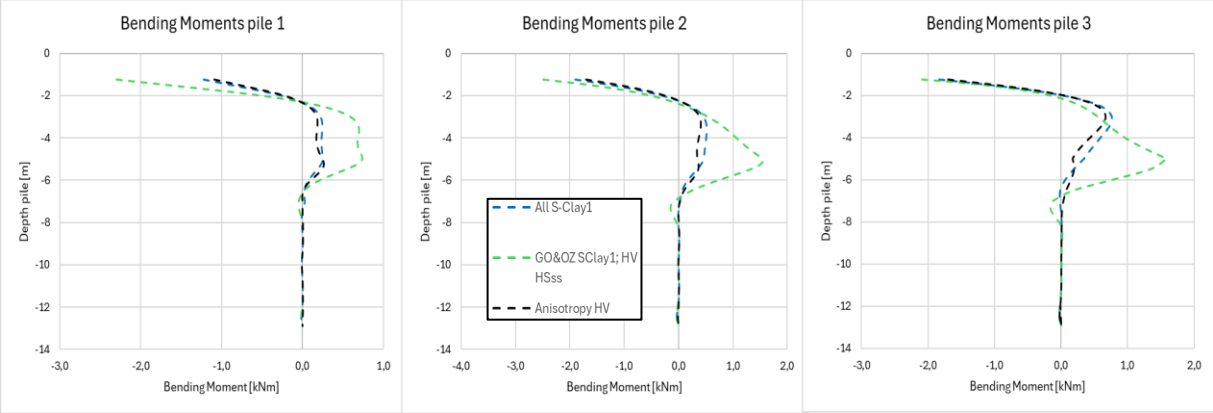

Figure 5.19. Maximum bending moments in foundation piles

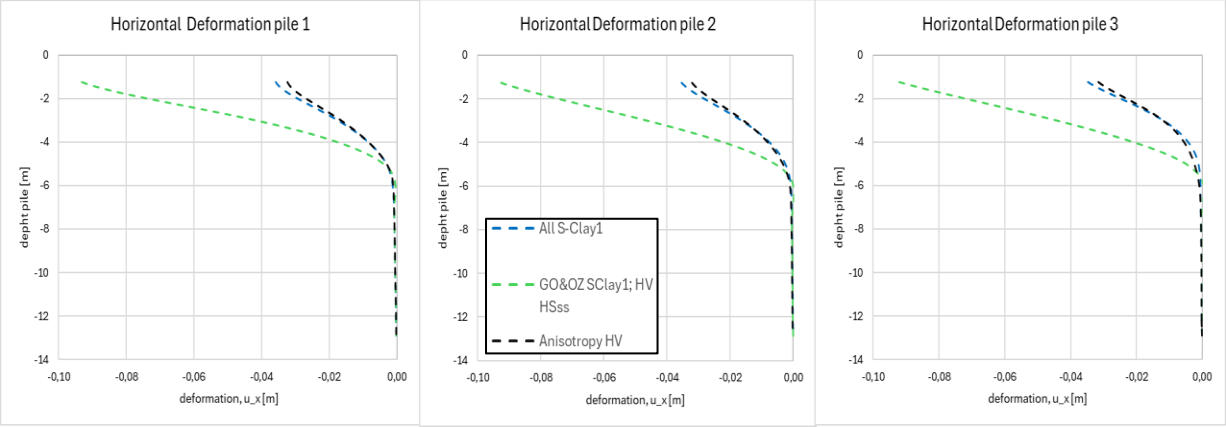

Figure 5.20. Maximum horizontal deformation in foundation piles

Figure 5.21 shows that the change in direction of the horizontal deformation at a distance of x is approximately 6-7 m from the face of the masonry in the Hollandveen and Oude zeeklei; in the Geulopvulling the change in direction is at a distance of approximately x = 10 m.

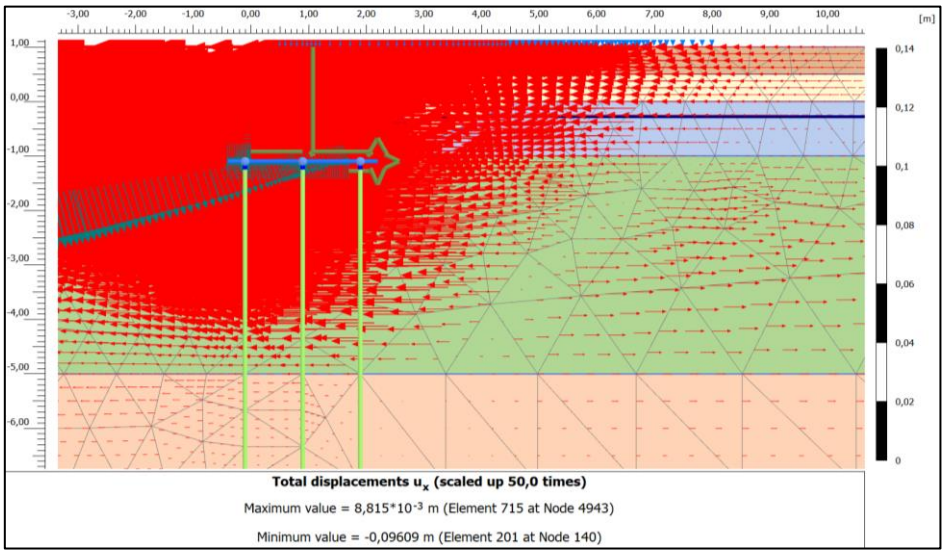

Figure 5.21. Horizontal deformation directions of extra simulation (geulopvulling SClay1; Hollandveen HSss; Oude zeeklei SClay1)

Figure 5.22 shows the contour plot of the extra simulation for the horizontal deformations. In this case the expected failure plane is occurring as a wedge sliding plane, which is clearly visible. Furthermore,

it is found as well that there is a greater amount of horizontal deformation in the soil layers right under the quay wall towards the canal.

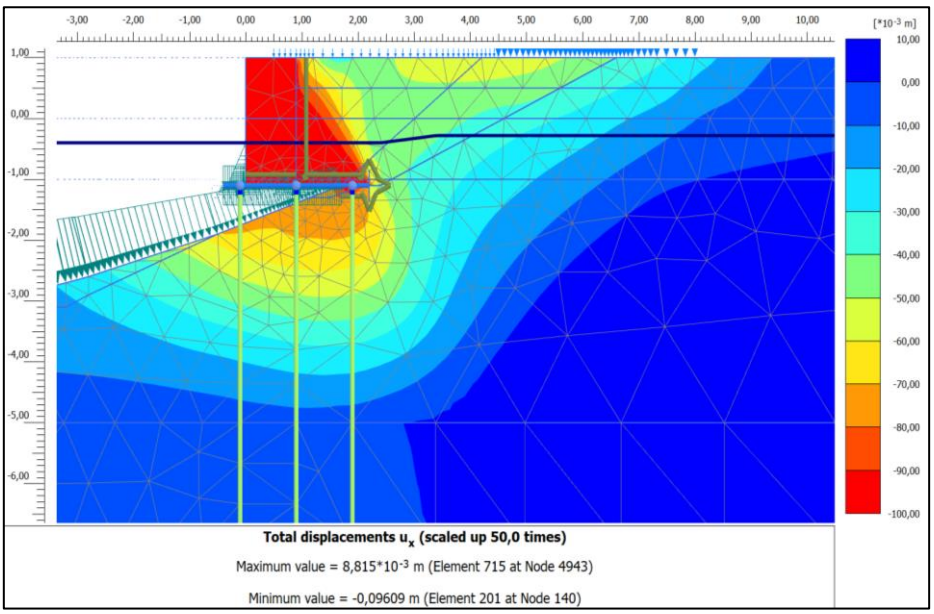

Figure 5.22. Horizontal deformations contour plot of extra simulation (geulopvulling SClay1; Hollandveen HSss; Oude zeeklei SClay1)

It may be that when considering the S-Clay1 model in Hollandveen, no wedge sliding plane is observed, because the deformation of the soil has not developed that far yet, and not so much the combination of models, since with the isotropic S-Clay1 model, combined with the isotropic HSss model, a perfect wedge sliding plane is observed in the output results as can be seen in figure 5.21 above.

5.4 Calculation of Forces, Bending Moments, and Deformations in the Piles according to TAK 3.2 approach

5.4.1 Output Results of Simulations 5-8

In this section shear and normal forces, bending moments, and horizontal deformations in the wooden piles are analyzed for various FEM-calculations performed with the HSss model used for Geulopvulling, the SS model for Hollandveen and Oude zeeklei, and the S-Clay1 model for Hollandveen. For these simulations, small adjustments had to be made in the strength parameters of the soil layers often to prevent errors, hence:

Simulation 5: c’ = 3.6 kPa from HSss model and ϕ’= 32.8° from SS model in Hollandveen.

Simulation 6: c’ increased from 2.0 to 3.3 kPa and locally increased in dredging profile (Figure 5.29) to 4.0 kPa Hollandveen.

Simulation 7: c’ increased from 6.0 to 7.0 kPa, 2.0 to 3.0 kPa and 2.0 to 3.0 kPa for respectively Geulopvulling, Hollandveen and Oude zeeklei.

Table 5.2 shows which material model and parameter set is used for each soil layer during the FEM calculation in Plaxis 2D. To make a clear comparison analysis on the results of the simulations, the HSss model is used for Geulopvulling in all simulations, because TAK 3.2 only consists of parameters for the HSss model for Geulopvulling. In simulation 8 the HSss and SS model parameters are from

parameter set Study. The remaining soil layers are modeled with the Hardening Soil small strain model and parameters from TAK 3.2 (see attachment H).

Table 5.2. Material models and parameter sets, used for each soil layer during the FEM-calculation; simulations 5 - 8

	Geulopvulling	Hollandveen	Oude zeeklei	Legend
Simulation 5	Hardening Soil ss	Soft Soil	Soft Soil	TAK 3.2 (characteristic values)
Simulation 6	Hardening Soil ss	Soft Soil	Soft Soil	Study (all laboratory results)
Simulation 7	Hardening Soil ss	Soft Soil	Soft Soil	Optimized
Simulation 8	Hardening Soil ss	S-Clay1	Soft Soil	Anisotropy HV

Shear Forces

In Figure 5.22 the shear forces are plotted against the depth of the piles in the subsurface. The development of shear forces is approximately identical for each simulation, where simulation 7 with the optimized parameter set causes the highest maximum shear forces in the piles and simulation 8 with anisotropy considered in Hollandveen yields the lowest maximum shear forces.

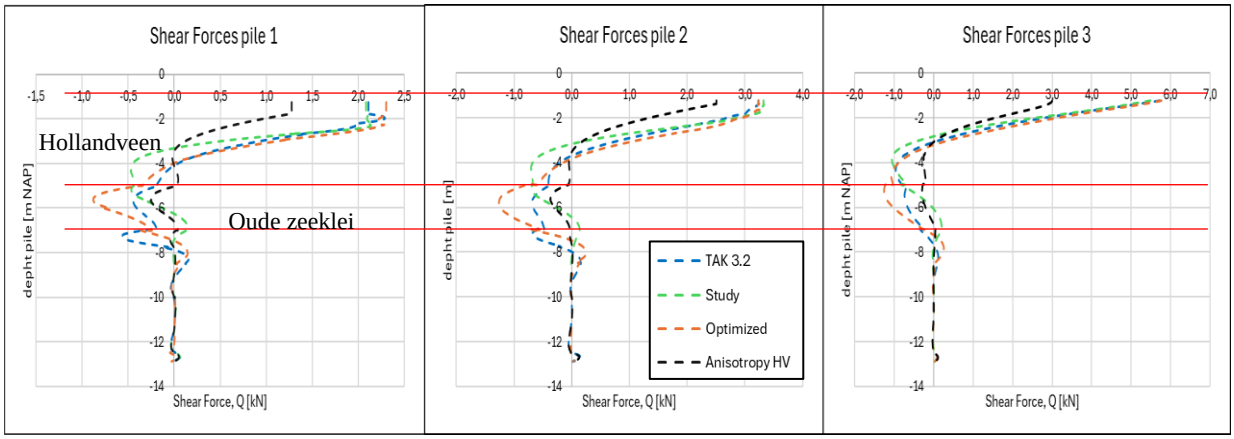

Figure 5.23. Shear force development in the piles simulation 5 - 8

Normal Forces

In Figure 5.24 the normal forces are plotted against the depth of the piles in the subsurface. The largest normal forces are noticed in pile 2 and for the different model parameters there is no significant difference in the normal forces developed in pile 1 and 2. In pile 3, a greater difference is noticed in normal forces between the different simulations, whereby simulation 8 with anisotropic behavior in Hollandveen in particular produces a larger normal force.

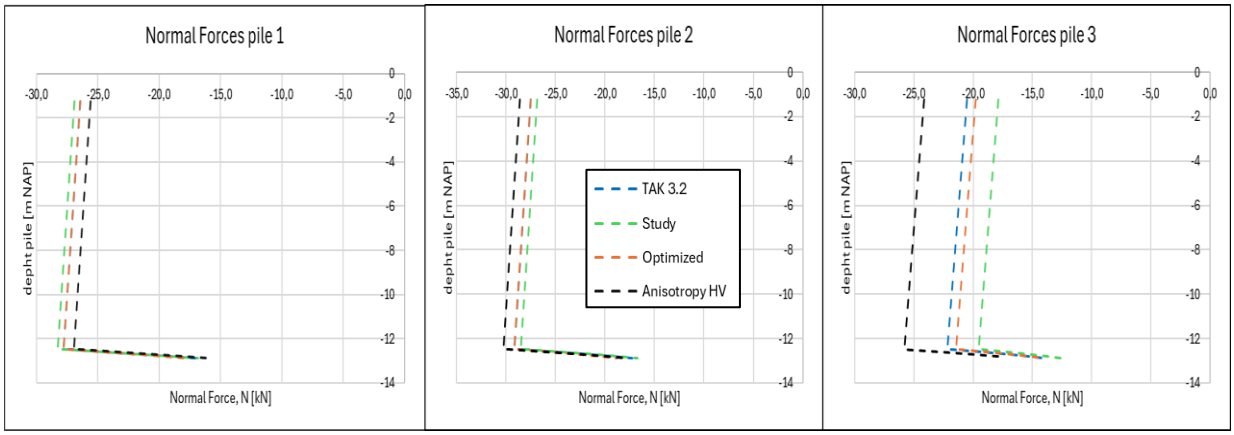

Figure 5.24. Normal force development in the piles simulation 5 - 8

Bending Moments

Similar to the shear force development in the piles, the bending moments (Figure 5.25) decrease when anisotropy is considered in Hollandveen. The decrease in shear forces and bending moments is expected, because with assumed isotropic behavior in Hollandveen (peat) the horizontal properties in Hollandveen are misjudged as explained before in section 5.3. Simulation 7 (optimized) yields the highest maximum bending moments, followed by simulation 5 (TAK 3.2), simulation 6 (Study) and simulation 8 (Anisotropy HV). There is again, a large reduction in maximum bending moments of the piles in simulation 8 compared to simulations 5 to 7, in percentages this is approximately between 74% and 80%.

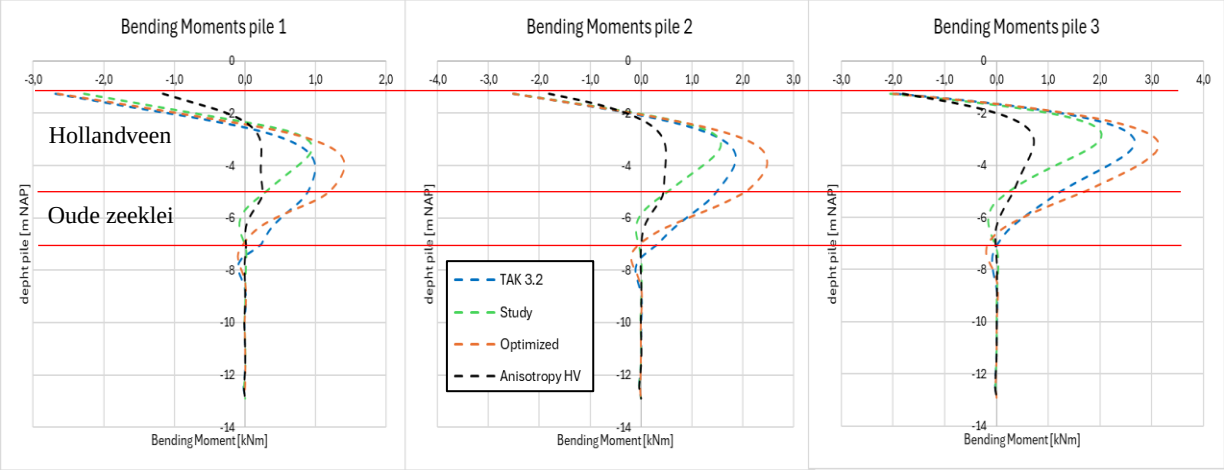

Figure 5.25. Bending moments in the piles simulation 5 - 8

Horizontal Deformation

The largest horizontal deformation (Figure 5.26) is observed at the head of the pile in Hollandveen towards the canal, with almost no deformation in Oude zeeklei. The largest deformations are noticed for simulation 6 with (Study), followed by simulation 5 (TAK 3.2), simulation 7 (Optimized) and the smallest deformations with simulation 8 (Anisotropy HV). The horizontal deformations are similar in all three piles for each simulation. As is the case with the bending moments, the reduction in maximum horizontal deformation of the piles in simulation 8 is quite large compared to simulations 5 to 7, in percentages this is approximately between 45% and 79%. Apparent upon comparison that simulation 3 and 7 (optimized) and simulation 4 and 8 (Anisotropy HV) give identical maximum horizontal deformations.

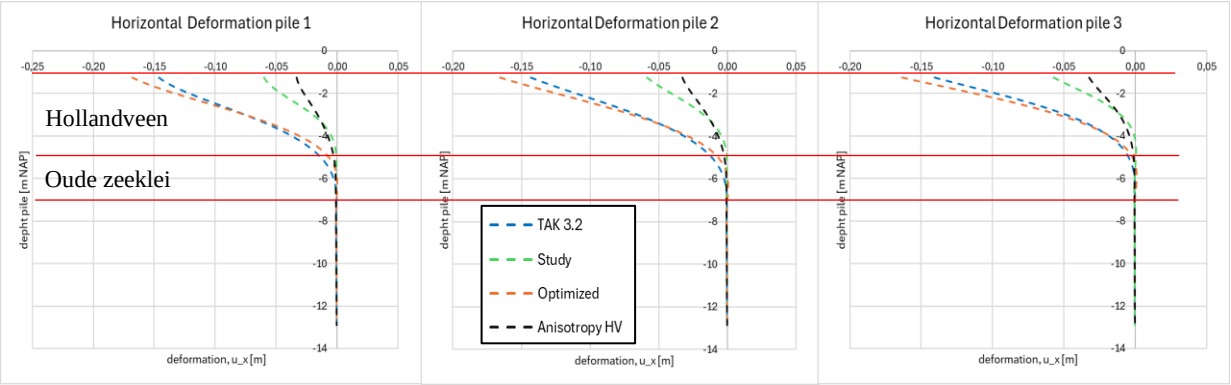

Figure 5.26. Horizontal deformation in the piles simulation 5 - 8

Quite disappointing that mainly the effective cohesion had to be adjusted for the simulations to run without errors. A global comparison between simulations 1-4 and simulations 5-8, shows that the optimized parameter set, when considering predominantly the HSss model, reduces the output results of forces and deformations in the piles between simulations 1-4, but in the case of predominantly the SS model, an increase can be seen in the output results for simulation 7 with optimized parameter set between simulations 5-8.

The optimized parameter set in the case of the Soft Soil model is mainly decreased in stiffness and strength to fit the graphs from laboratory data as shown in Chapter 4. Therefore, the soil absorbs less forces and these are absorbed by the piles, increasing the forces, bending moments and horizontal deformations in the piles.

5.4.2 Line cross-section analysis in Hollandveen and Oude zeeklei (simulations 5-8)

Just as in section 5.3.1 a line cross-section analysis is conducted to provide more insight into the effective principal stress distribution in mainly Hollandveen and Oude zeeklei. A line cross section (Figure 5.12) is drawn to the right of the foundation piles at a distance of x is 4 m from the frontside of the masonry wall and between y = -1 mNAP and y = -7 mNAP.

In Figure 5.27 the major and minor principal stress directions are shown, from which it is clear that the major and minor principal stresses are not identical to the vertical and horizontal stresses along the cross-section, as they are rotated.

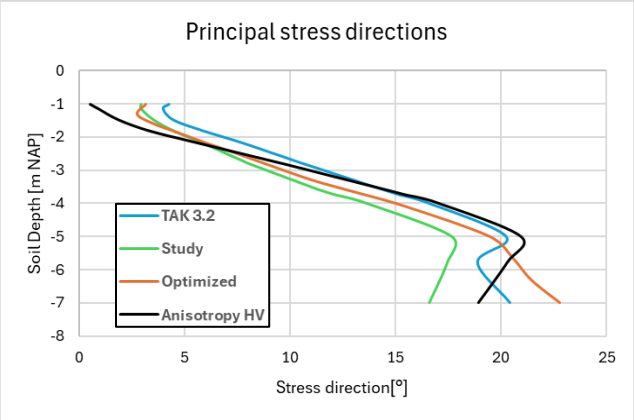

Figure 5.27. Effective principal stress paths in soil body at x = 4 m and y = -1 m to -7 m; simulations 5-8; SLS1 phase

Figure 5.28 shows the effective principal stress paths along the line cross-section. Overall simulation 8 with the S-Clay1 model for Hollandveen (Anisotropy HV) develops slightly lower major effective principal stresses, σ'_1, in the soil body compared to simulations 5-7, and the effective principal stresses in directions 2 and 3 (σ'_2 and σ'_3) are approximately identical for all simulations. Although there is a small difference in the effective principal stresses of approximately a maximum of 15% in the line cross-section of the soil body, quite large differences are observed in maximum bending moments and maximum horizontal deformation.

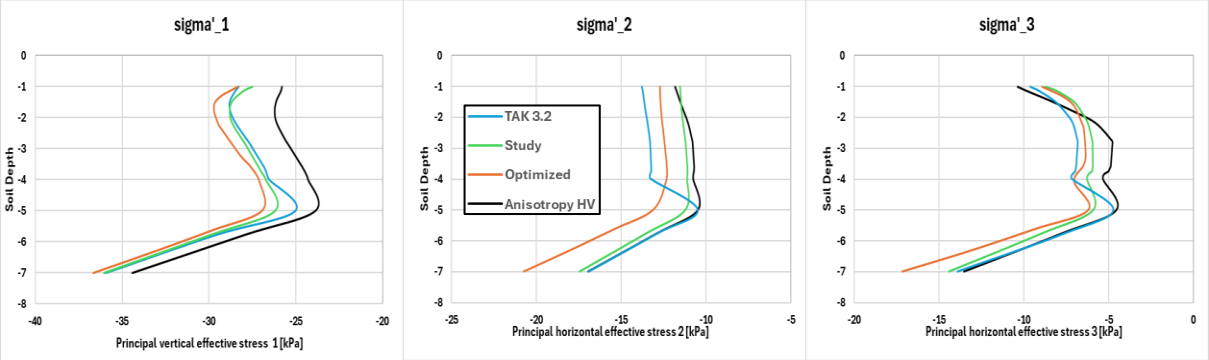

Figure 5.28. Effective principal stress paths in soil body at x = 4 m and y = -1 m to -7 m; simulations 5-8

5.4.3 Plaxis 2D horizontal deformation output results (simulations 6 and 8)

Figure 5.29 shows the deformation direction of simulation 6. It is observed that parts along the slope under the quay wall experience strong deformation inland, which is contrary to expectations. In simulation 6 the effective cohesion (c') for Hollandveen was increased to 3.3 kPa and locally in the dredging profile (dark green) the effective cohesion was increased to 4 kPa, otherwise the simulation bumped into errors. Similar output results are found as well for simulations 5 and 7 (see attachment I).

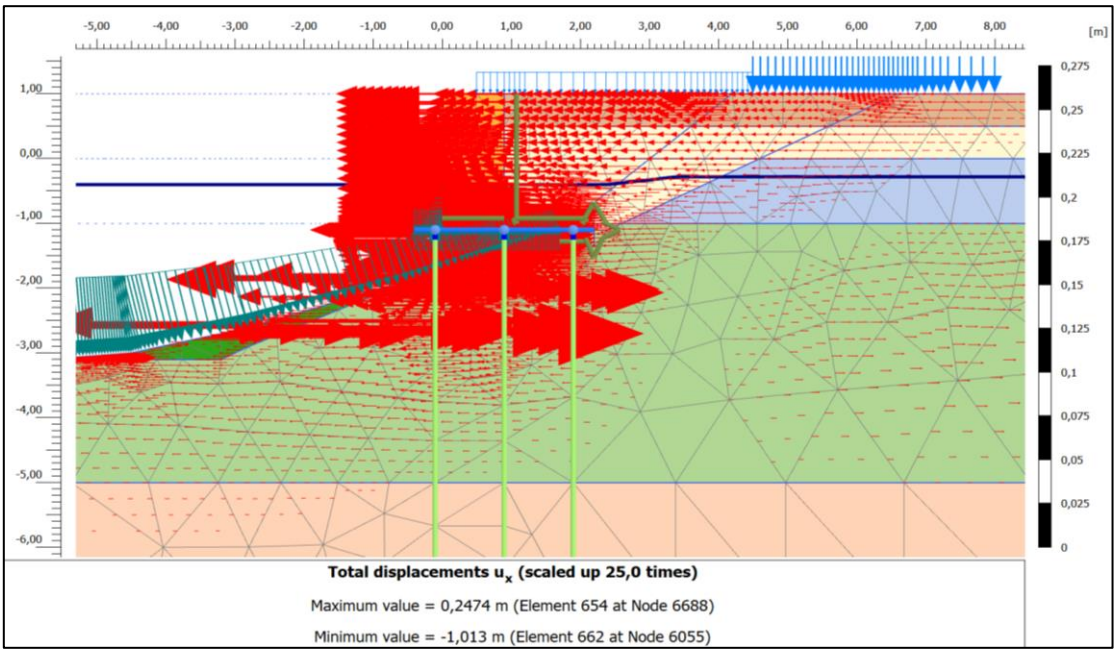

Figure 5.29. Horizontal deformation directions of Simulation 6 (Geulopvulling HSss; Hollandveen Soft Soil; Oude zeeklei Soft Soil)

The contour plot (Figure 5.30) clearly shows the locally located strong horizontal deformations in the slope of Hollandveen. No wedge sliding plane is observed.

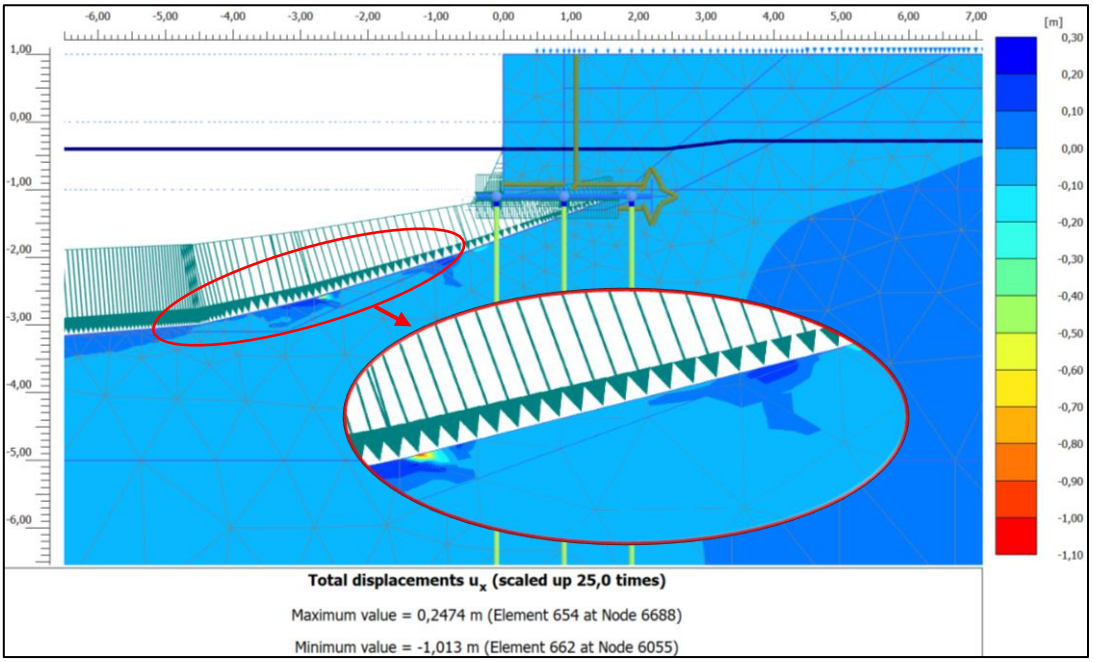

Figure 5.30. Horizontal deformations contour plot of Simulation 6 (Geulopvulling HSss; Hollandveen SS; Oude zeeklei SS)

In simulation 8, where the S-Clay1 model is used for Hollandveen, an improvement in the output results (Figure 5.31 and Figure 5.32) can be seen compared to the simulations with the SS model considered for Hollandveen and Oude zeeklei. There is no horizontal deformation observed along the slope inland. The failure sliding plane seems to be taking the shape of a wedge sliding plane, but not quite as expected.

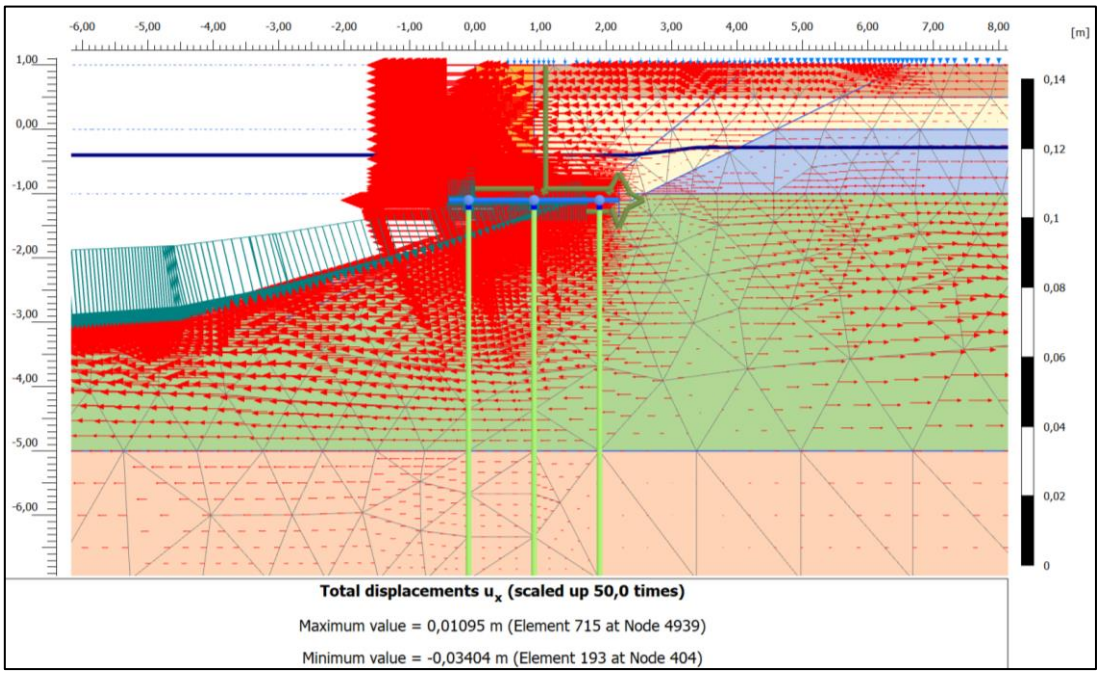

Figure 5.31. Horizontal deformations directions of Simulation 8 (Geulopvulling HSss; Hollandveen S-Clay1; Oude zeeklei SS)

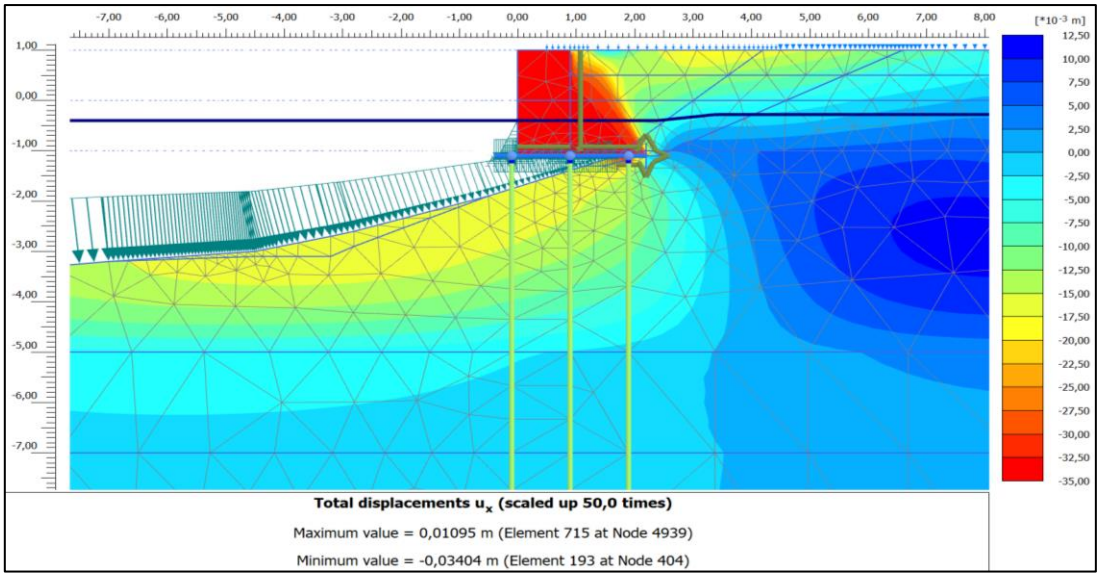

Figure 5.32. Horizontal deformations contour plot of Simulation 8 (Geulopvulling HSss; Hollandveen S-Clay1; Oude zeeklei SS)

5.5 Influence of the Initial Phase with K0-procedure and Gravity loading on the Stress Development in the Soil Body

In the first (initial) phase for every project in Plaxis 2D, a calculation of the initial stress field is included to configure the initial geometry. Three methods are available for consideration such as the K0-procedure, gravity loading and field stress. The first and second method are considered in this study for comparison.

The K0-procedure (used in previous sections) is one of the calculation methods to define the initial stresses for the model, where the stress history of the medium is considered by either the OCR or POP. The K0-procedure does not check for stress field equilibrium at the end of the initial phase. The K0-procedure is recommended for use in cases where a horizontal surface is present, and all soil layers and phreatic levels are parallel to the surface. In any other case the stress field equilibrium is not guaranteed as there are shear stresses required, which the K0-procedure does not generate. In the K0-procedure the vertical stresses are equal to the self-weight of the soil and the horizontal stresses are calculated with the value of K_0^{NC} (PLAXIS, Plaxis 2D; Reference Manual, 2020). The K0-procedure is carried out with an initial natural slope (1:3) as well according to TAK 3.2, but then a plastic-0 phase is introduced after the initial phase with the same geometry, which must ensure that stress field equilibrium is achieved. The stage in which the canal is excavated is therefore excluded from the phases.

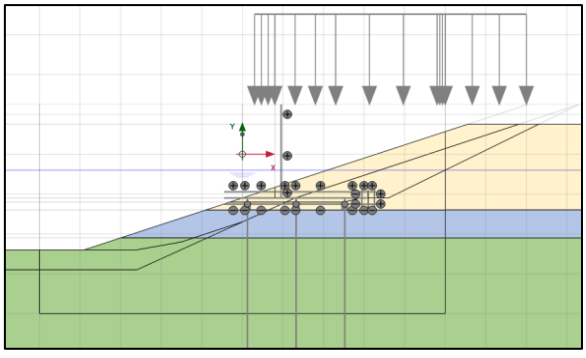

Figure 5.33. Initial phase with natural slope (1:3)

The Gravity Loading (GL) method is recommended for an initial situation with a slope. In the case of Gravity loading, the initial stresses are generated by applying the soil self-weight in the initial phase. For Gravity loading, the K0-value is equal to the K_0^{NC}- parameter in the material data set, when advanced soil models are used. The stress history of the medium is not considered.

Table 5.3. K_0^{NC} - values considered in the soil layers and simulations

	TAK 3.2	Anisotropy HV
Soil layer	K_0^{NC}-value	K_0^{NC}-value
Geulopvulling	0.66	0.40
Hollandveen	0.69	0.39
Oude zeeklei	0.56	0.43

In the following figures a comparison is made between the three above-mentioned methods to generate initial stresses in the soil. For each method, 2 simulations are carried out using material models according to Table 5.1 (TAK 3.2 = simulation 1 and Anisotropy HV = simulation 4). The OCR and volumetric weights are identical for all simulations, the K_0^{NC} is not identical between TAK 3.2 and Anisotropy HV.

Figure 5.34 shows the principal stress directions for the initial phase and the SLS1 phase, from which it can be seen that in the initial phase the effective major principal stress and the effective minor principal stress are identical to the vertical and horizontal effective stress, respectively, as the principal stress directions are constant with depth and equal to 0 degrees. In the SLS1 phase the major and minor effective principal stress are not identical to the effective vertical and horizontal stress, respectively, as their stress directions are not constant and not equal to 0 degrees.

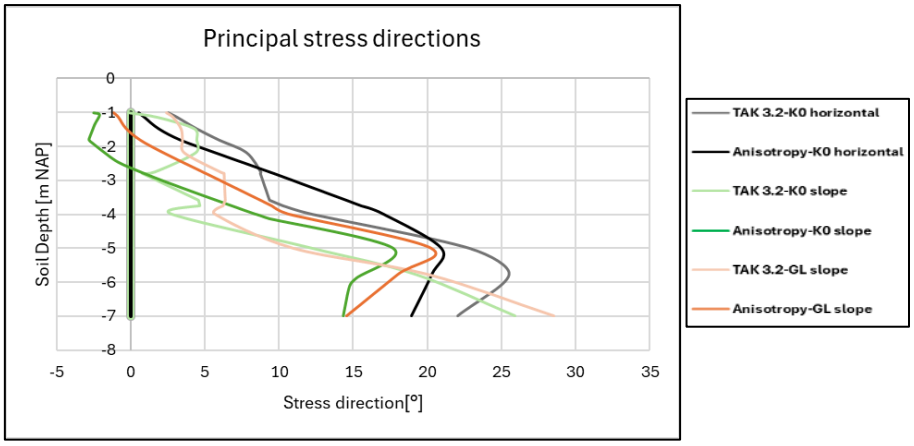

Figure 5.34. Effective principal stress paths in soil body at x = 4 m and y = -1 m to -7 m; Initial and SLS1 phase

K0-procedure with horizontal layers

In the initial phase (Figure 5.35), the course of the major effective principal stress (σ_1') according to the K0-procedure with horizontal layers is identical for both simulations. The horizontal effective principal stresses (σ_2' and σ_3') are smaller for Anisotropy-K0 than TAK 3.2-K0, due to the lower K_0^{NC}-values. In the case of the K0-procedure with horizontal layers the horizontal effective principal stresses in directions 2 and 3 are identical. In the case of the K0-procedure with horizontal layers, the largest effective principal stresses are achieved compared to K0-slope and GL-slope in the initial phase.

K0-procedure with slope

The results with the K0-procedure with a slope are obtained from output results at the end of the plastic-0-step and are shown in Figure 5.35. The K0-procedure with plastic-0-step shows a clear difference in the course of the major effective principal stress (σ_1') in the initial phase. The effective principal stress (σ_2') is more or less identical for both simulations but is not equal in effective principal stress directions 2 and 3. The expectation is that the results after the plastic-0-step are approximately equal to the results obtained from the K0-procedure with horizontal layers, but that is by no means the case in Hollandveen. The resulting graphs from this method for the deeper layer of Oude zeeklei seem to converge.

Gravity Loading with slope

Illustrated in Figure 5.35 with the Gravity Loading method, the course of the initial major effective principal stress (σ_1') is approximately identical as well for both simulations. An approximately equal progression is observed in effective principal stress direction 2 as well for both simulations. The difference in Hollandveen for the minor effective principal stress (σ_3') may be due to the implementation of the S-Clay1 model. The results of this method with a slope seem more reliable than the results of the K0-procedure with a slope.

The difference in major effective principal effective stress is less than or approximately equal to 10 kPa (26%), for all three methods and simulations. The difference in effective principal stress directions 2 and 3 is less than or approximately equal to 14 kPa (56%), between all simulations.

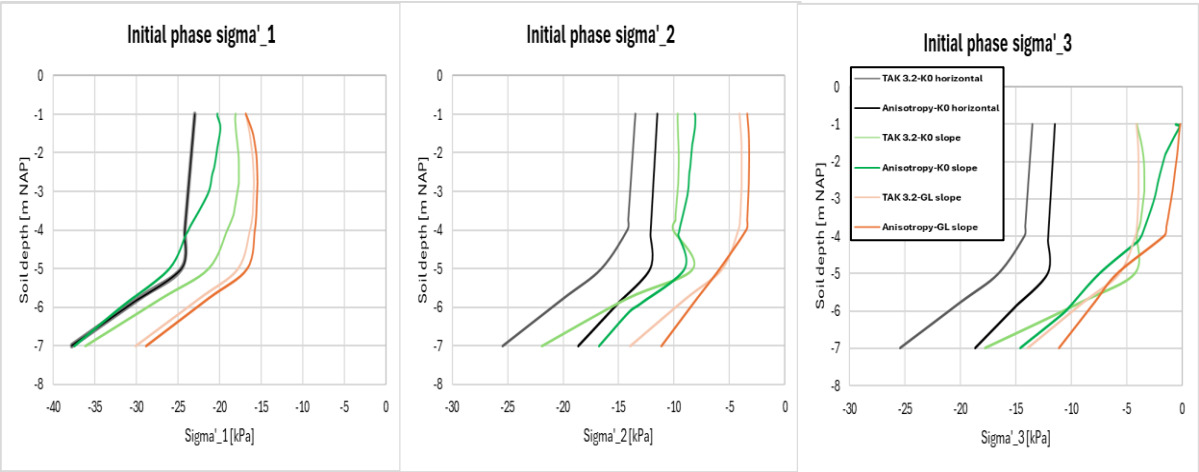

Figure 5.35. Principal effective stress development in Hollandveen and Oude zeeklei in the initial phase

It is interesting to observe the development of the effective principal stress paths in the SLS1 phase shown in Figure 5.36. The simulations with TAK 3.2 model parameters give approximately the same progression for the major effective principal stress (σ_1'), whether the simulation consists of a slope, horizontal layers or different initial phase method. The simulations containing TAK 3.2 parameters with a slope give approximately the same progression for the effective principal stress in directions 2 and 3; TAK 3.2 K0-horizontal yields greater effective principal stresses in directions 2 and 3. The Anisotropy K0-procedure with a slope yields different results for the major effective principal stress development, compared to Anisotropy-K0 horizontal and Anisotropy-GL slope in which the two latter have identical progressions. Anisotropy-K0 horizontal has identical effective stress development in directions 2 and 3. In directions 2 and 3 all three methods with Anisotropy follow their own progression.

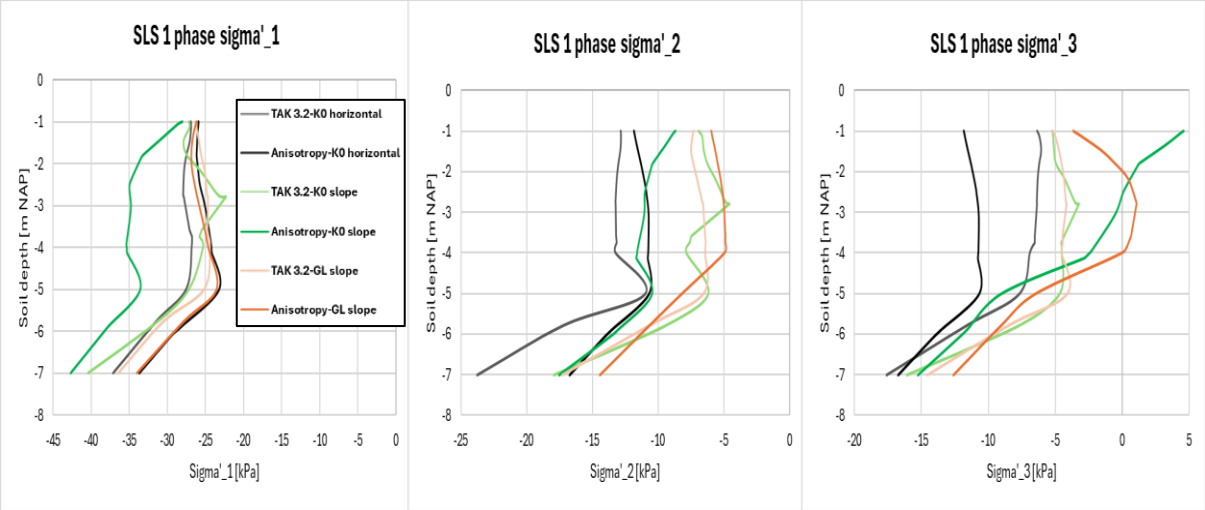

Figure 5.36. Principal effective stress development in Hollandveen and Oude zeeklei in the Serviceability Limit State (SLS1)

Figure 5.37 shows the developed mobilized shear strength with depth in the initial phase and in the SLS1 phase. With TAK 3.2 material model parameters, approximately the same progression is obtained for the mobilized shear strength in the SLS1 phase. The mobilized shear strength increased in the SLS1 phase compared to the initial phase. In the SLS1 phase, greater mobilized shear strength is obtained in situations with a slope than an initial situation with horizontal soil layers.

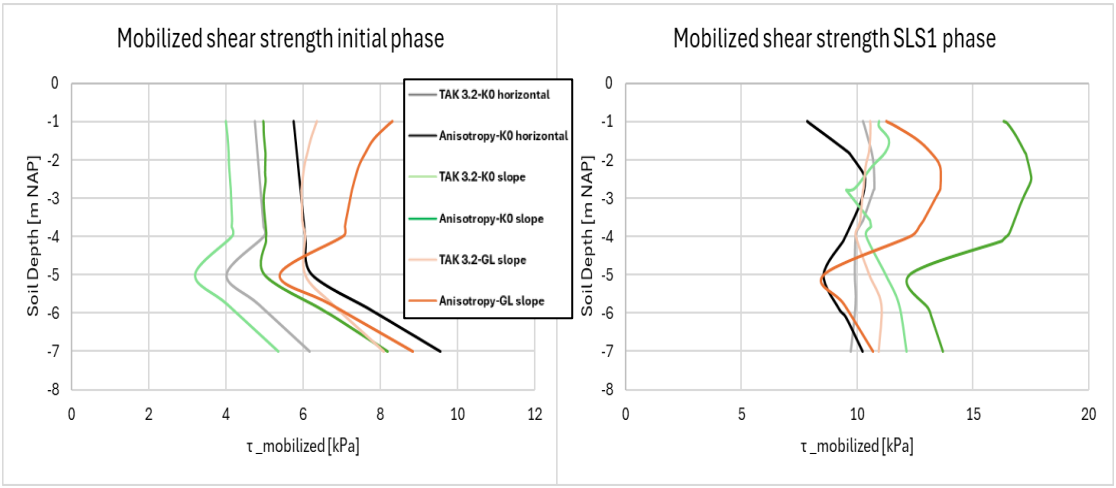

Figure 5.37. Mobilized shear strength development in Hollandveen and Oude zeeklei; initial phase and SLS1 phase

It can be seen in Figure 5.38 that much larger bending moments and horizontal deformations are developed in an initial phase with a slope than in an initial phase with horizontal layers, independently of the considered material model.

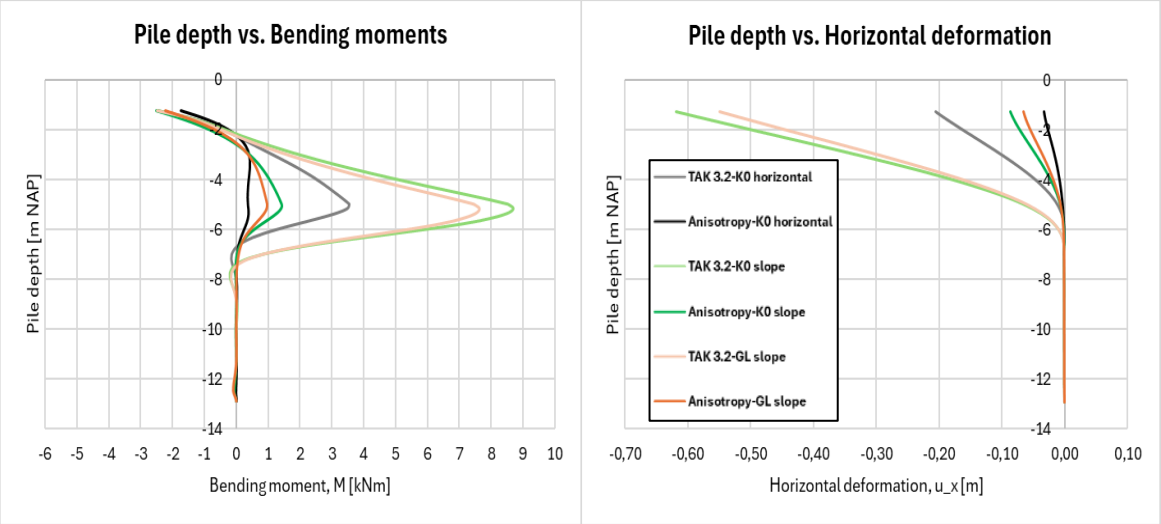

Figure 5.38. Bending moments and horizontal deformations in pile 2; SLS1 phase

In conclusion, the results with the K0-procedure with a slope look numerically unstable, especially in the SLS1 phase. The GL-method seems to provide better and more stable results in the case of an initial situation with a slope. Therefore, the GL method is recommended in the case of initial situation with a slope, unfortunately this method does not include the stress history, while in fact the stress history is essential in the case of old quay walls, especially with the excavation of the canals that took place.

If the initial situation is related to practice, the K0-procedure with horizontal layers is the best way to consider the initial situation. After all, the construction of historic quay walls took place with an initial situation in which the soil layers are horizontal as illustrated in Section 5.2 and appendix J.

5.6 Sensitivity Analysis (simulation 4)

For simulation 4, a sensitivity analysis is conducted to analyze the influence on the output results of the foundation piles, in which the anisotropy parameters of the S-Clay1 model considered in Hollandveen are varied and output results (normal forces, shear forces, bending moments, horizontal deformation) are examined in pile 2. Furthermore, it is examined to what extent this influences effective principal stress development in the soil body at x = 4 m and y = -1 m to -7 m.

Table 5.4. The varied anisotropic parameters values for the sensitivity analysis

Case	α_0 [-]	ω [-]	ω_d [-]
1	[0.0, 0.25, 0.59,1.0]	17	1.0
2	0.59	[0.0,17,34,200]	1.0
3	0.59	17	[0.0,0.5,1.0]

In Figure 5.39 the output results are shown for the cases in table 5.4. The graphs are identical, therefore there is no legend included for the different cases of Table 5.6. Varying the anisotropy parameters has no influence on the output results for pile 2 or on the effective principal stresses at the line cross-section. With the S-Clay1 model, no plasticity occurs in Hollandveen and the soil behavior is therefore elastic (Figure 5.41). Variation in the elastic unloading-reloading parameter, κ*, determines the change in the

output results which is kept constant in this case, hence no changes occur when varying the anisotropy parameters. Soil behavior with the S-Clay1 model is indeed elastic as κ* is changed from 0.021 to 0.01 and it becomes evident from Figure 5.39 that the output results in pile 2 decrease, as the soil has become stiffer. The effective principal stress paths are influenced as well upon varying of κ*.

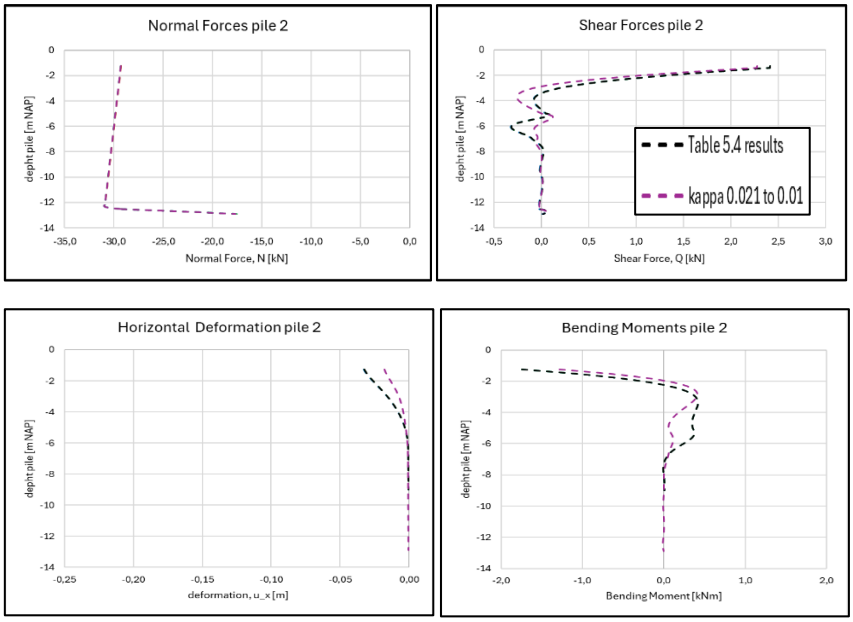

Figure 5.39. Output results for pile 2 for all cases of table 5.4 and κ = 0.021 to 0.01*

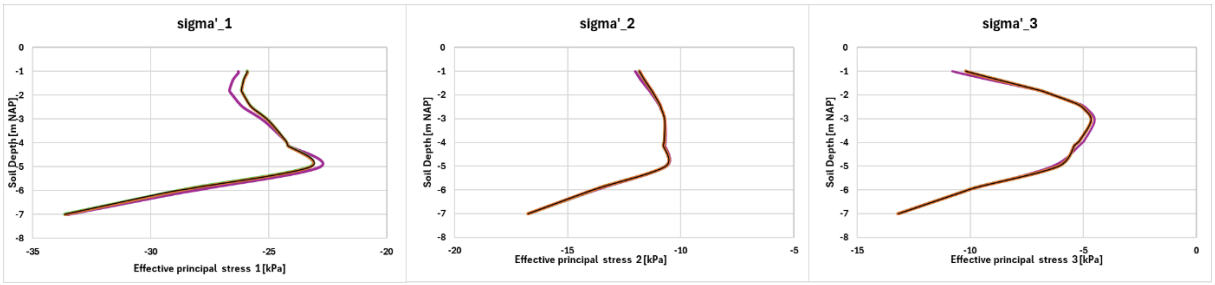

Figure 5.40. Effective principal stress development in the SLS1 at x = 4 m and y = -1 m to -7 m.

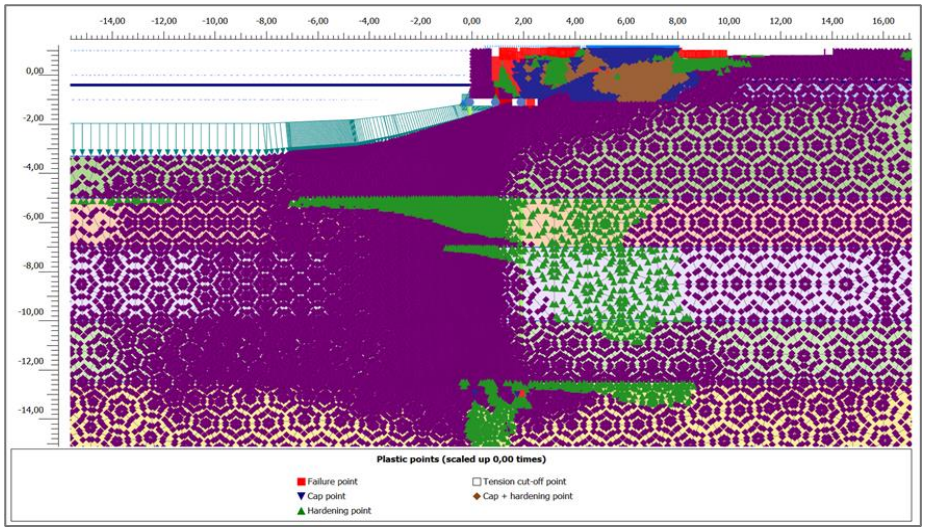

Figure 5.41. Plastic and elastic points (purple) output results with S-Clay1 model Hollandveen

6. Discussion, Conclusions and Recommendations

In this chapter, a discussion is given on the assumptions and simplifications in this study, answers are given to the sub-research questions and to the main question based on the findings of this research after which recommendations are provided to improve the quality of the findings in further research.

6.1 Discussion

The first point of discussion is the Soft Soil model included in TAK 3.2 and the consideration of the Soft Soil model in this study as well, although literature explicitly suggests that this material model is unsuitable for unloading stress paths, since this material model considers unloading stress paths as elastic and the advances of this model are constituted on compression stress paths. In the staged construction of the historic quay walls, unloading stress paths occur when excavating the canal and the construction pit, followed by reloading (water entering the canal and refilling the construction pit). The suitability of the Soft Soil model for correctly simulating these stages is in question.

The second point of discussion are the material models considered for the soil layers in the eight FEM-simulations. The material models with different parameter sets have been chosen in such a way to provide a good insight into the changes that occur in output results with different parameter sets. Multiple combinations of material models considered in the soil layers are possible, where it can be opted for each soil layer, to consider the material model and parameter set that yields the best fit in the strain versus stress graphs.

The third point is the fact that the material model parameters in this study have been determined based on available laboratory results from Kloveniersburgwal (quay wall) and these parameters are used in the case study for which the quay wall in Plaxis 2D is constructed based on the quay wall at Herengracht. Ideally, the material model parameters come from laboratory results from the same location as the case study.

The fourth point is the S-Clay1 model, which is reasoned to give promising results, but with necessary caution, as the target values (3q/4p' and q/ 3p') in Equation 2.28 for the evolution of anisotropy are based on findings for Otaniemi clay and not for clay/peat in the center of Amsterdam/the Netherlands.

The final point of discussion is the order of the phases included in the staged construction of the historic quay wall, in which the canal is first excavated and then the quay wall is constructed, while archive drawings show a different order, in which the quay wall is constructed first, whereafter the canal is excavated. The difference in the order of the phases can certainly have consequences for the output results.

6.2 Conclusions

What are the criteria in choosing a suitable constitutive model for geotechnical finite element method analyses?

Considering loading scenarios such as shearing, compression, and extension that occur in the staged historic quay wall assessment in Plaxis 2D, it is concluded that the features of the Hardening Soil (small strain) model are best tailored to the situation for the assessment of historic quay walls in Amsterdam. The HSss model includes a shear hardening and compaction hardening rule, and a more accurate

description of stiffnesses by defining three different stiffness parameters (secant stiffness, unloading-reloading stiffness from triaxial test and the oedometer stiffness from 1D compression test), making it a more favorable isotropic material model over the Soft Soil model, which is only based on a compaction hardening rule and two stiffness parameters (compression index and swelling index) obtained from 1D oedometer test.

The Soft Soil model (PLAXIS, Material Models Manual, 2023) and S-Clay1 model (Wheeler J. , Näätänen, Karstunen, & Lojander, 2003) are unsuitable for strictly unloading scenarios (excavations), because of isotropic elastic behavior in unloading scenarios. Difficulties are experienced with the Soft Soil model in the calculation of the excavation phase, even in simulations where the initial situation starts with a slope, errors are encountered during the excavation phase of the construction pit.

Isotropic soil behavior happens sporadically, especially in the case of retaining structures where soil behavior is rather anisotropic, hence the interest in including anisotropic models such as the Sekiguchi-Ohta and the S-Clay1 model in this study. Preference is given to the S-Clay1 model, because of the explicit anisotropic parameters considered in the model which provide more insight into the behavior of the material, and consideration of extension in soil through the approximation of the critical state line parameter, M_e.

How should laboratory tests be interpreted to derive the appropriate model parameters for the corresponding constitutive soil model? **and** *What methods can be employed to validate selected model parameters for different constitutive soil models in geotechnical finite element method analyses?*

Despite the lack of necessary laboratory test results to obtain certain material model parameters, realistic estimates can be made by choosing the Poisson's ratio equal to 0.2 based on research of Mayne, Coop, Springman, Huang, & Zornberg (2009), approximation of the earth pressure coefficient based on Jaky's formula (1948), determination of the HSss model drained stiffness parameters with the guidelines from Plaxis manual (2023), the relations of Obrzud & Truty (2018) and the small strain parameters with the approximations of B. Hardin and W. Black (1969), determination of the 1-Dimensional stiffness parameters for the Soft Soil, Sekiguchi-Ohta and S-Clay1 model using Bjerrum one dimensional parameters, and estimation of the anisotropy parameters using the guidelines of Wheeler et al. (2003) and Leoni et al. (2008).

The stiffness parameters for the Soft Soil model, Sekiguchi-Ohta model and S-Clay1 model can be easily determined with the oedometer test and the strength parameters with triaxial and DSS tests. The stiffness parameters of the HSss model can be determined from triaxial test results. With the anisotropic models, performing isotropically consolidated triaxial test simulations in PST anomalous results are obtained. The DSS test provides the opportunity to perform K0-consolidation PST simulations, yielding improved results.

Validating the material model parameters using graphs from PST simulations against graphs from measured laboratory data from the representative test at three consolidation stresses is a suitable method, since the maximum deviatoric stress is more or less well estimated, especially for Oude zeeklei and Hollandveen. There is a significant discrepancy in stiffnesses between grahps from PST and graphs from measured laboratory data, but by optimizing the parameter set the PST graphs are better fitted to the graphs from measured lab data.

How do the structural forces in the wooden foundation piles differ, with the considered constitutive models, when applying the standard approach for historical quay wall assessment according to Toetskader Amsterdamse Kademuren 3.2 in Plaxis 2D?

Simulations 1-4, predominantly performed with the HSss model with different parameter sets (TAK 3.2, Study, Optimized, Anisotropy HV) in which simulation 2 is performed with stiffnesses almost twice as high and a significantly lower effective cohesion as considered in simulation 1 in Oude zeeklei,

approximately the same progression of bending moments is observed in the piles in Oude zeeklei and Hollandveen. Parameter sets with completely different parameter values, can yield approximately the same output results, meaning that if the effective cohesion and internal friction angle are greater in one simulation, but the stiffness parameters are lower and in the other simulation the stiffness parameters are higher, but the effective cohesion and internal friction angle are lower, approximately the same output results can be found.

Between simulations 1-4 and simulations 5-8 in which for the latter predominantly the Soft Soil model is considered, the optimized parameters result in a reduction for simulations 1-4 and an increase for simulations 5-8 in output results. Despite the HSss model and the SS model yielding approximately identical results in chapter 4 in terms of maximum deviatoric stress, a significant difference is observed in the results of the maximum bending moments in the piles (Figure 5.10 and Figure 5.25) and the horizontal deformation (Figure 5.11 and Figure 5.26), but the maximum deformations of the pile head are identical in simulations 3 and 7 (Optimized) and in simulations 4 and 8 (Anisotropy HV).

The S-Clay1 model enhances the soil, hence a significant reduction is observed in the output results of the piles, however, it has become evident that the soil behavior is elastic, rather than plastic in the soil layer in which this model is considered. Furthermore, it is observed with the S-Clay1 model that adjustment of the anisotropy parameters has no influence on the output results given, because of elastic behavior in which the anisotropy parameters play no role.

What is the influence of different ways of modelling the initial situation of an existing retaining wall in Plaxis 2D?

Initial phase

In case the K0-procedure with horizontal layers is used in the initial phase, the development of σ_1' appears to be independent of the considered material model, but σ_2' and σ_3' are dependent on the considered material model. When implementing the K0-procedure with plastic-0-step in the initial situation with a slope, there is dependence on the considered material model as different developments of σ_1', σ_2' and σ_3' are observed. The differences in the K0-procedure with plastic-0-step may come from equilibrium which has not been sufficiently obtained by the plastic-0-step calculation. In the case of Gravity loading method with an initial situation with a slope, approximately the same progression of σ_1' and σ_2' is found between both simulations, but σ_3' differs.

Serviceability Limit State (SLS1) phase

In the SLS, an initial calculation with GL seems to give a more numerically stable progression than the K0 procedure with slope. In case the initial phase starts with a slope, a significant increase bending moments and horizontal deformations is observed. In practice the initial situation for the historic quay walls of Amsterdam consisted of horizontal soil layers, with a horizontal surface making the initial phase with the K0-procedure and horizontal layers the best choice for the determination of the initial phase. Furthermore, the K0-procedure includes the stress history of soil, which is essential in the case of historic quay walls, especially with the excavation of the canal in the past.

Main research question:

How can the current parameter set, as given in Toetskader Amsterdamse Kademuren 3.2, of the most influencing Holocene soil layers for Historical Quay Wall Assessment be improved based on a better selection of parameters and by taking into consideration the applied constitutive soil models?

The Hardening Soil small strain model is preferred in the assessment of the historic quay walls for Amsterdam. The axial strain levels are unknown for which the current parameter set of the HSss model included in TAK 3.2 is determined. It is important to conduct the assessment of the historic quay walls with a material parameter set tailored to the maximum deviatoric stress, as failure of the quay wall

occurs after reaching the maximum absorbable deviatoric stress. To assure that the strength parameters in TAK 3.2 have been determined at the maximum strength of the soil, the strength parameters of the Soft Soil model in TAK 3.2 can be permanently included in the HSss model parameters.

In case unsatisfactory results are obtained in the assessment of the historic quay wall with the parameter set from TAK 3.2, a parameter set can be determined based on laboratory results from the concerned location and these parameters can be further optimized using representative test results and Plaxis Soiltest, as conducted in this study.

Upon examination of the FEM-calculation results, it becomes evident that the largest structural forces and deformations occur mainly in Hollandveen, which makes it more important to compile improved material parameter sets for Hollandveen rather than Geulopvulling and Oude zeeklei. In Oude zeeklei no significant differences are observed in output results between simulations (1-3) with parameter sets that do contain significant differences in parameter values for the HSss model.

Furthermore, it is a good prospect as well to consider a material model such as the S-Clay1 model, since the soil behavior in especially soft soils is anisotropic rather than isotropic. The results with the S-Clay1 model in Hollandveen strengthen the soil behavior and decreased structural forces and deformations are observed in the piles, compared to the results of an isotropic HSss model.

6.3 Recommendations

The recommendations are divided into recommendations regarding the analysis that has been carried out in this study and recommendations regarding the improvement of TAK3.2. This list of recommendations may be of added value if this research is further expanded.

Recommendations regarding this study:

- Ideally for the HSss model to perform drained triaxial tests, since the reference secant stiffness, E_{50}^{ref}, is in terms of effective stress. The linear Equation 3.4 is used to go from undrained to drained reference secant stiffness. The difference in values of drained secant stiffness between the method using the linear equation and by performing a drained triaxial test can be determined and judgement can be given if the reference secant stiffness is reasonably estimated with the equation.
- For the unloading-reloading stiffness, E_{ur}^{ref}, of the HSss model, perform isotropically consolidated drained compression triaxial tests with unloading/reloading phase at the required stress level, since the unloading-reloading stiffness is in terms of effective stress as well.
- Include material model parameters obtained from triaxial extension tests in the phases in which unloading takes place during staged construction.
- Carrying out anisotropically consolidated triaxial compression tests on Geulopvulling and Oude zeeklei, which allows the S-Clay1 model to be validated with more certainty against laboratory results, without turning off the initial anisotropy parameter, α_0.
- The oedometer stiffness parameters (λ^*, κ^*) are optimized in PST using triaxial test simulations and laboratory results, but it is recommended to fit the oedometer test results from the laboratory with PST oedometer simulations and analyze the results obtained with this parameter set for FEM-simulations.
- Consider an additional laboratory test as representative test and perform PST simulations to verify the representativeness of the derived parameter set for the entire soil layer.

Recommendations regarding the improvement of TAK 3.2:

- Compiling a material model parameter set for the HSss model with characteristic values at maximum deviatoric stress.
- Excluding the initial phase with a slope and plastic-0-step and consider the K0-procedure with horizontal soil layers and surface.
- Revising the sequence in the phases of the staged construction (excavation of the canal and construction of the quay wall).

References

Alkema, S. H. (2018). *Influence of the initial soil stress state on the cone factor.*

Backhausen, U., & van der Stoel, A. (2014). *Reader Geotechniek voor het HBO.* Denhaag: KIVI.

Benz, T. (2006). *Small-Strain Stiffness of Soils and its Numerical Consequences.*

Brinkgreve, R. B. (1994). *Geomaterial Models and Numerical Analysis of Softening.* Delft.

Brinkgreve, R. B. (2021). TUDelft Lectures Behaviour of Soils and Rocks. Delft.

Brinkgreve, R. (z.d.). *Materiaalmodellen voor grond en gesteente.*

Chao, C., Jommi, C., & Muraro, S. (2023). Numerical investigation of the equipment set-up in triaxial testing of soft soils. *In 10th European Conference on Numerical Methods in Geotechnical Engineering.* London: Edited by K. Zdravkovic, Taborda, Tsiampous.

Correia, A., Santos, J., Barros, C., & Niyama, S. (2001). An Approach To Predict Shear Modulus of Soils in the Range of 10^-6 to 10^-2 Strain Levels. *Proceedings: Fourth International Conference on Recent Advances in Geotechnical Earthquake Engineering and Soil Dynamics*.

de Gans, W. (2011). *De Bodem onder Amsterdam; Een geologische wandeling.*

Duncan, M., & Chang, C. (1970). Non Linear Analysis of Stress and Strains in Soils. *Soil Mechanics and Foundations Division,* 1629-1651.

Hardin, B., & Black, W. (1969). Vibration Modulus of Normally Consolidated Clay. *Journal of the Soil Mechanics and Foundations Division 94(2)*.

Hardin, B., & Drnevich, V. (1972). Shear modulus and damping in soils: Design equations and curves.Proc. ASCE. *Journal of the Soil Mechanics and Foundations Division,* 667-692.

Janbu, N. (1985). Soil models in offshore engineering. *Geotechnique volume 35* (pp. 241-281). Thomas Telford Ltd.

Karstunen, M., & Amavasai, A. (2017). *Best Soil: Soft Soil modelling and parameter determination.* Sweden.

Lefebvre, G., Langlois, P., Lupien, C., & Lavallée, J. G. (1984). Laboratory testing and in situ behaviour of peat as embankment foundation. *Canadian Geotechnical Journal 21(2),* 322–337.

Leoni, M., Karstunen, M., & Vermeer, P. A. (2008). Anisotropic creep model for soft soils. *Ge´otechnique 58, No. 3,* 215–226.

Mayne, P., Coop, M., Springman, S., Huang, A., & Zornberg, J. (2009). State-of-the-art paper (soa-1): Geomaterial behavior and testing. *In ICSMGE, editor, 17th Int Conf Soil Mech And Geotech Engng,* (pp. volume 4, 2777-2872). Alexandria, Egypt: Millpress/IOS Press Rotterdam.

Muir Wood, D. (1990). Soil Behaviour and Critical State Soil Mechanics. *Cambridge University Press 1*, 355-358.

Muraro, S. (2019). *The deviatoric behaviour of peat: A route between past empiricism and future perspectives (PhD dissertation).* Delft: Delft University of Technology.

Muraro, S., & Jommi, C. (2020). Pre-failure behaviour of reconstituted peats in triaxial compression. *Acta Geotechnica 16(3),* 789–805.

Neijzing, L., Cherkaoui, A., Pijpers, R., & Weststein, R. (2023). *Toetskader Amsterdamse Kademuren TAK 3.2.* Amsterdam.

Obrzud, R. F., & Truty, A. (2018). *The Hardening Soil Model- A Practical Guidebook.* Switzerland: Zace Services Ltd.

PLAXIS. (2020). *Plaxis 2D; Reference Manual.*

PLAXIS. (2023). *Material Models Manual.*

Post, M., & Luijendijk, M. S. (2018). *POV-M Parameterbepaling Deltares.*

Prins, J., Spannenburg, T. M., & Antea Group. (2023). *Toetsing Amsterdamse Kademuren; Rapportage Technisch Advies Kademuur HEG0201.* Amsterdam.

Rowe, P. W. (1962). The Stress-Dilatancy Relation for Static Equilibrium of an Assembly of Particles in Contact.

Santos, J. A., & Correia, A. G. (2001). Reference threshold shear strain of soil. its application to obtain a unique strain-dependent shear modulus curve for soil. *15th International Conference on Soil Mechanics and Geotechnical Engineering*, (pp. volume 1, 267-270). Istanbul, Turkey.

Schanz, T., & Vermeer, P. (1996). *Angles of friction and dilatancy of sand.*

Schanz, T., Vermeer, P., & Bonnier, P. (1999). *The Hardening Soil Model: Formulation and verification.* Rotterdam: Balkema.

Smits, E. (1999). *OMEGAM (12)11.435 Parameterset Holocene grondlagen Noord Zuidlijn.*

van Duinen, A. (2014). *Handreiking voor het bepalen van schuifsterkte parameters, WTI 2017.* Deltares.

Van oorsprong tot heden: de evolutie van de Amsterdamse kademuren. (n.d.). Retrieved from kade2020.nl: https://kade2020.nl/kademuren-amsterdam/#:~:text=De%20eerste%20stenen%20kademuur%20werd,kilometer%20%C3%A9cht%20aan%20vervanging%20toe.

Verruijt, A. (2012). *Soil Mechanics.* Delft .

Verweij, A. (2023). *Grondparameters TAK 3.2.*

Wheeler, J., Näätänen, A., Karstunen, M., & Lojander, M. (2003). An anisotropic elastoplastic model for soft clays. *Canadian Geotechnical Journal vol.40*, 403-418.

Wheeler, S. J., Cudny, M., Neher, H., & Wiltafsky, C. (2003). *Some developments in constitutive modelling of soft clays.*

Wheeler, S., Näätänen, A., Karstunen, M., & Lojander, M. (2003). An anisotropic elastoplastic model for soft clays. *Canada Geotechnical Journal vol. 40*, 403-418.

A. Geulopvulling laboratory results

Samples M002-b1, M002-b2, M003-b2 (black lines) were not considered in the determination of parameters due to the abnormal course of the graphs at given consolidation stresses in the triaxial test (Attachment figure A.1). The course of the graph could be associated with an incorrect estimation of the in-situ stress and the chosen consolidation stresses.

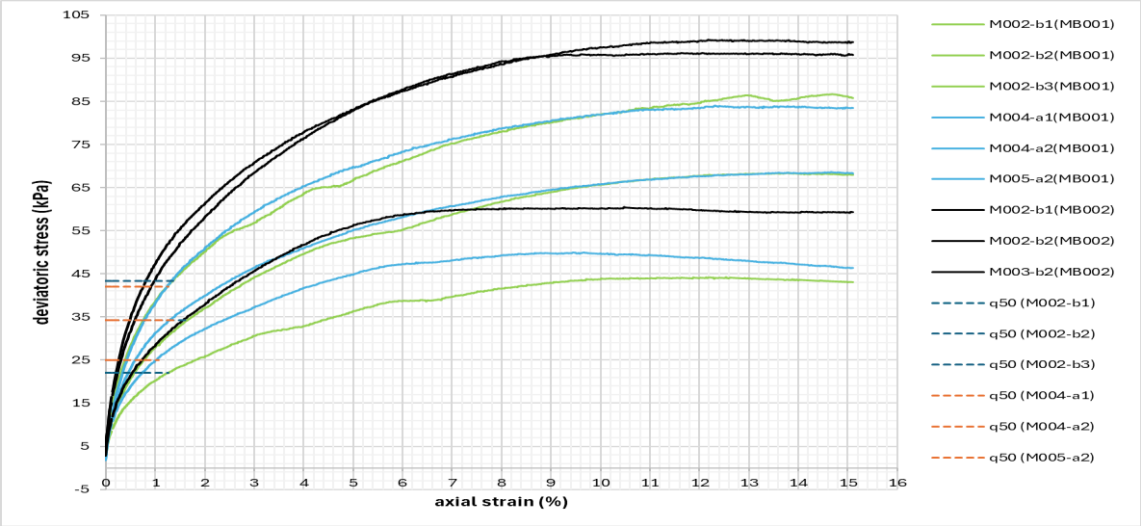

Attachment figure A.1. Deviatoric stress vs. Axial strain from triaxial tests Geulopvulling

Attachment table A.1. Sample properties and strength parameters Geulopvulling.

					Peak deviator stress		Regression	
Bore #	Sample #	Depth [mNAP]	Initial sat. density [kN/m^3]	Consolidation stress [kPa]	ϕ' [°]	c' [kPa]	ϕ' [°]	c' [kPa]
MB001 (KBW0301-LB01)	M004-a1	-2.71 to -2.79	13.83	29	33.48	10.39	36.87	8
MB001 (KBW0301-LB01)	M004-a2	-2.87 to -2.95	12.50	59	33.48	10.39	36.87	8
MB001 (KBW0301-LB01)	M005-a2	-3.10 to -3.18	11.27	88	33.48	10.39	36.87	8
MB001 (KBW0301-LB01)	M002-b1	-1.90 to -1.97	12.22	25	42.36	3.6	36.87	8
MB001 (KBW0301-LB01)	M002-b2	-1.97 to -2.05	12.23	50	42.36	3.6	36.87	8
MB001 (KBW0301-LB01)	M002-b3	-2.05 to -2.13	12.10	76	42.36	3.6	36.87	8
*[2] MB002 (KBW0201-LB02)	M002-b1	-1.87 to -1.95	11.72	25	*[1]	*[1]	36.87	8
*[2] MB002 (KBW0201-LB02)	M002-b2	-1.95 to -2.03	12.49	50	*[1]	*[1]	36.87	8
*[2] MB002 (KBW0201-LB02)	M003-b2	-2.14 to -2.22	12.19	76	*[1]	*[1]	36.87	8

*[1] cannot be determined; *[2] Not considered in the analysis; Triaxial: page 308; 317; 362 Kloveniersburgwal report.

The cohesion and internal friction angle of samples from borehole MB002 (KBW0201-LB02) cannot be determined in the event of failure due to the undesirable spread of the Mohr circles (Attachment figure A.2). Failure occurs at different strain levels, so such a phenomenon is not strange.

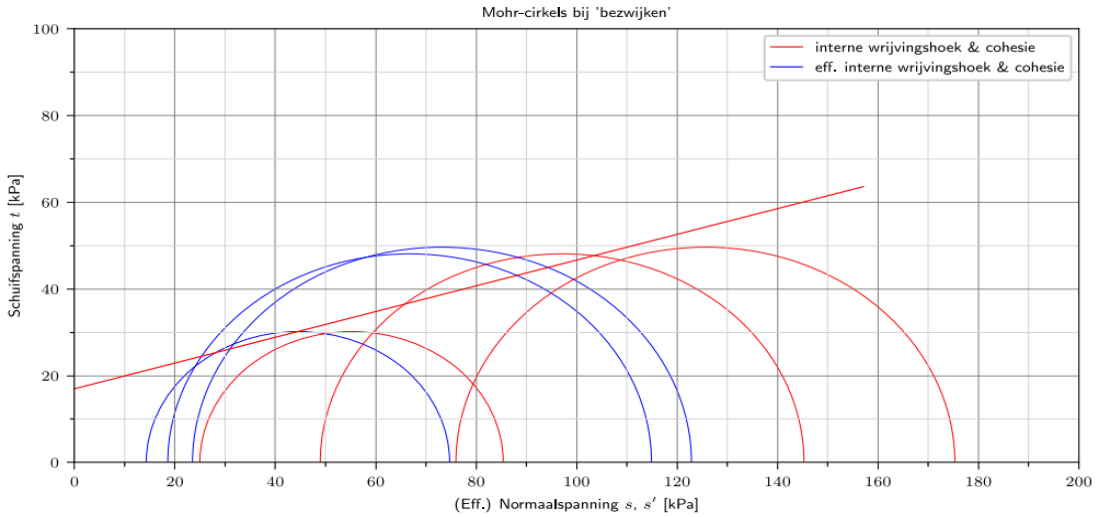

Attachment figure A.2. Mohr Circles samples MB002 (KBW0201-LB02) at failure

Determination of stiffness exponent parameter, m, conform the procedure in Section 3.4, as shown in Attachment figure A.3 **.**

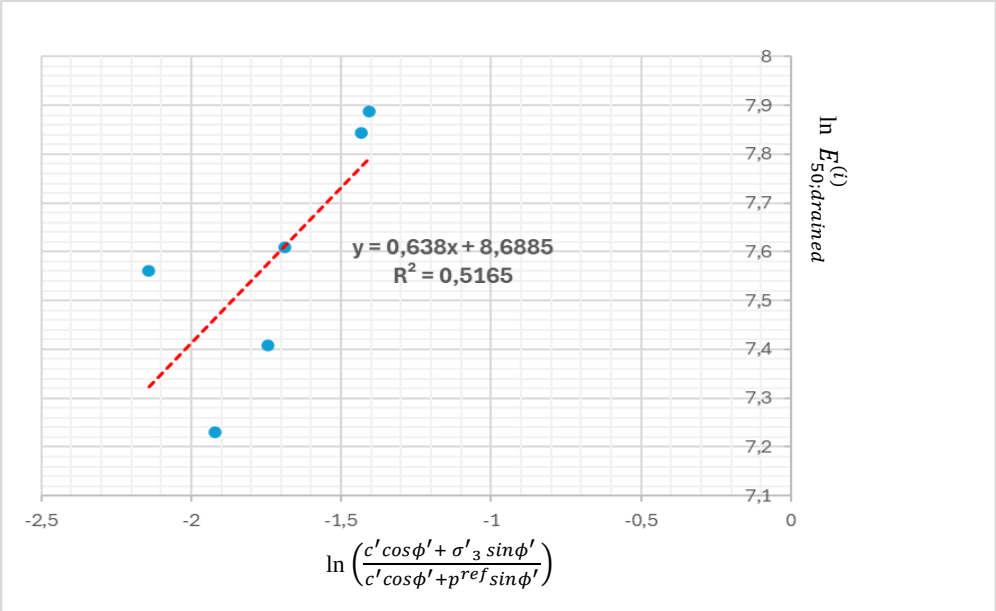

Attachment figure A.3. Stiffness exponent parameter, m, Geulopvulling.

Determination of strength parameters, c' and ϕ', conform the procedure in Section 3.4, as shown in Attachment figure A.4**.**

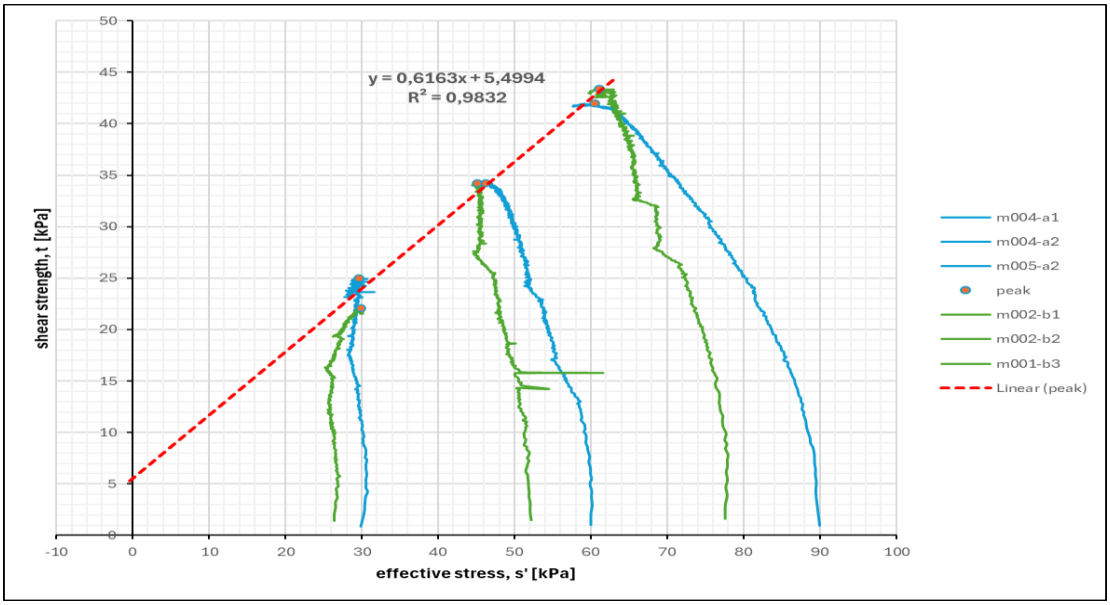

Attachment figure A.4. Linear regression to obtain strength parameters Geulopvulling

Geulopvulling stiffness model parameters for each sample given in Attachment table A.2**.**

Attachment table A.2. Stiffness parameters and coefficient of lateral earth pressure for Geulopvulling

Bore #	Sample #	$E_{50;undr}$ $[kPa]$	$E_{50;dr}$ $[kPa]$	$E_{50;dr}^{ref}$ $[kPa]$	$E_{ur;dr}^{ref}$ $[kPa]$	K_0^{nc} [-]	m	G_0^{ref} [kPa]	$\gamma_{0.7}$[-] *10^{-4}
MB001 (KBW0301-LB01)	M004-a1	1726,56	1381.25	4911.55	17190	0.4	0.64	17190	4.2
MB001 (KBW0301-LB01)	M004-a2	2060,24	1648.19	5207.19	18225	0.4	0.64	18225	5.6
MB001 (KBW0301-LB01)	M005-a2	3183.82	2547.06	6552.85	22935	0.4	0.64	22935	5.7
MB001 (KBW0301-LB01)	M002-b1	2403.85	1923.08	7898.53	27645	0.4	0.64	27645	2.7
MB001 (KBW0301-LB01)	M002-b2	2522.06	2017.65	6140.81	21493	0.4	0.64	21493	4.8
MB001 (KBW0301-LB01)	M002-b3	3333.33	2666.67	6740.41	23591	0.4	0.64	23591	5.5
Average		2538	2031	6242	21847	0.4	0.64	21847	4.8

The stiffness parameters for soft soil, Sekiguchi-Ohta and sclay1 models, are obtained from oedometer results on Geulopvulling via the relations with the NEN Bjerrum parameters Cc and Cs, shown in Attachment table A.3.

Attachment table A.3. Oedometer sample properties and stiffness parameters Geulopvulling

Bore #	Sample #	Depth [m NAP]	Ini. Sat. Weight [kN/m^3]	e_0 [-]	In situ stress [kPa]	Pre-cons.stress [kPa] Bjerrum	OCR [-]	Cc [-]	Cs [-]	λ^* [-]	κ^* [-]	$\lambda^*/\ \kappa^*$	E_{oed}^{ref} [kPa]
MB001 (KBW03 01-LB01)	M001-b1	-1.78 tot -1.82	12.88	2.85	34.7	39.4	1.14	0.698	0.0599	0.079	0.0135	5.85	1094
MB001 (KBW03 01-LB01)	M004-a3	- 2.83 tot -2.87	12.73	3.44	38.4	38.9	1.01	1.085	0.1033	0.106	0.0202	5.25	1100
MB002 (KBW02 01-LB02)	M003-b1	- 2.27 tot -2.31	11.81	3.40	40.1	43.1	1.07	0.810	0.0948	0.080	0.0188	4.26	833
Average	-	-	12.47	-	-	-	1.07	-	-	0.088	0.0175	5.12	1009

Oedometer p. 97; 111; 167

Attachment figure A.5. Oedometer test results and reference oedometer moduli Geulopvulling illustrates how the reference oedometer moduli are obtained from the experimental results.

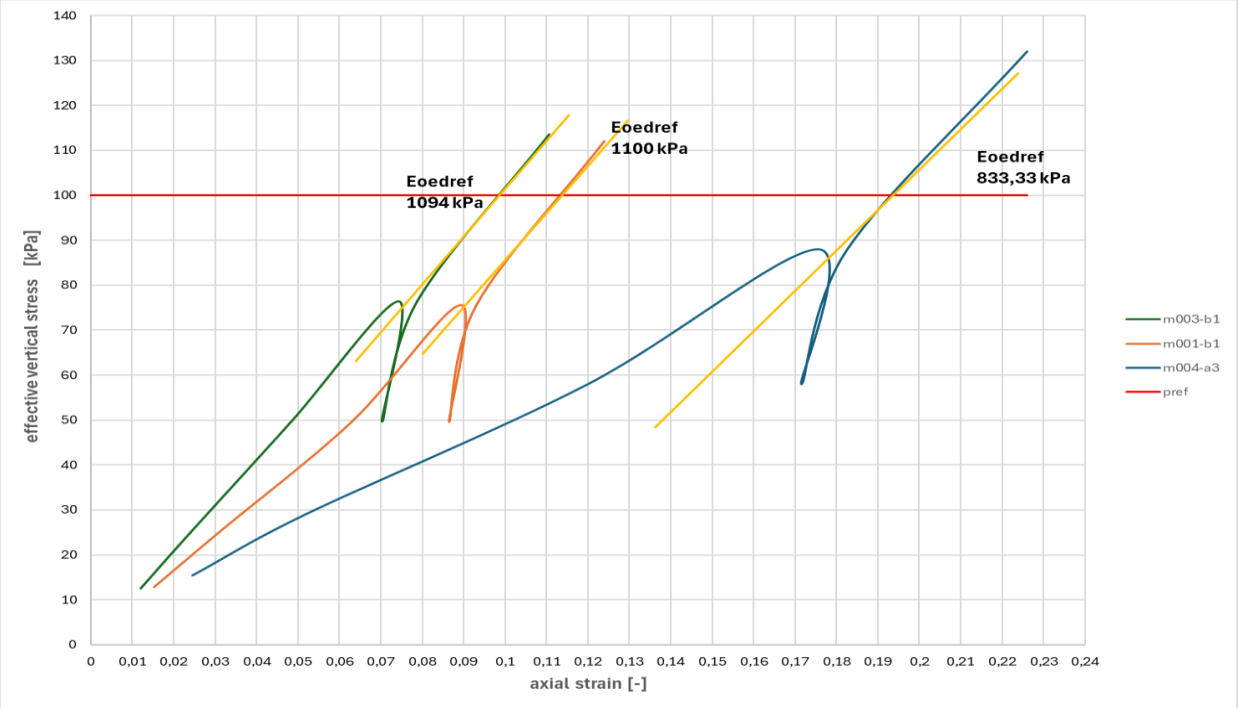

Attachment figure A.5. Oedometer test results and reference oedometer moduli Geulopvulling

B. Oude Zeeklei laboratory results

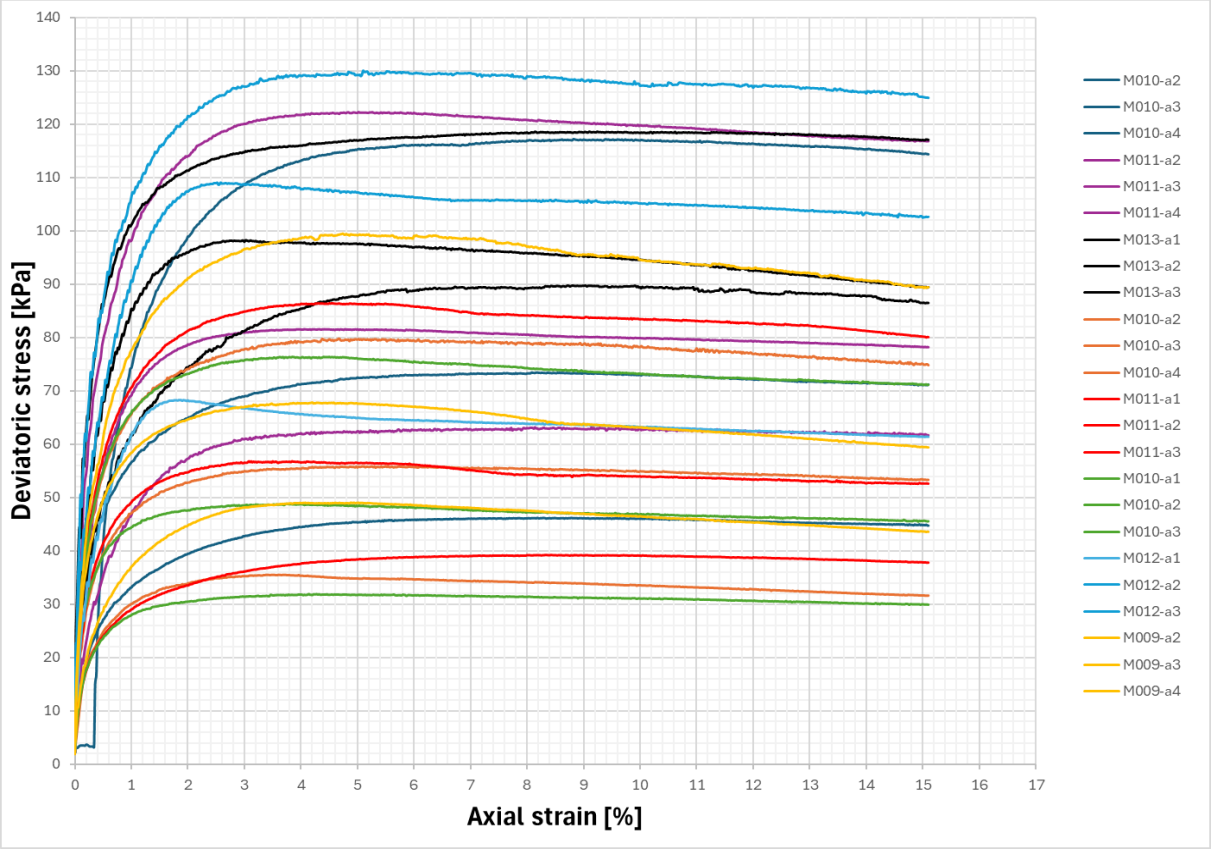

Attachment figure B.1. Deviatoric stress vs. Axial strain from triaxial tests Oude zeeklei Landside

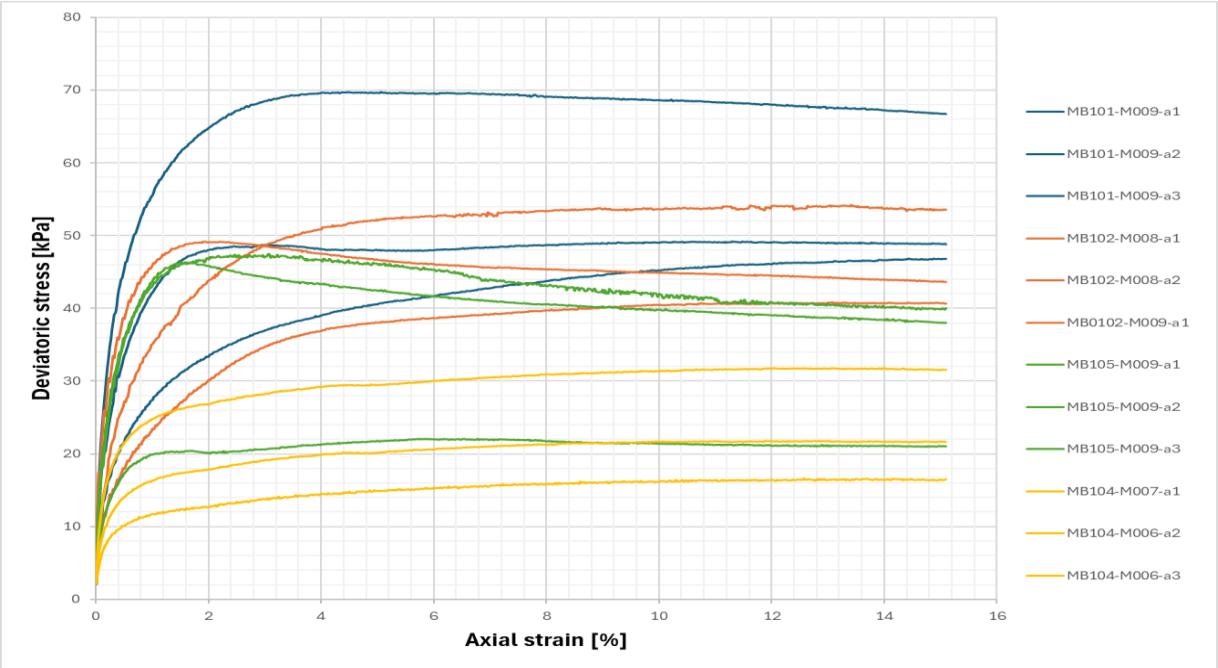

Attachment figure B.2. Deviatoric stress vs. Axial strain from triaxial tests Oude zeeklei Waterside

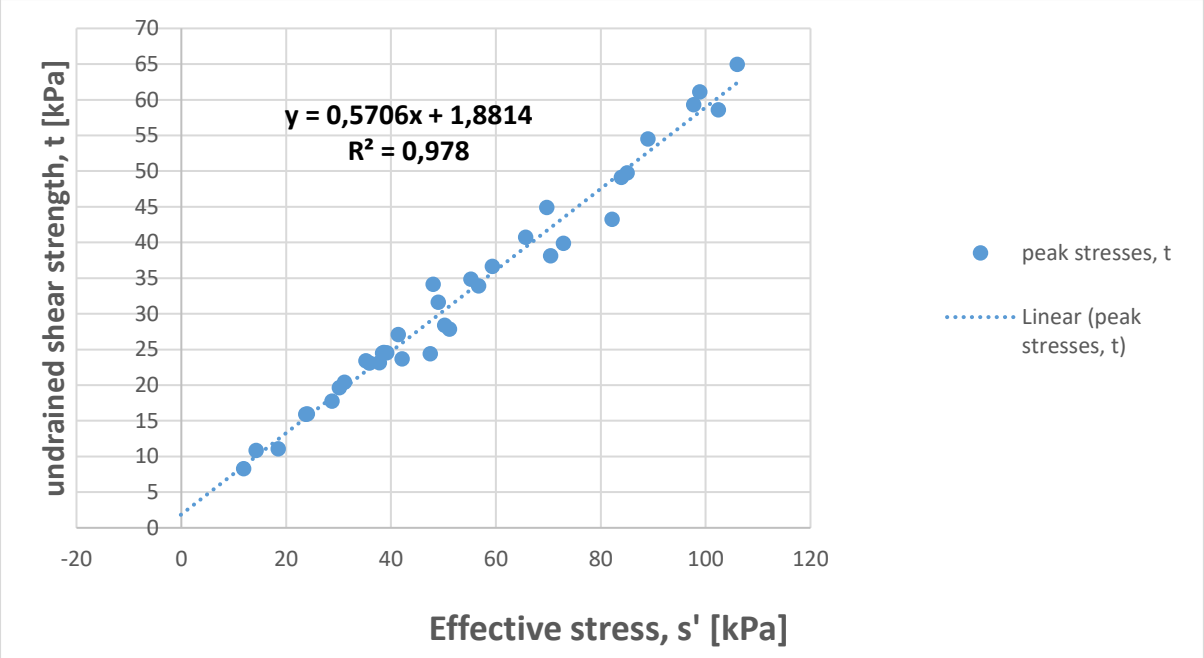

Attachment figure B.3. Linear regression to obtain strength parameters Oude zeeklei

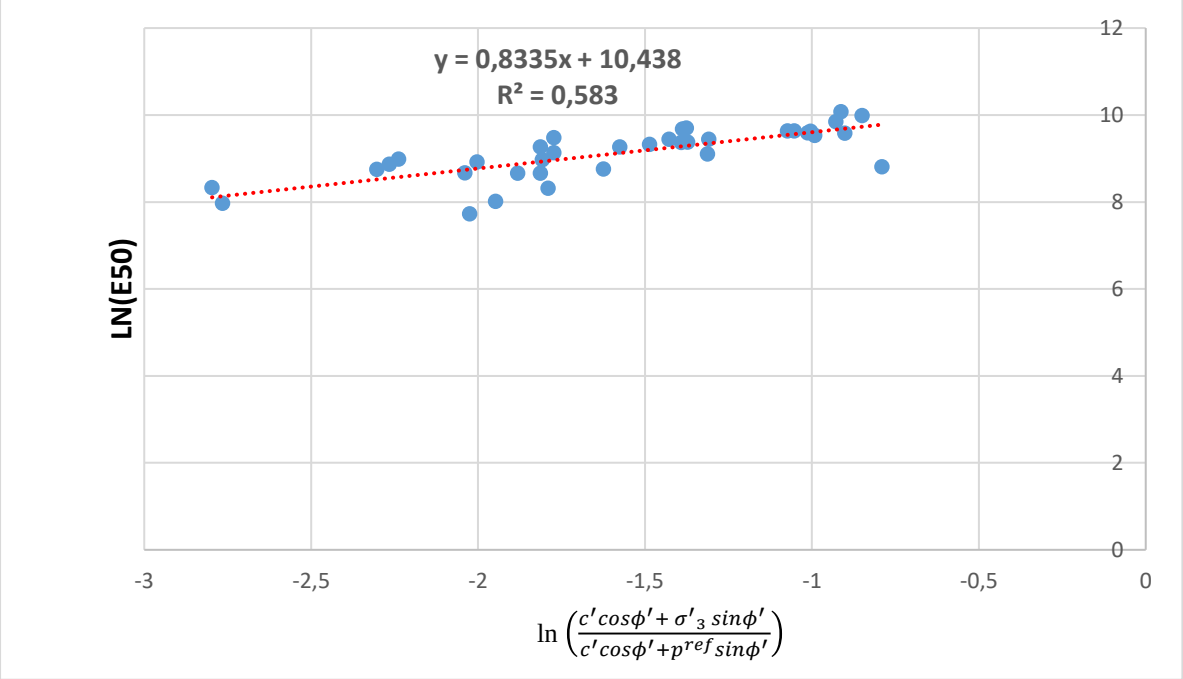

Attachment figure B.4. Stiffness exponent parameter, m, Oude zeeklei.

Attachment table B.1. Sample properties and strength parameters Oude zeeklei

						Peak deviator stress		Regression	
Bore # (Land)	Sample #	Depth (m NAP)	Initial Volumetric weight [kN/m^3]	Void ratio e_0 [-]	Consolidation stress [kPa]	ϕ' [°]	c' [kPa]	ϕ' [°]	c' [kPa]
MB001(KBW0301-LB01)	M010-a2	-5.14	16.54	1,41	38	32.06	5.30	34.82	2
MB001(KBW0301-LB01)	M010-a3		16.37	1,42	76	32.06	5.30	34.82	2
MB001(KBW0301-LB01)	M010-a4	-5.44	17.06	1,20	133	32.06	5.30	34.82	2
MB001(KBW0301-LB01)	M011-a2	-5.54	16.15	1,52	39	36.51	2.67	34.82	2
MB001(KBW0301-LB01)	M011-a3		15.92	1,56	78	36.51	2.67	34.82	2
MB001(KBW0301-LB01)	M011-a4	-5.84	17.18	1,22	118	36.51	2.67	34.82	2
MB001(KBW0301-LB01)	M013-a1	-6.30	15.89	1,61	46	30.18	10.39	34.82	2
MB001(KBW0301-LB01)	M013-a2		15.36	1,84	92	30.18	10.39	34.82	2
MB001(KBW0301-LB01)	M013-a3	-6.63	16.53	1,44	139	30.18	10.39	34.82	2
MB002(KBW0201-LB02)	M010-a2	-4.87	15.82	1,66	35	30.02	3.54	34.82	2
MB002(KBW0201-LB02)	M010-a3		15.98	1,55	70	30.02	3.54	34.82	2
MB002(KBW0201-LB02)	M010-a4	-5.20	15.94	1,57	105	30.02	3.54	34.82	2
MB002(KBW0201-LB02)	M011-a1	-5.25	16.22	1,55	38	27.03	6.52	34.82	2
MB002(KBW0201-LB02)	M011-a2		16.03	1,48	76	27.03	6.52	34.82	2
MB002(KBW0201-LB02)	M011-a3	-5.55	15.05	1,88	113	27.03	6.52	34.82	2
MB003(KBW0101-LB03)	M010-a1	-5.03	15.89	1,60	34	28.41	4.16	34.82	2
MB003(KBW0101-LB03)	M010-a2		16.29	1,45	67	28.41	4.16	34.82	2
MB003(KBW0101-LB03)	M010-a3	-5.33	16.21	1,45	101	28.41	4.16	34.82	2
MB003(KBW0101-LB03)	M012-a1	-5.84	16.20	1,48	39	31.60	10.25	34.82	2
MB003(KBW0101-LB03)	M012-a2		16.67	1,26	78	31.60	10.25	34.82	2
MB003(KBW0101-LB03)	M012-a3	-6.14	16.50	1,33	118	31.60	10.25	34.82	2
MB004(KBW0102-LB04)	M009-a2	-5.08	16.49	1,38	38	32.86	4.16	34.82	2
MB004(KBW0102-LB04)	M009-a3		16.47	1,39	76	32.86	4.16	34.82	2
MB004(KBW0102-LB04)	M009-a4	-5.41	15.43	1,79	113	32.86	4.16	34.82	2
MB101(KBW0301-WB01)	M009-a1	-6.17	16.43	1,38	21	35.80	3.03	34.82	2
MB101(KBW0301-WB01)	M009-a2		16.34	1,40	42	35.80	3.03	34.82	2
MB101(KBW0301-WB01)	M009-a3	-6.50	16.09	1,54	63	35.80	3.03	34.82	2
MB102(KBW0201-WB02)	M008-a1	-5.61	15.55	1,62	14	37.19	1.92	34.82	2
MB102(KBW0201-WB02)	M008-a2		15.66	1,65	28	37.19	1.92	34.82	2
MB102(KBW0201-WB02)	M009-a1	-6.15	16.32	1,40	42	37.19	1.92	34.82	2
MB105(KBW0202-WB05)	M009-a1	-5.85	14.88	1,48	20	33.84	1.24	34.82	2
MB105(KBW0202-WB05)	M009-a2		15.10	1,71	40	33.84	1.24	34.82	2

MB105(KBW0202-WB05)	M009-a3	-6.18	15.01	1,57	55	33.84	1.24	34.82	2
MB104(KBW0102-WB04)	M007-a1	-5.23	16.31	1,83	11	36.75	2.18	34.82	2
MB104(KBW0102-WB04)	M006-a2		15.59	1,74	22	36.75	2.18	34.82	2
MB104(KBW0102-WB04)	M006-a3	-5.53	15.79	1,84	34	36.75	2.18	34.82	2

Landzijde: Pagina 326; 335; 344; 371; 380; 398; 407; 425; Waterzijde: 452; 479; 515; 524 KBW proefresultaten

Attachment table B.2. Stiffness parameters and coefficient of lateral earth pressure for Oude zeeklei

Bore #	Sample #	$E_{50;undr}$ $[kPa]$	$E_{50;dr}$ $[kPa]$	$E_{50;dr}^{ref}$ $[kPa]$	$E_{ur;dr}^{ref}$ $[MPa]$	K_0^{nc} [-]	m	G_0^{ref} [MPa]	$\gamma_{0.7}$ *10^{-4}[-]
MB001(KBW0301-LB01)	M010-a2	7219	5775	27526	55051	0.415	0.7	33	2,4
MB001(KBW0301-LB01)	M010-a3	14660	11728	37235	74470	0.415	0.7	33	3,9
MB001(KBW0301-LB01)	M010-a4	8371	6697	12905	25810	0.415	0.7	47	4,5
MB001(KBW0301-LB01)	M011-a2	7900	6320	24330	48661	0.415	0.7	28	3,9
MB001(KBW0301-LB01)	M011-a3	15673	12538	37173	74345	0.415	0.7	26	5,5
MB001(KBW0301-LB01)	M011-a4	23500	18800	40610	81220	0.415	0.7	46	4,6
MB001(KBW0301-LB01)	M013-a1	11225	8980	26703	53406	0.415	0.7	23	6,5
MB001(KBW0301-LB01)	M013-a2	18885	15108	34777	69553	0.415	0.7	15	11,8
MB001(KBW0301-LB01)	M013-a3	29650	23720	50618	101237	0.415	0.7	32	6,5
MB002(KBW0201-LB02)	M010-a2	9342	7474	39417	78835	0.415	0.7	21	3,0
MB002(KBW0201-LB02)	M010-a3	14684	11747	36702	73403	0.415	0.7	26	4,1
MB002(KBW0201-LB02)	M010-a4	19000	15200	36440	72880	0.415	0.7	25	5,9
MB002(KBW0201-LB02)	M011-a1	7278	5822	31657	63314	0.415	0.7	26	2,6
MB002(KBW0201-LB02)	M011-a2	15778	12622	41283	82567	0.415	0.7	30	3,6
MB002(KBW0201-LB02)	M011-a3	18021	14417	30459	60918	0.415	0.7	14	12,1
MB003(KBW0101-LB03)	M010-a1	9969	7975	51097	102195	0.415	0.7	24	2,4
MB003(KBW0101-LB03)	M010-a2	20333	16267	50983	101967	0.415	0.7	31	3,1
MB003(KBW0101-LB03)	M010-a3	19075	15260	37187	74375	0.415	0.7	31	4,6
MB003(KBW0101-LB03)	M012-a1	13135	10508	47342	94684	0.415	0.7	30	3,7
MB003(KBW0101-LB03)	M012-a2	18167	14533	33677	67355	0.415	0.7	43	4,4
MB003(KBW0101-LB03)	M012-a3	27063	21650	43834	87668	0.415	0.7	38	5,9
MB004(KBW0102-LB04)	M009-a2	7206	5765	25973	51945	0.415	0.7	35	2,4
MB004(KBW0102-LB04)	M009-a3	19941	15953	50485	100969	0.415	0.7	34	3,5
MB004(KBW0102-LB04)	M009-a4	17155	13724	31248	62496	0.415	0.7	16	10,8
MB101(KBW0301-WB01)	M009-a1	3774	3019	15201	30401	0.439	1.94	35	2,3
MB101(KBW0301-WB01)	M009-a2	9840	7872	35292	70585	0.439	1.94	34	2,6
MB101(KBW0301-WB01)	M009-a3	13940	11152	38287	76573	0.439	1.94	27	4,6

MB102(KBW0201-WB02)	M008-a1	2833	2267	12174	24347	0.439	1.94	23	3,1
MB102(KBW0201-WB02)	M008-a2	5113	4091	18073	36146	0.439	1.94	22	4,3
MB102(KBW0201-WB02)	M009-a1	16367	13093	57023	114047	0.439	1.94	34	2,6
MB105(KBW0202-WB05)	M009-a1	3609	2887	28662	57324	0.439	1.94	30	1,1
MB105(KBW0202-WB05)	M009-a2	5167	4133	42118	84237	0.439	1.94	19	2,0
MB105(KBW0202-WB05)	M009-a3	8833	7067	46331	92662	0.439	1.94	25	2,2
MB104(KBW0102-WB04)	M007-a1	7893	6314	42731	85463	0.439	1.94	15	2,9
MB104(KBW0102-WB04)	M006-a2	11575	9260	40329	80657	0.439	1.94	18	4,6
MB104(KBW0102-WB04)	M006-a3	13167	10533	38962	77925	0.439	1.94	15	6,1
Average		13204	10563	35968 → 14721 landzijde	71936 → 39746.7	0.439	1.94	29	4,5

Attachment table B.3. Oedometer sample properties and stiffness parameters Oude zeeklei

Bore #	Sample #	Depth [m] M.V.	Ini. Sat. Weight [kN/m^3]	e_0 [-]	In-situ stress [kPa]	Pre-cons.stress [kPa] Bjerrum	OCR [-]	Cc [-]	Cs [-]	λ^* [-]	κ^* [-]	$\lambda^*/\ \kappa^*$	E_{oed}^{ref} [kPa]
MB001 (KBW0301-LB01)	M010-a1	-5.10 to -5.14	16.4	1.51	40.8	42.3	1.04	0.379	0.015	0.066	0.005	12.80	1250
MB001 (KBW0301-LB01)	M011-a1	-5.50 to -5.54	18.7	0.85	43.0	60.3	1.40	0.121	0.006	0.028	0.003	10.25	3500
MB002 (KBW0201-LB02)	M010-a1	-4.84 to -4.87	15.5	1.74	37.82	45	1.19	0.573	0.019	0.091	0.006	15.08	1000
MB002 (KBW0201-LB02)	M011-a4	-5.55 to -5.59	15.2	2.17	42.4	52.4	1.24	0.757	0.031	0.104	0.009	12.21	941
MB003 (KBW0101-LB03)	M010-a4	-5.33 to -5.36	16.3	1.52	36.1	52.7	1.46	0.426	0.0113	0.0735	0.004	18.85	1111
MB004 (KBW0102-LB04)	M009-a1	-5.04 to -5.08	16.5	1.46	32.2	58.1	1.80	0.489	0.013	0.087	0.005	18.95	1000
Average	-	-	16.4	-	-	-	1.36	-	-	0.073	0.005	14.42	1467→ 7450

Pagina 139; 153; 195; 209; 237; 265

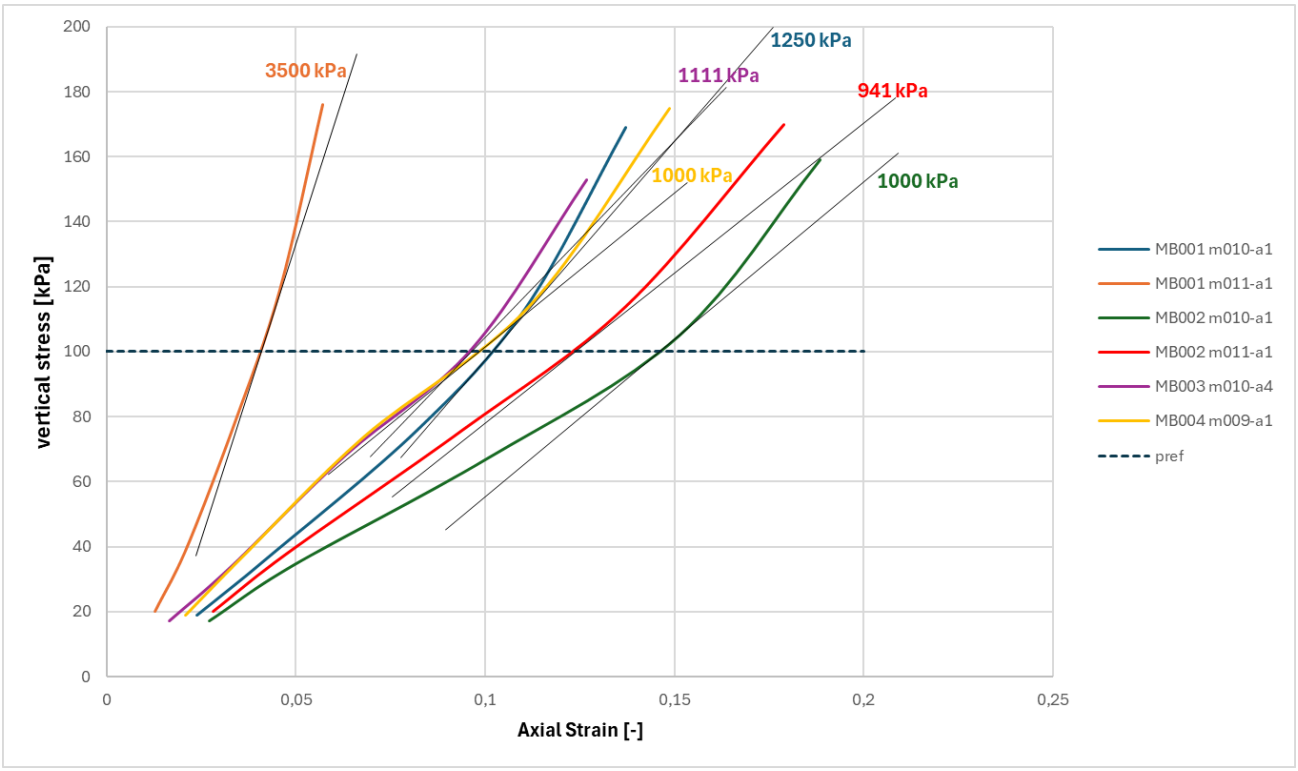

Attachment figure B.5. Oedometer test results and reference oedometer moduli Oude zeeklei (unloading reloading phase not included in graph)

C. Hollandveen Laboratory results

Attachment table C.1. Sample properties and strength parameters Hollandveen

							Peak shear stress		Regression	
Bore # (Land)	Sample #	Depth (m NAP)	Initial Volumetric weight [kN/m^3]	Consolidation stress [kPa]	In-situ stress [kPa]	G_{50} [kPa]	ϕ' [°]	c' [kPa]	ϕ' [°]	c' [kPa]
MB001(KBW0301-LB01)	M007-a2	- 4.03	9.89	34.03	48	225.9	29	3.4	37.3	2.0
MB001(KBW0301-LB01)	M007-a3		9.90	67.00	48	386.0	29	3.4	37.3	2.0
MB001(KBW0301-LB01)	M007-a4	- 4.15	10.01	101.00	48	580.4	29	3.4	37.3	2.0
MB002(KBW0201-LB02)	M005-a1	- 2.87	9.81	28.98	42	324.5	-	-	37.3	2.0
MB002(KBW0201-LB02)	M005-a2		9.90	58.99	42	446.6	-	-	37.3	2.0
MB002(KBW0201-LB02)	M005-a3	-2.93	9.91	88.01	42	774.7	-	-	37.3	2.0
MB003(KBW0101-LB03)	M005-a1	-3.02	9.87	29.01	42	271.1	31.2	3.3	37.3	2.0
MB003(KBW0101-LB03)	M005-a2		9.96	58.99	42	542.1	31.2	3.3	37.3	2.0
MB003(KBW0101-LB03)	M005-a3	-3.10	9.69	88.01	42	732.2	31.2	3.3	37.3	2.0
MB102(KBW0201-WB02)	M004-b1	-4.03	9.41	7.95	10	115.2	27.2	1.9	37.3	2.0
MB102(KBW0201-WB02)	M004-b2		9.50	15.99	10	190.7	27.2	1.9	37.3	2.0
MB102(KBW0201-WB02)	M004-b3	-4.12	9.96	24.00	10	203.4	27.2	1.9	37.3	2.0
MB103(KBW0101-WB03)	M003-b1	-3.93	9.78	7.98	6	92.8	-	-	37.3	2.0
MB103(KBW0101-WB03)	M003-b2		9.52	15.99	6	151.3	-	-	37.3	2.0
MB103(KBW0101-WB03)	M004-a1	-4.24	9.31	24.00	6	226.2	-	-	37.3	2.0

p. 552; 561; 570; 588; 597 KBW laboratory results

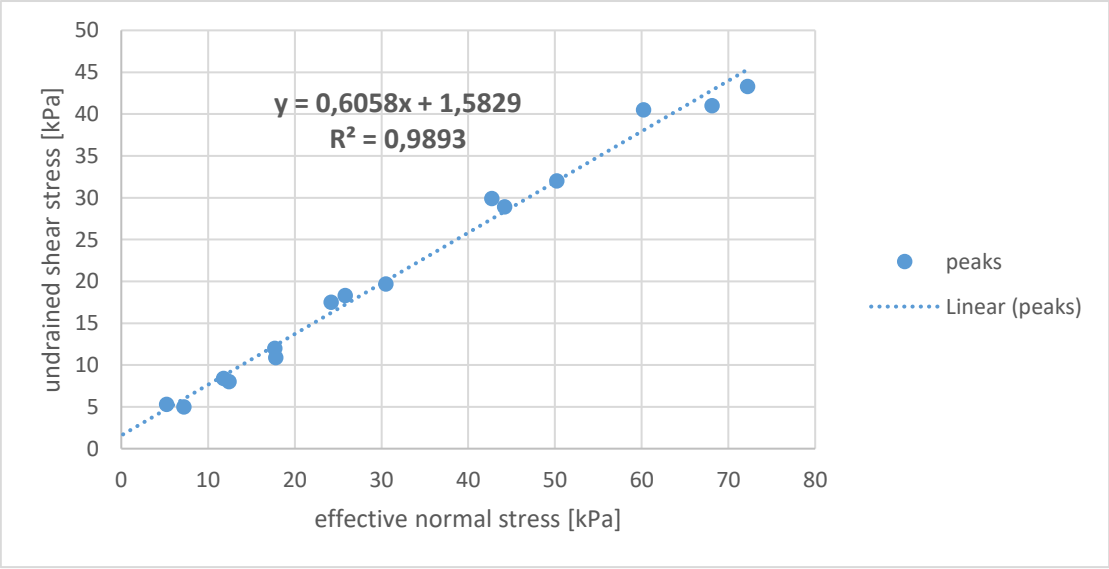

Attachment figure C.1. Linear regression to obtain strength parameters Hollandveen

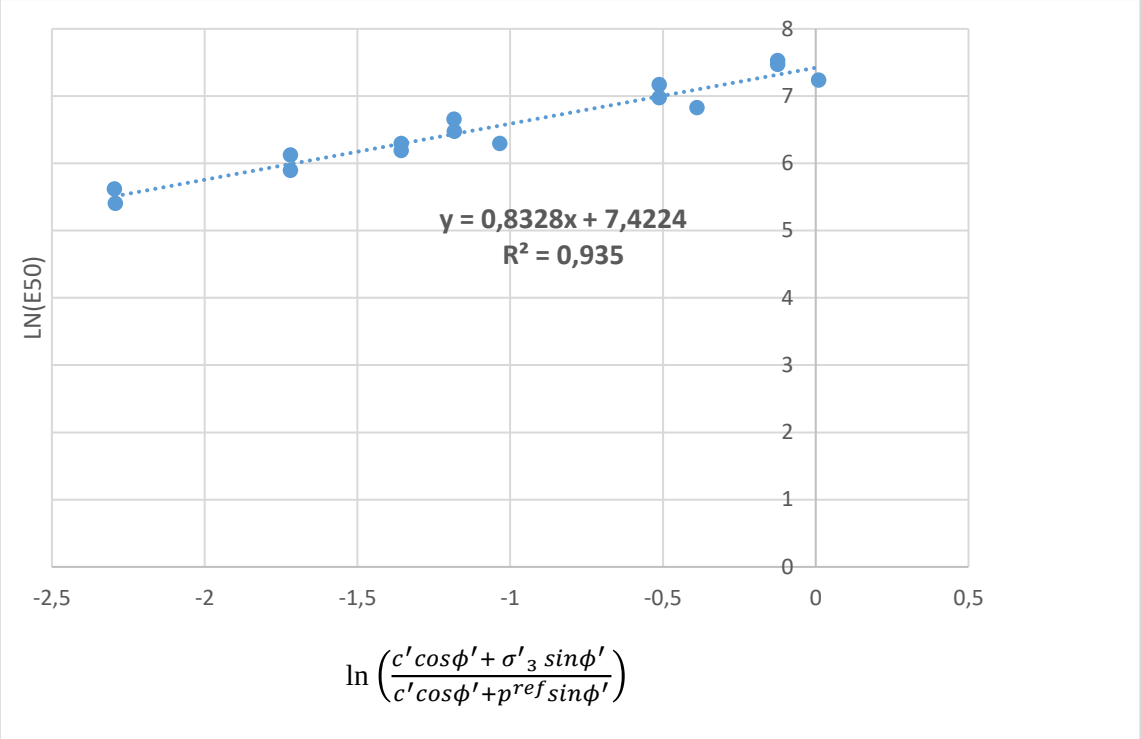

Attachment figure C.2. Stiffness exponent parameter, m.

Attachment table C.2. Oedometer sample properties and stiffness parameters Hollandveen

Bore #	Sample #	Depth [m NAP]	Ini. Sat. Weight [kN/m^3]	e_0 [-]	In-situ stress [kPa]	Pre-cons.stress [kPa] Bjerrum	OCR [-]	Cc [-]	Cs [-]	λ^* [-]	κ^* [-]	$\lambda^*/\ \kappa^*$	E_{oed}^{ref} [kPa]
MB001 (KBW0301-LB01)	M007-a1	-3.95 to -4.03	10.22	9.42	39.4	34.1	1.0	4.120	0.2790	0.1719	0.0248	6.9	516
MB002 (KBW0201-LB02)	M006-a1	-3.33 to -3.39	11.23	5.77	36.9	45.7	1.24	2.718	0.0986	0.1746	0.0127	13.8	600
MB002 (KBW0201-LB02)	M005-a1	- 3.15 to -3.23	10.35	7.087	37.1	42.8	1.15	3.144	0.1531	0.1690	0.0165	10.3	600
MB003 (KBW0102-LB04)	M007-a4	-4.39 to -4.47	10.56	6.641	32.4	52.7	1.62	3.639	0.3702	0.2071	0.0421	4.9	545
MB102 (KBW0201-WB02)	M003-b1	-3.74 to -3.80	10.63	11.329	5.9	12.1	2.04	4.440	0.1096	0.1566	0.0077	20.3	-
Average	-	-		-	-	-	1.41	-	-	0.1758	0.0207	8.5	565 → 920

p. 125; 181; 223; 251; 279

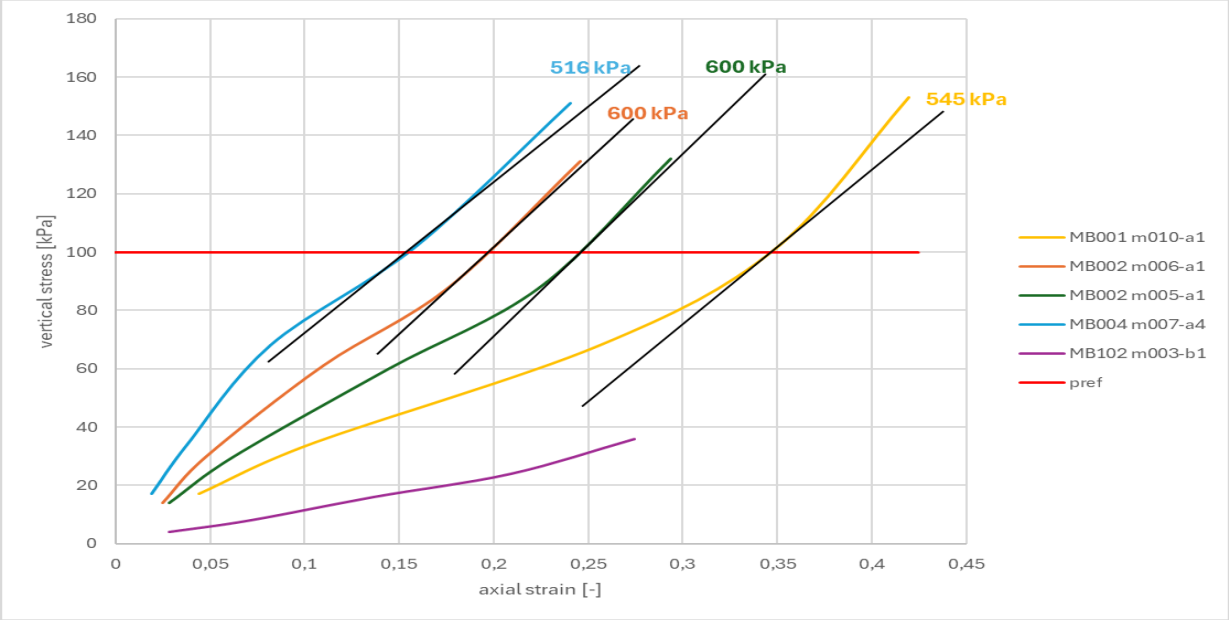

Attachment figure C.3. Oedometer test results and reference oedometer moduli Hollandveen (unloading reloading phase not included in graph)

Attachment table C.3. Stiffness parameters and coefficient of lateral earth pressure for Hollandveen

Bore #	Sample #	G_{50} $[kPa]$	E_{50} $[kPa]$	E_{50}^{ref} $[kPa]$	E_{ur}^{ref} $[MPa]$	K_0^{nc} [-]	m	G_0^{ref} [kPa]	$\gamma_{0.7}$ *10^{-4}[-]
MB001(KBW0301-LB01)	M007-a2	225.9	542,16	1281,74	4486,097	0.394	0.83	4486,097	8.4
MB001(KBW0301-LB01)	M007-a3	386.0	926,40	1280,62	4482,161	0.394	0.83	4482,161	15.5
MB001(KBW0301-LB01)	M007-a4	580.4	1392,96	1381,74	4836,085	0.394	0.83	4836,085	20.2
MB002(KBW0201-LB02)	M005-a1	324.5	778,80	2084,86	7297,016	0.394	0.83	7297,016	6.0
MB002(KBW0201-LB02)	M005-a2	446.6	1071,84	1640,93	5743,253	0.394	0.83	5743,253	10.4
MB002(KBW0201-LB02)	M005-a3	774.7	1859,28	2062,34	7218,18	0.394	0.83	7218,18	11.4
MB003(KBW0101-LB03)	M005-a1	271.1	650,64	1740,39	6091,363	0.394	0.83	6091,363	5.9
MB003(KBW0101-LB03)	M005-a2	542.1	1301,04	1991,82	6971,379	0.394	0.83	6971,379	8.8
MB003(KBW0101-LB03)	M005-a3	732.2	1757,28	1949,20	6822,191	0.394	0.83	6822,191	13.6
MB102(KBW0201-WB02)	M004-b1	115.2	276,48	1866,26	6531,9	0.394	0.83	6531,9	1.7
MB102(KBW0201-WB02)	M004-b2	190.7	457,68	1912,49	6693,716	0.394	0.83	6693,716	2.9
MB102(KBW0201-WB02)	M004-b3	203.4	488,16	1509,16	5282,058	0.394	0.83	5282,058	5.2
MB103(KBW0101-WB03)	M003-b1	92.8	222,72	1499,75	5249,107	0.394	0.83	5249,107	2.6
MB103(KBW0101-WB03)	M003-b2	151.3	363,12	1517,36	5310,746	0.394	0.83	5310,746	3.9
MB103(KBW0101-WB03)	M004-a1	226.2	542,88	1678,33	5874,147	0.394	0.83	5874,147	4.6
Average	-	350.9	842,096	1693,13	5925,96	0.394	0.83	5925,96	8.1

D. Sampler conditions

Sampler MB001(KBW0301-LB01) Landside p.68 KBW laboratory results.

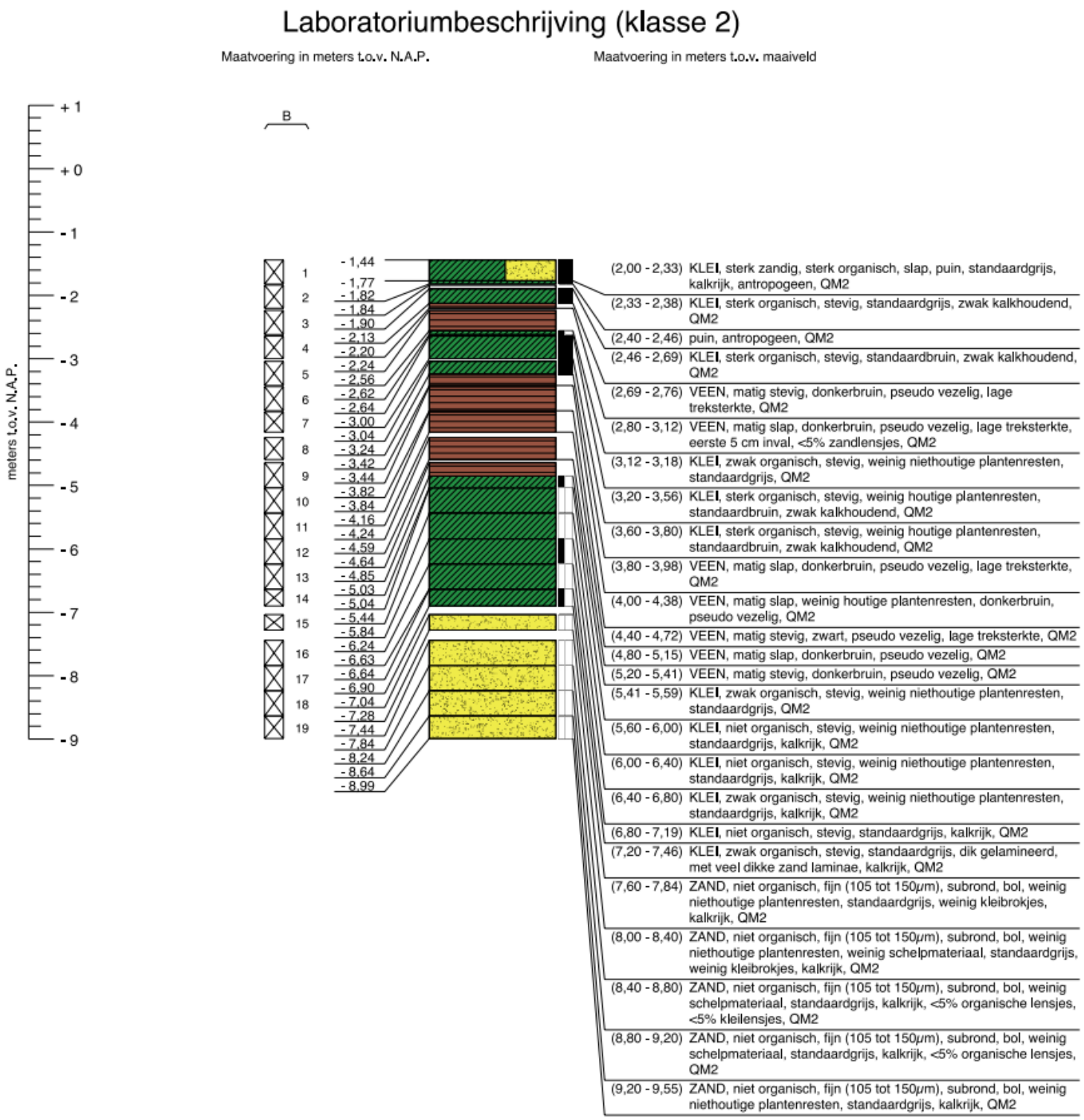

Sampler MB002 (KBW0201-LB02) Landside p.70 KBW laboratory results.

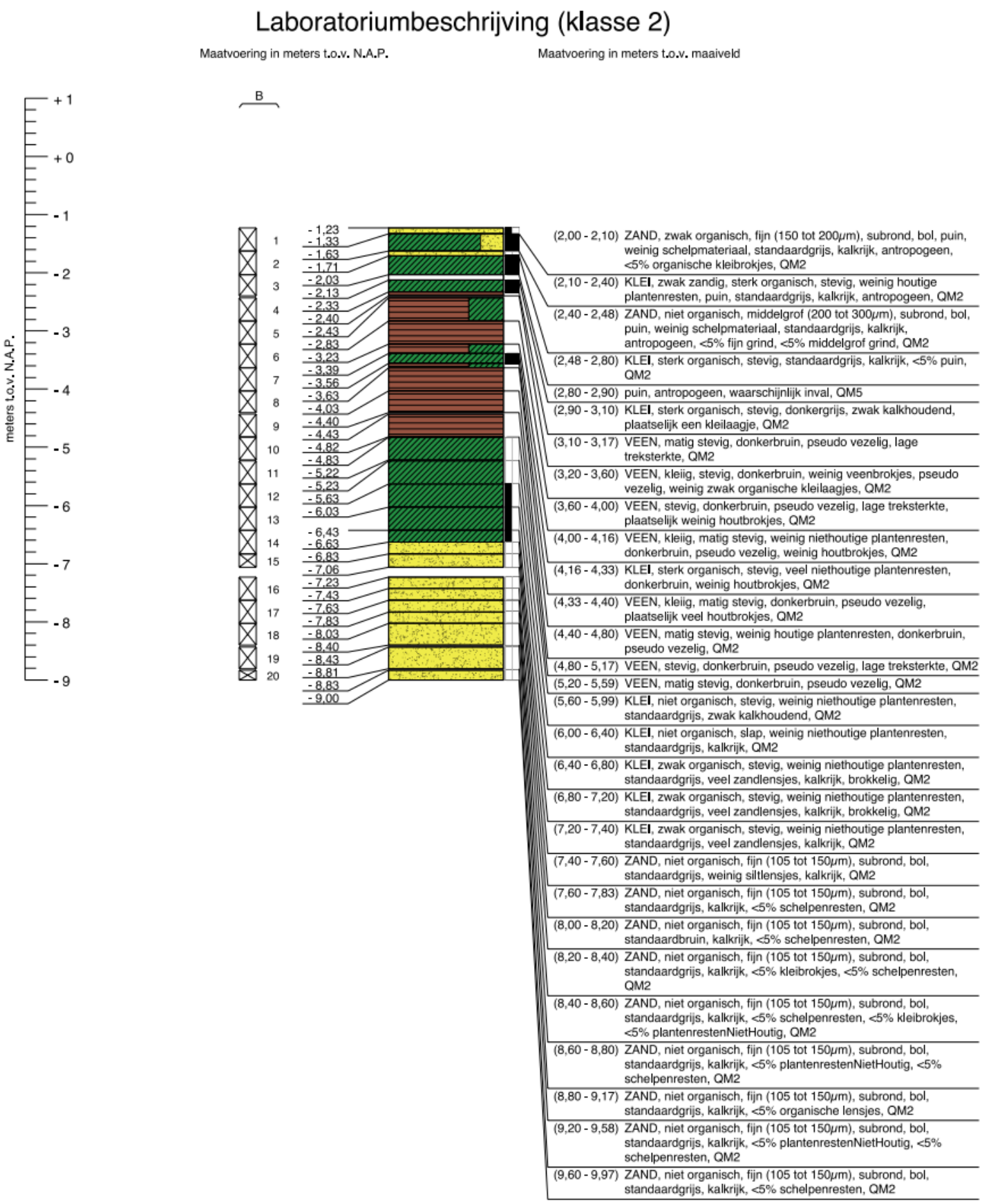

Sampler MB003 (KBW0101-LB03) Landside p.72 KBW laboratory results.

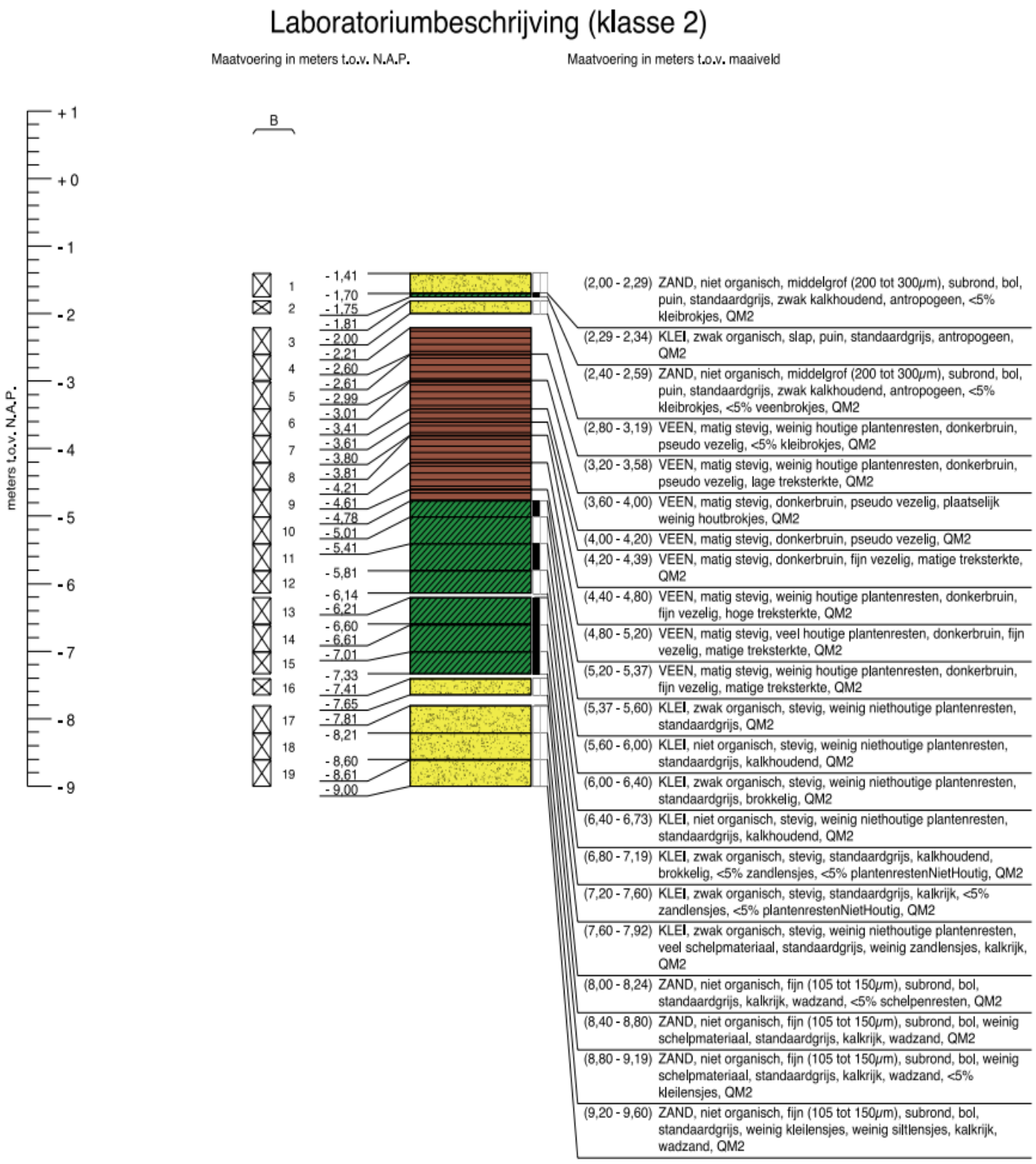

Sampler MB004 (KBW0102-LB04) Landside p.74 KBW laboratory results.

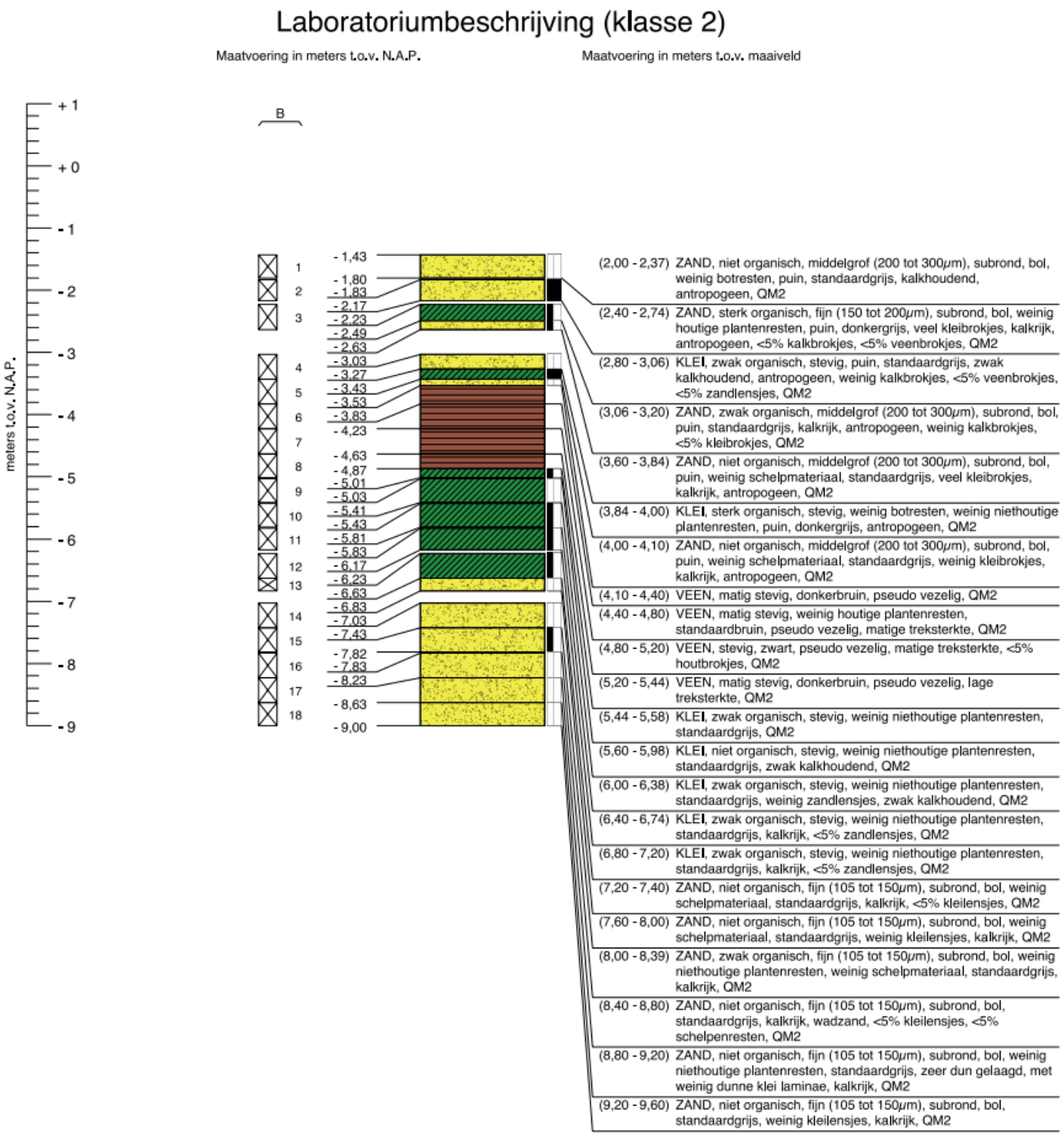

Sampler MB102 (KBW0201-WB02) Waterside p.78 KBW laboratory results.

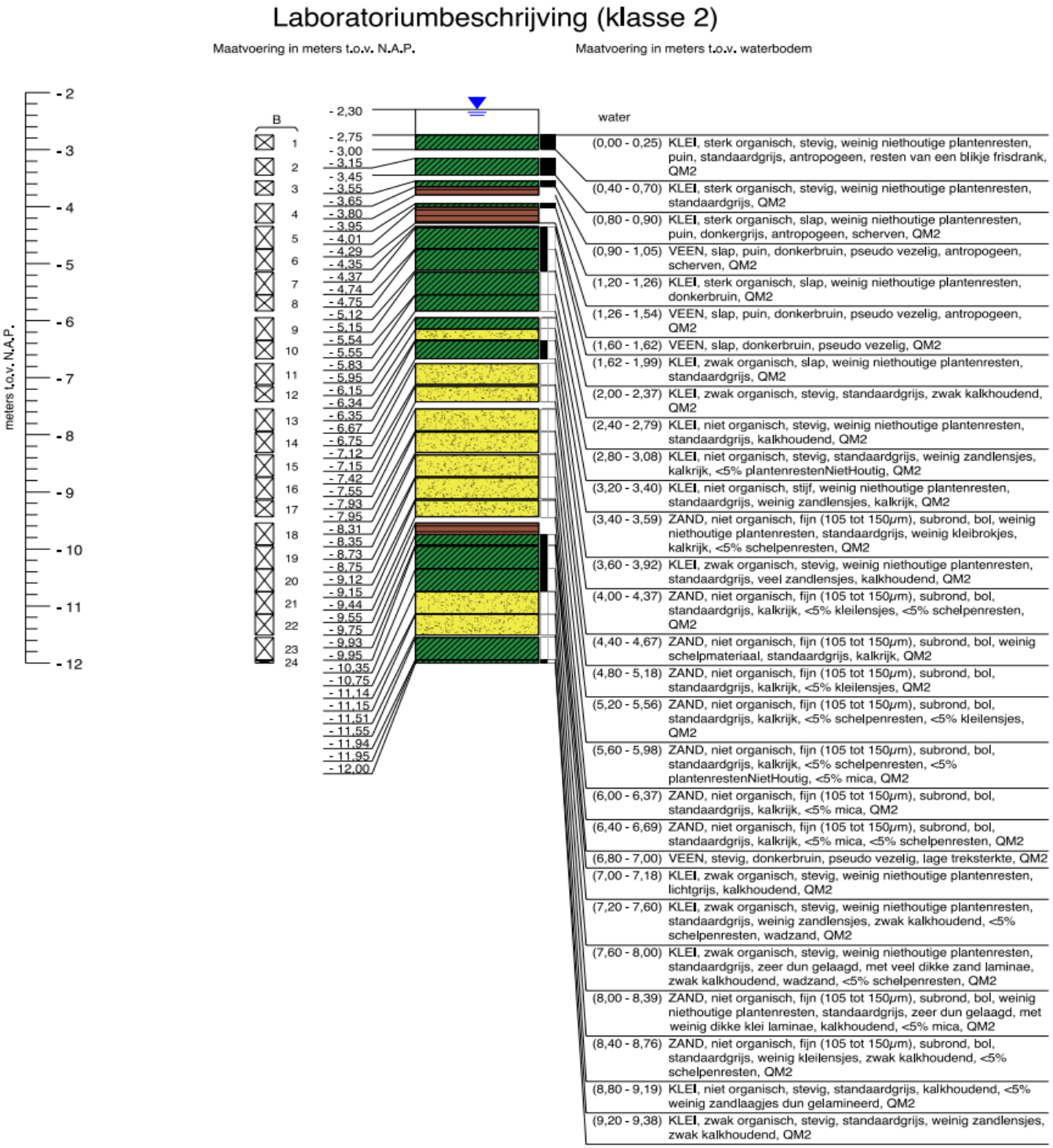

E. Simulation results with soil test

Reference = All laboratory results; optimized = optimized parameters from tables in chapter 4.

E.1 Geulopvulling Hardening Soil Small Strain Model

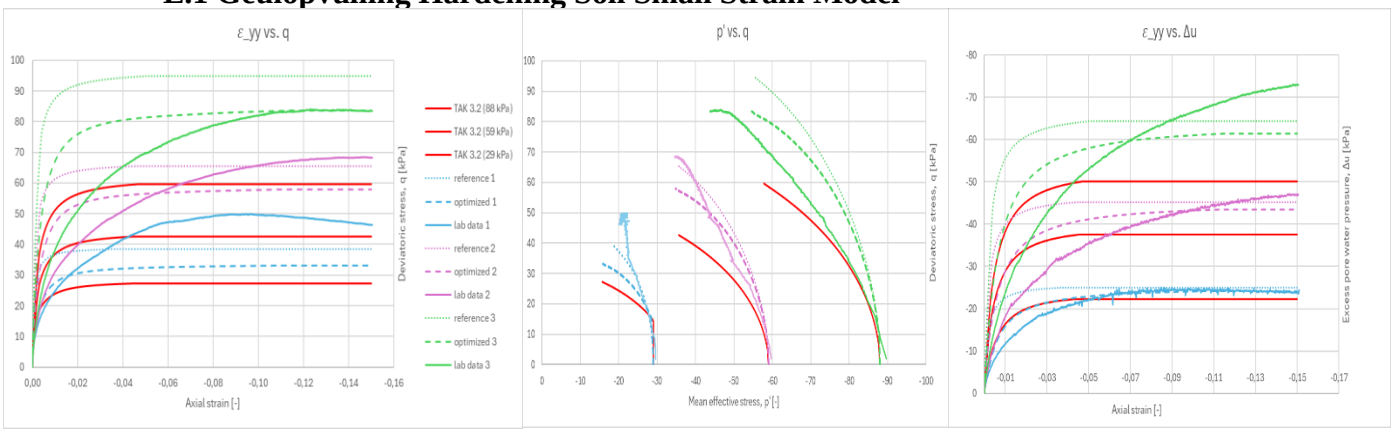

E.2 Geulopvulling Soft Soil Model

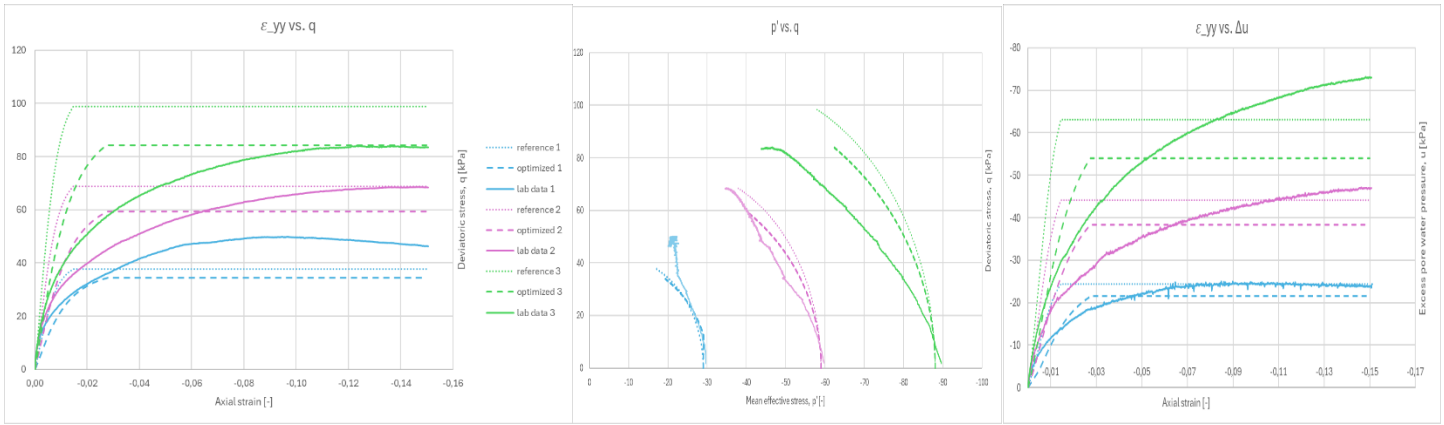

E.3 Geulopvulling Sekiguchi-Ohta Model

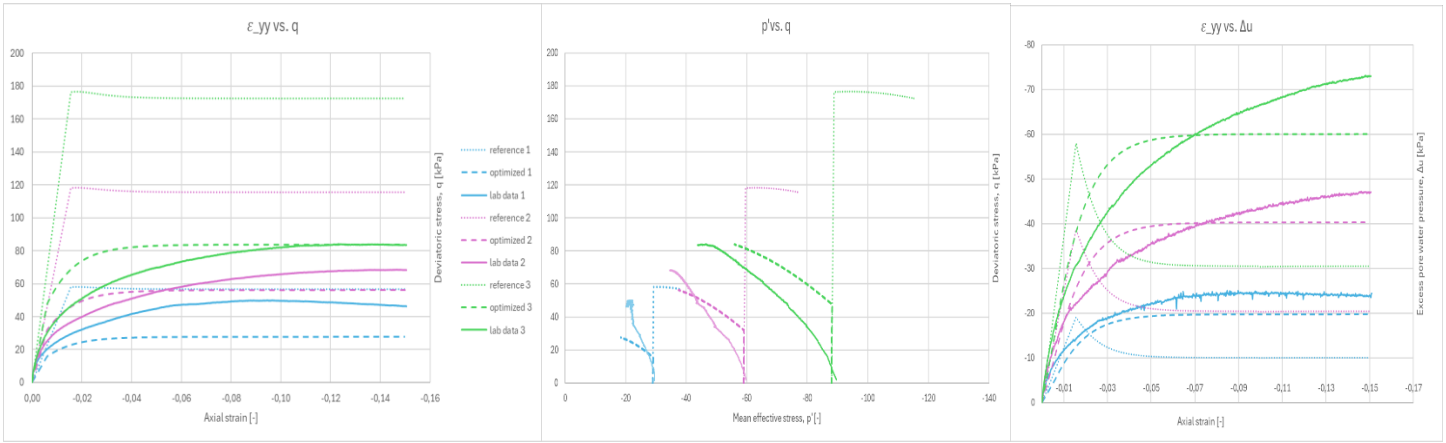

E.4 Geulopvulling S-Clay1 Model

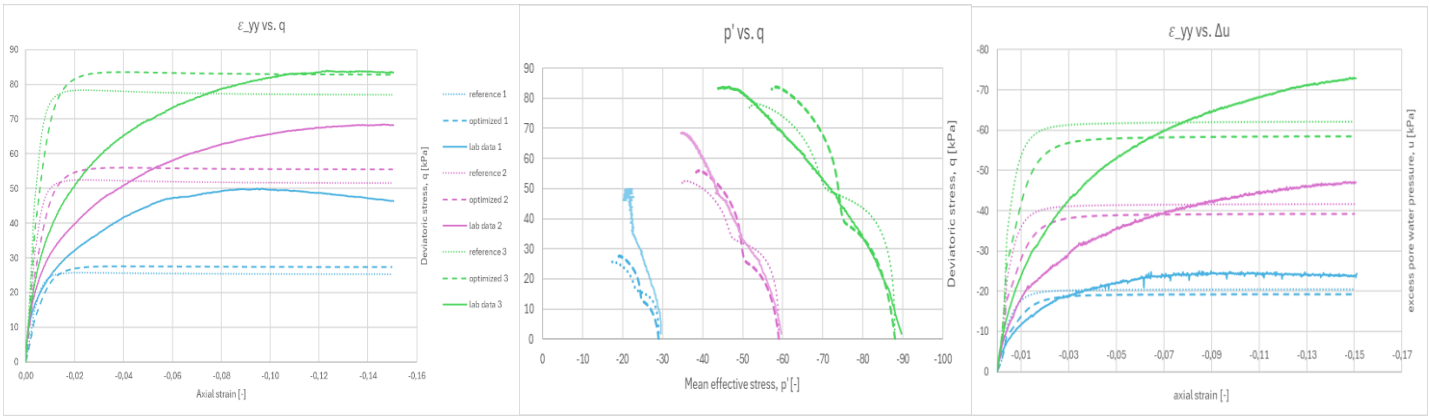

E.5 Oude zeeklei Hardening Soil Small Strain Model

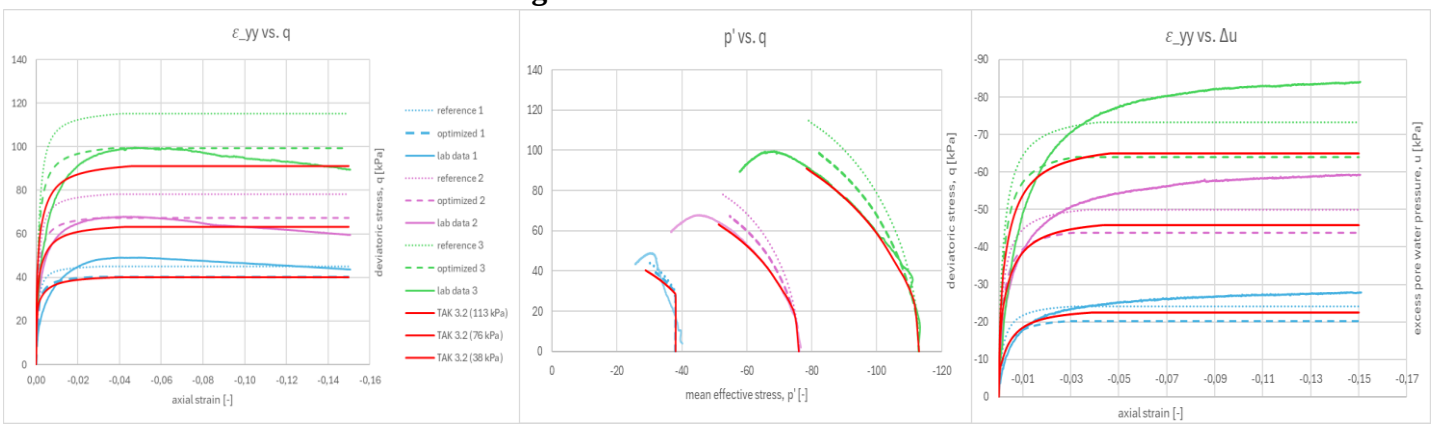

E.6 Oude zeeklei Soft Soil Model

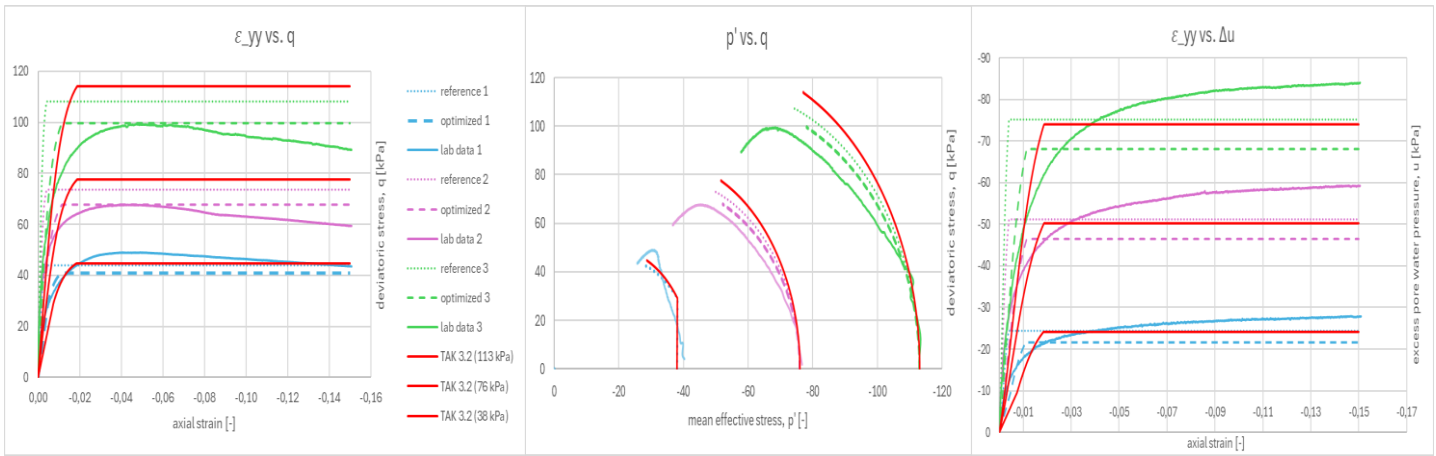

E.7 Oude zeeklei Sekiguchi-Ohta Model

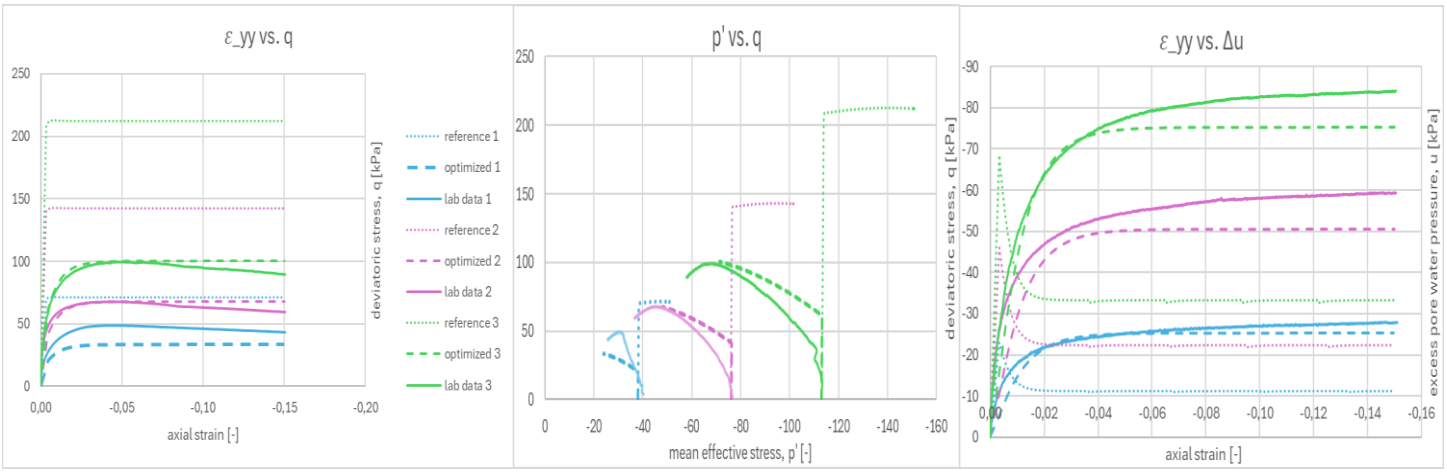

E.8 Oude zeeklei S-Clay1 Model

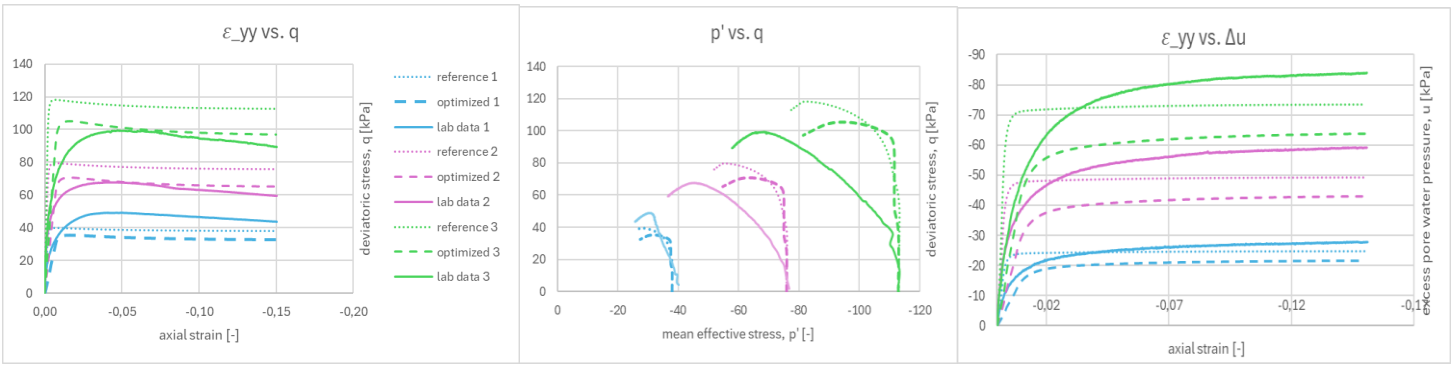

E.9 Hollandveen Hardening Soil Small Strain Model

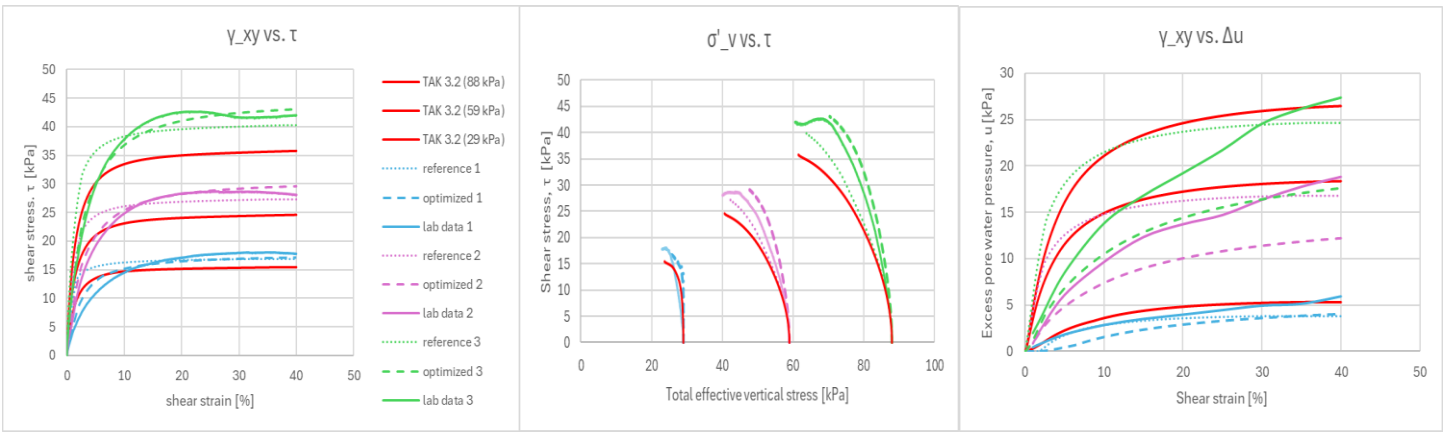

E.10 Hollandveen Soft Soil Model

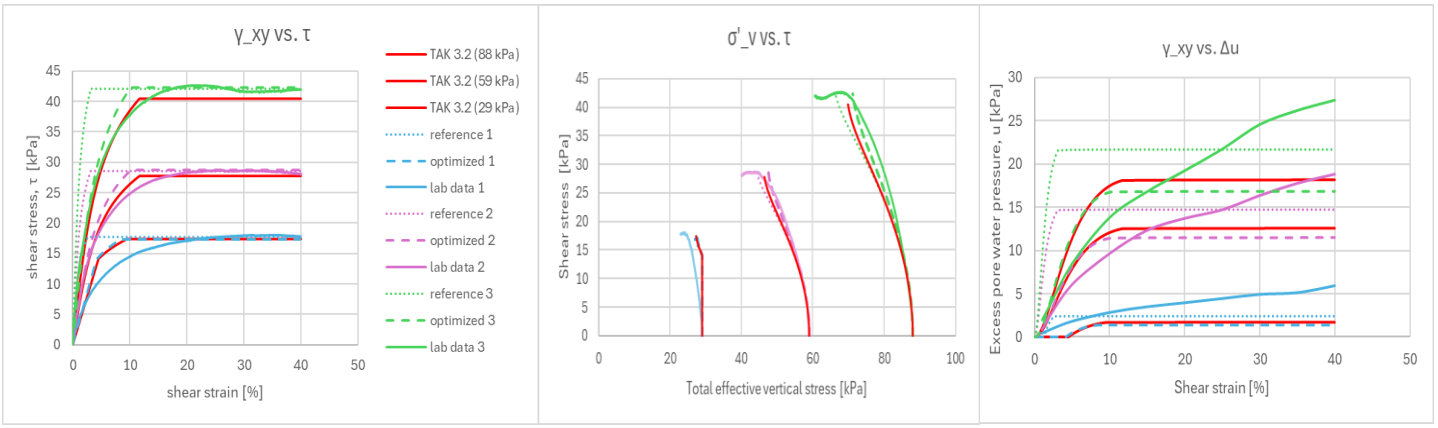

E.11 Hollandveen Sekiguchi-Ohta Model

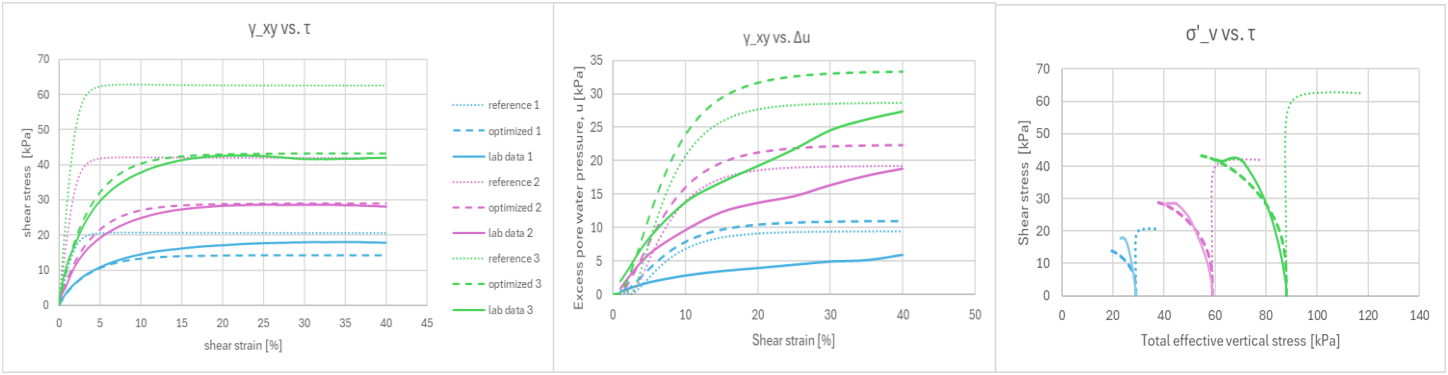

E.12 Hollandveen S-Clay1 Model

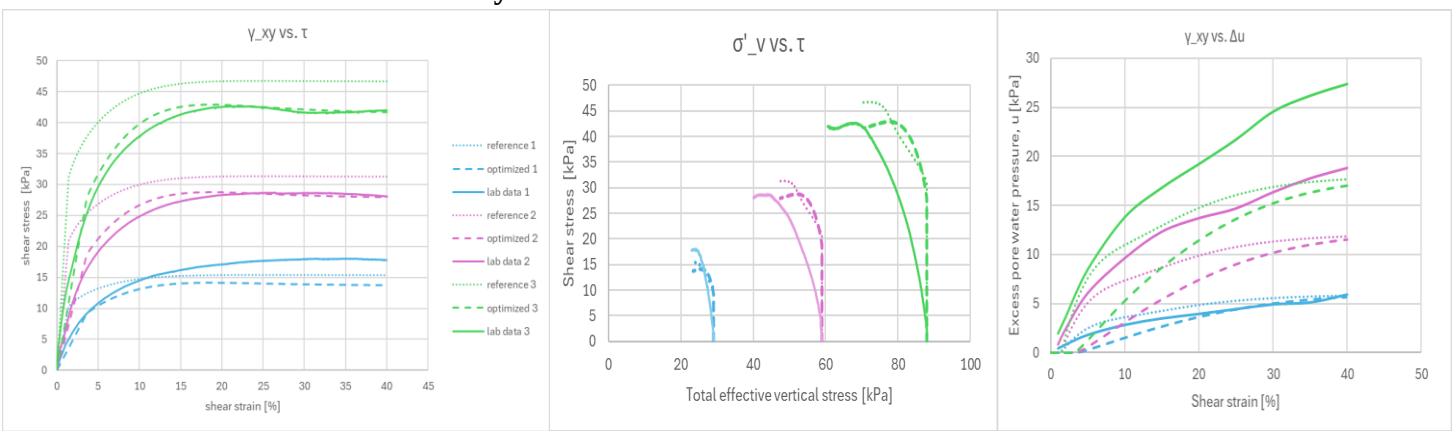

F. Construction phases in FEM calculation Plaxis 2D

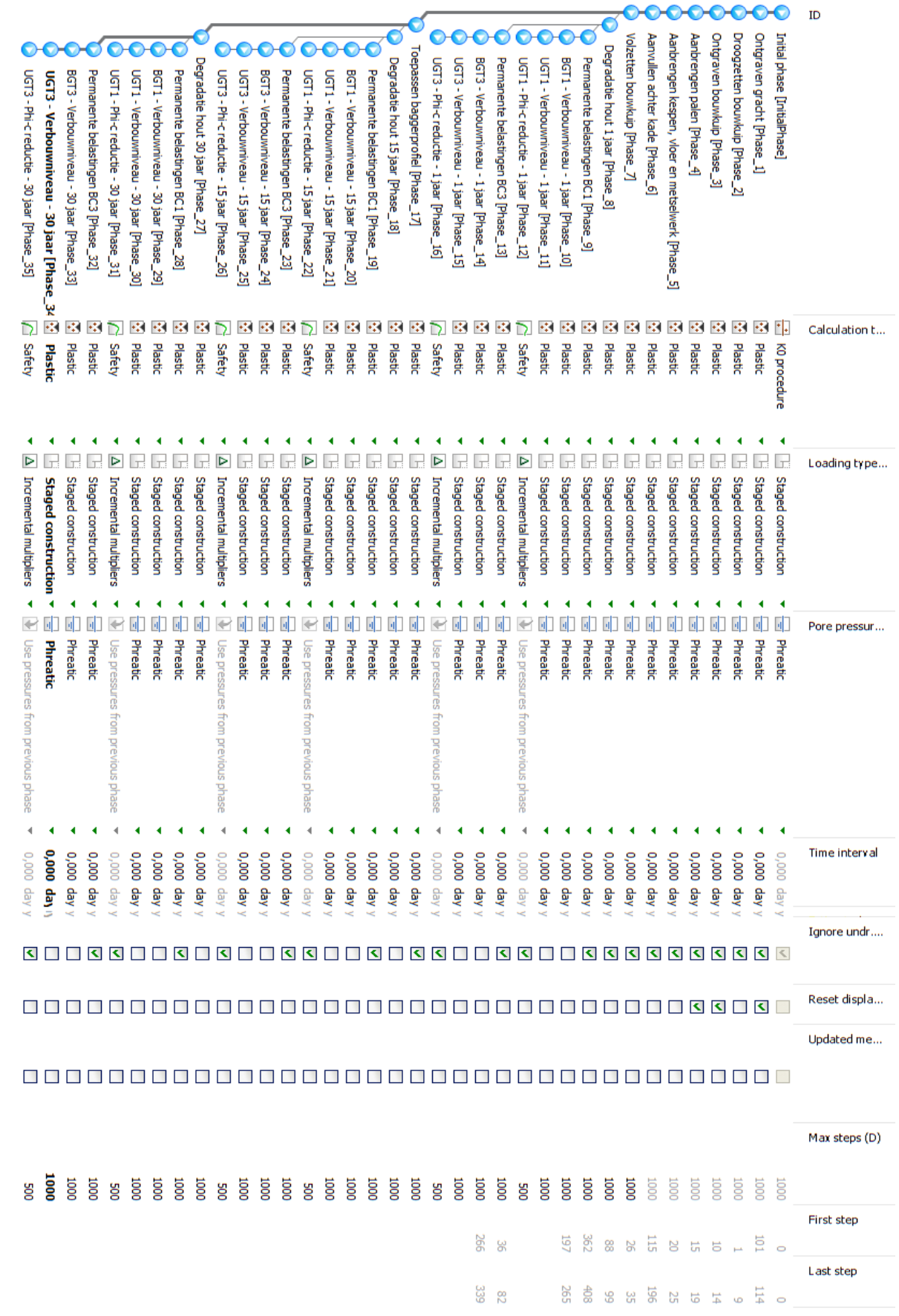

G. Subsurface subdivision for case study with the use of CPT results (Dinoloket) and Robertson chart (1980)

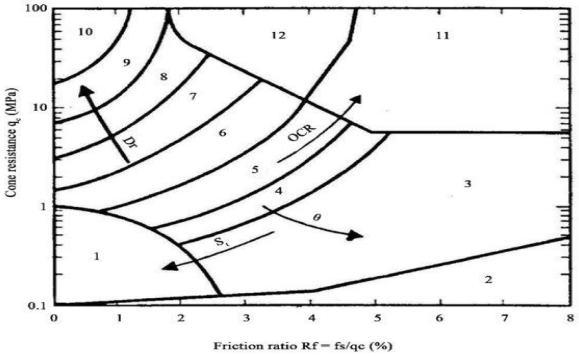

Zone: Soil Behaviour Type:

1. Sensitive fine grained
2. Organic material
3. Clay
4. Silty clay to clay
5. Clayey silt to silty clay
6. Sandy silt to clayey silt
7. Silty sand to sandy silt
8. Sand to silty sand
9. Sand
10. Gravelly sand to sand
11. Very stiff fine grained*
12. Sand to clayey sand*

* *Overconsolidated or cemented.*

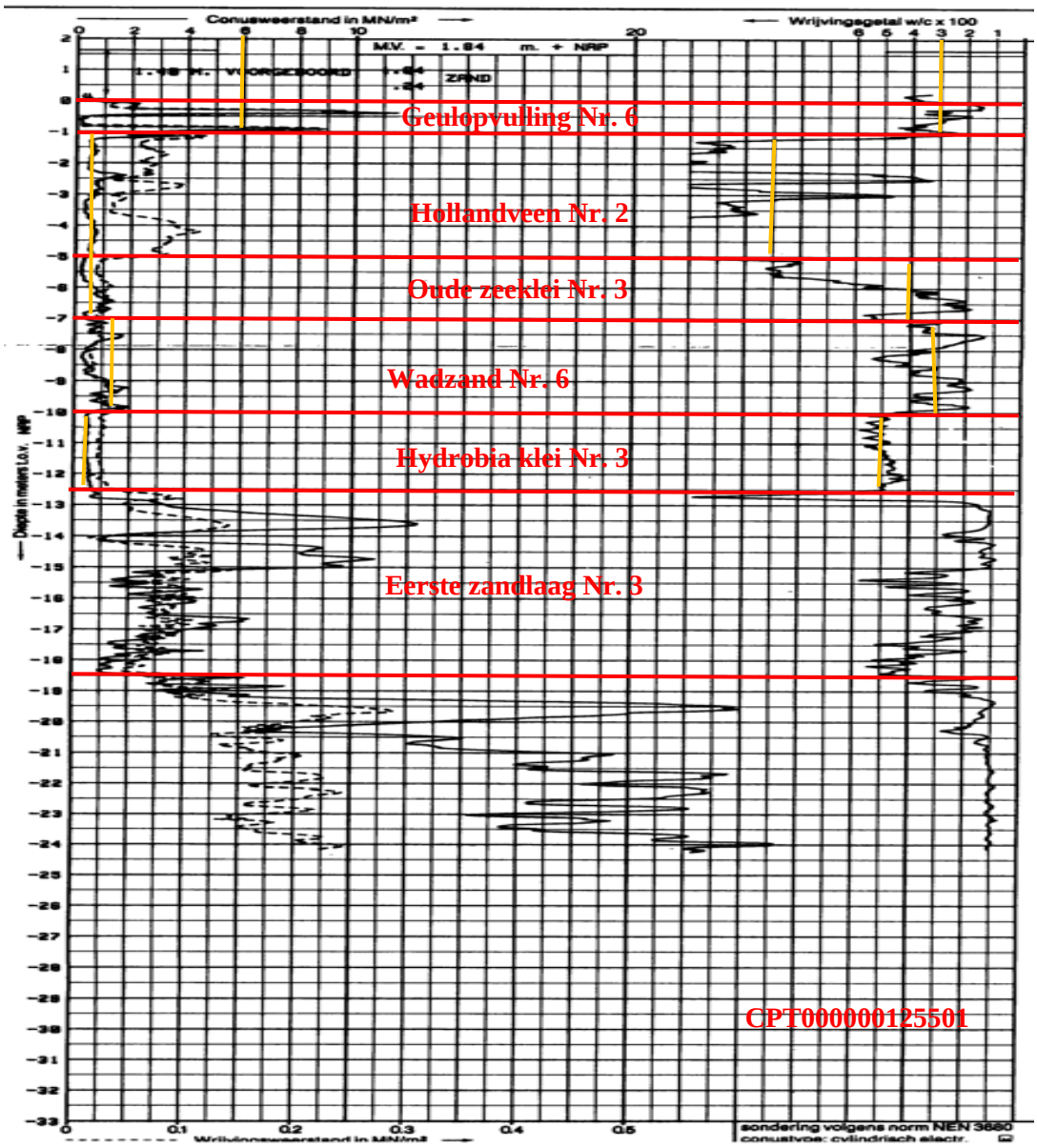

H. Hardening Soil small strain parameters and substantiation in TAK 3.2

6.3.2.1 Hardening Soil small strain parameters

In Tabel 6-1 is een overzicht gegeven van de laag karakteristieke grondparameters t.b.v. Plaxis 2D voor het Hardening Soil Small Strain model.

De oranje gemarkeerde parameters in Tabel 6-1 wijken af van of zijn toegevoegd aan de parameterset van de Noord-Zuidlijn, met de volgende onderbouwing:

- In de Noord-Zuidlijn parameterset zijn alleen de verwachtingswaardes van c' gegeven. De laag karakteristieke waardes van c' zijn bepaald o.b.v. de variatiecoëfficiënt van 0,2 van c' conform de NEN 9997-1 en 3 à 4 proeven per grondlaag [17].
- De E_{50}^{ref} van Hydrobiaklei is verlaagd van 10.000 kN/m² naar 5.000 kN/m² om te voldoen aan de voorwaarde in Plaxis 2D dat $E_{UR}^{ref} > 2 \cdot E_{50}^{ref}$. De verlaging in stijfheid is enigszins conservatief, maar heeft vanwege de diepteligging van de kleilaag naar verwachting weinig invloed.
- De E_{oed}^{ref} van verschillende grondlagen is verlaagd om te voldoen aan de verhoudingen in Plaxis 2D tussen E_{oed}^{ref} met E_{UR}^{ref} en E_{50}^{ref}. Door de verlaging in stijfheid is dit een enigszins conservatief uitgangspunt; daarbij heeft E_{oed}^{ref} relatief weinig invloed op de resultaten, omdat er vooral is ontgraven i.p.v. opgehoogd.
- Ter aanvulling op de Noord-Zuidlijn parameterset is een verhardingslaag van 0,5 m toegevoegd. De verhardingslaag bestaat uit bestrating en waarschijnlijk menggranulaat, bims en/of verdicht zand. De geotechnische parameters van deze laag zijn ingeschat, mede op basis van de NEN 9997-1.
- Het soortelijk gewicht en de hoek van interne wrijving (ϕ') van de ophooglaag, zand is ingeschat op basis de NEN 9997-1.
- De parameters voor kleine rekken $\gamma_{0,7}$ en G_o^{ref} van het HSss model ontbreken in de Noord-Zuidlijn parameterset. De $\gamma_{0,7}$ is bepaald conform de Plaxis 2D manual [27]. G_o^{ref} is voor de zandlagen en siltige kleilagen bepaald o.b.v. de relaties van Alpan (1970) tussen dynamisch en statisch grondgedrag. De G_o^{ref} van de relatief slappe lagen Geulopvulling (klei), Hollandveen en Basisveen worden met de relaties van Alpan sterk overschat. Zie ook Kishida et al. [28]. Daarom is voor deze lagen aangehouden $G_o^{ref} = E_{UR}^{ref}$.
- Verder geldt ν_{ur} = 0,2 voor alle grondlagen en hebben alle grondlagen een POP van 10 kN/m², behalve de Eerste Zandlaag (13) een OCR van 1,2 conform de parameterset [17].
- Bepaling K_o via regel van Jaky.
- De R_{inter} is bepaald o.b.v. vergelijking [27]: $R_{inter} = \frac{\tan(\delta)}{\sin(\varphi)}$. De δ is ingeschat op ¾ ϕ', op basis van een ruw oppervlak. Dit leidt tot een R_{inter} voor zand 0,8, voor klei en wadzand 0,7 en voor veen 0,3.

Tabel 6-1 Grondparameters laag karakteristiek t.b.v. Plaxis 2D (Hardening Soil Small Strain) o.b.v. NZ-lijn set

Laag	Naam	γ_{droog} [kN/m³]	γ_{nat} [kN/m³]	c' [kPa]	ϕ' [°]	ψ' [°]	E_{50}^{ref} [kN/m²]	E_{oed}^{ref} [kN/m²]	E_{UR}^{ref} [kN/m²]	$\gamma_{0,7}$ 10^{-4} [-]	G_o^{ref} [kN/m²]	m [-]
-	Verharding	18,0	20,0	0,5	32,5	2,5	20.000	20.000	60.000	1,0	89.500	0,5
01A	Ophooglaag	17,0	19,0	1,0	30	0	17.134	15.000	50.000	1,0	81.000	0,5
07A	Geulopv. Klei [2]	13,9	13,9	7,1	20	0	4.284	2.200	15.000	2,0	15.000	0,8
08	Hollandveen	10,5	10,5	3,6[1]	18[1]	0	2.000	1.085	7.000	2,0	7.000	0,8
09	Oude Zeeklei	16,5	16,5	5,0[1]	26[1]	0	7.500	3.780	20.000	2,0	47.000	0,8
10	Wadzand	17,9	17,9	1,4	27	0	10.000	5.890	25.000	1,0	53.500	0,5
11	Hydrobiaklei	15,2	15,2	5,7	27	0	5.000	2.850	10.000	2,0	33.000	0,8
12	Basisveen	11,7	11,7	4,3	18	0	2.000	1.065	7.000	2,0	7.000	0,8
13	1e zandlaag	16,6	19,7	0,1	33	3	35.000	20.000	100.000	1,0	121.500	0,5
14	Allerød	18,5	18,5	0,1	28	0	15.000	7.000	30.000	1,0	59.500	0,8
16	Geulopvulling	18,6	18,6	0,1	27	0	8.400	4.000	25.000	1,0	53.500	0,8
17	2e zandlaag	18,0	20,0	0,1	33	3	32.000	25.000	80.000	1,0	105.500	0,5

[1] De (verhoogde) sterkteparameters afgeleid in Bijlage E en gepresenteerd in Tabel 6-2 zijn onafhankelijk van het grondmodel en kunnen ook in HSss worden toegepast

[2] Deze laag is erg heterogeen en wisselend van samenstelling. Bij schematisatie grondprofiel ook rekening houden met archiefboringen van Waternet/Omegam.

I. Graphical horizontal deformation output results Plaxis 2D

Simulation 1 with TAK 3.2 parameter set (Geulopvulling HSss; Hollandveen HSss; Oude zeeklei HSss)

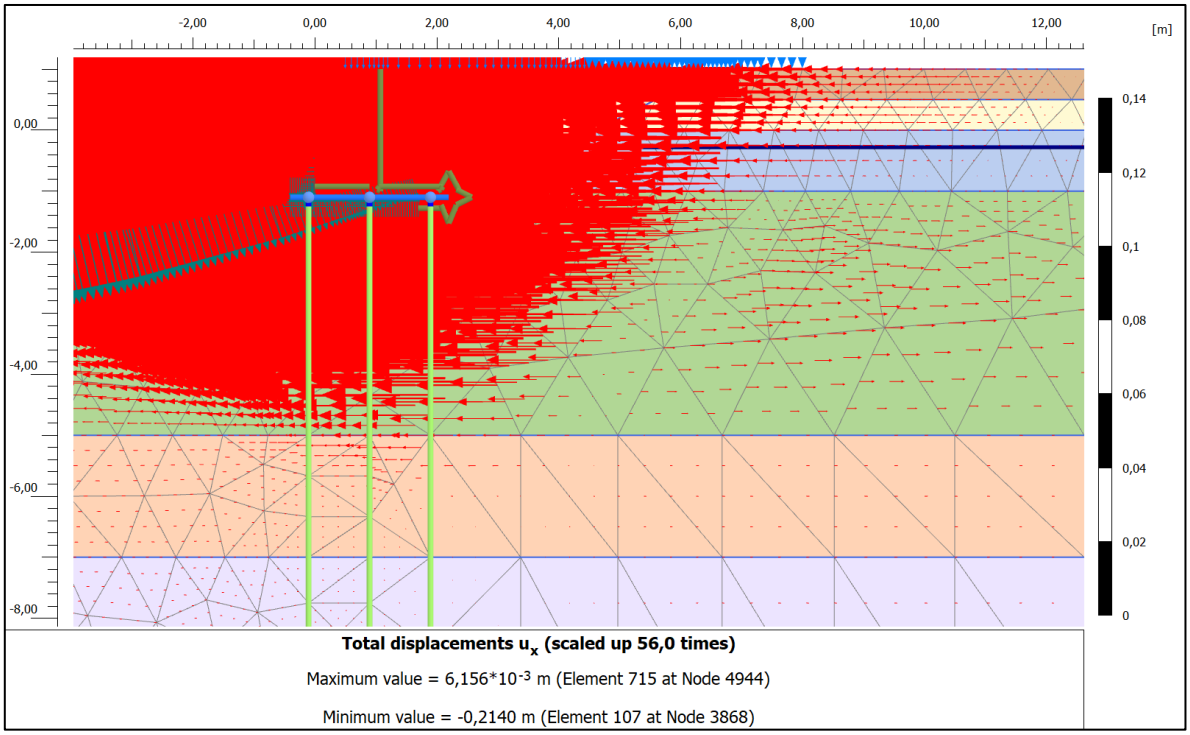

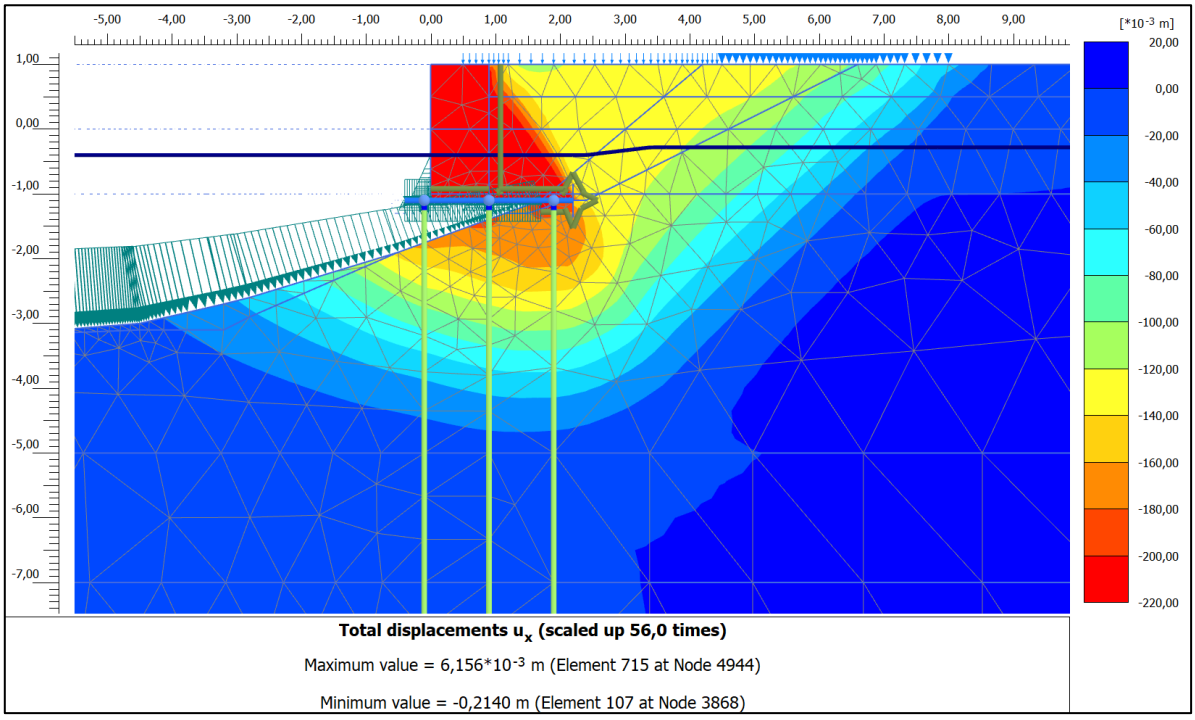

Simulation 3 with Optimized parameter set (Geulopvulling HSss; Hollandveen HSss; Oude zeeklei HSss)

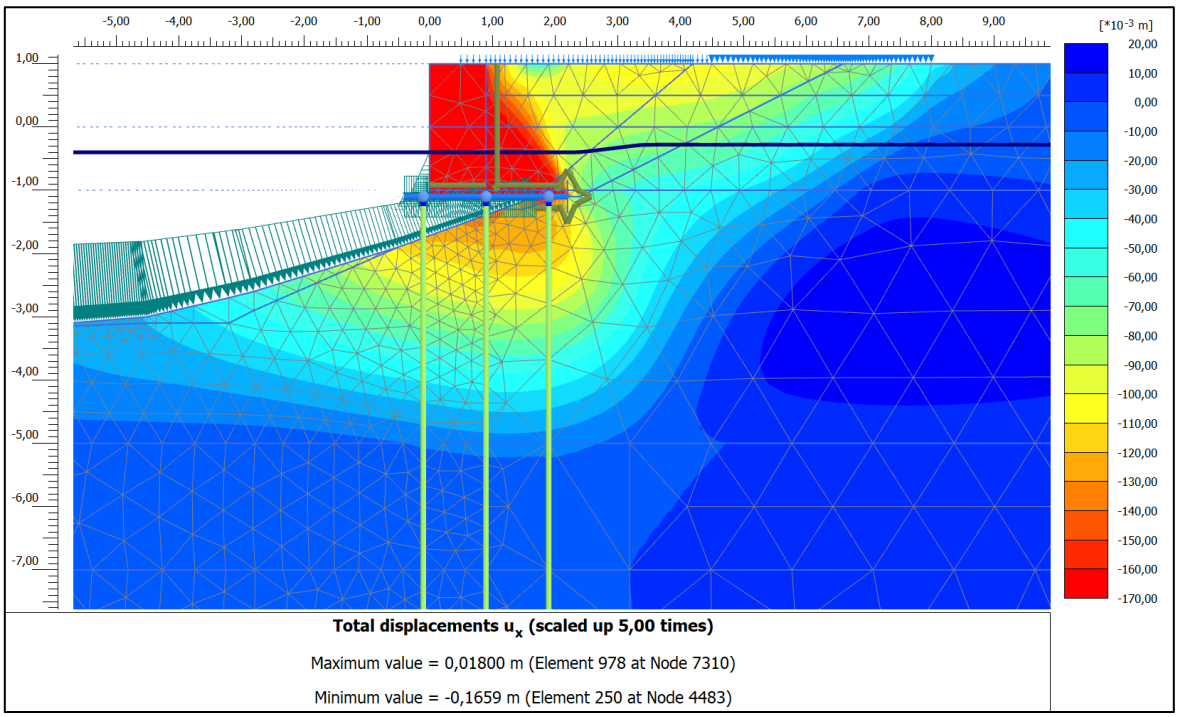

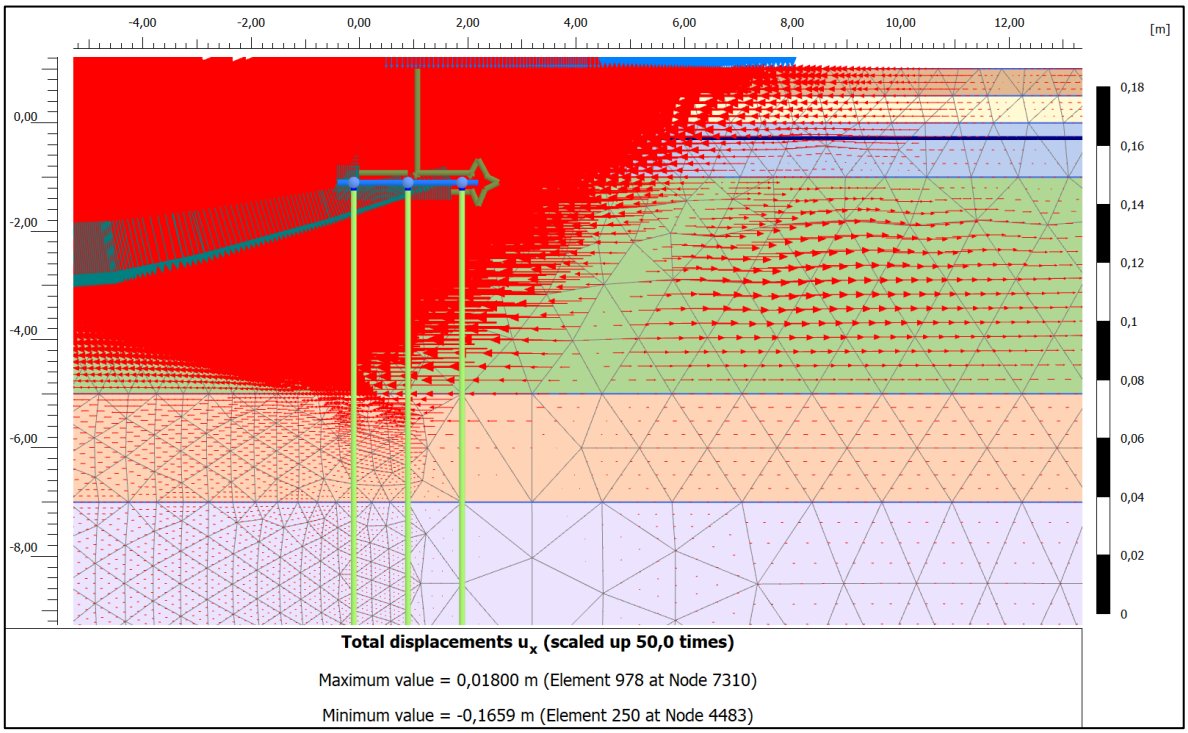

Simulation 5 with TAK 3.2 parameter set (Geulopvulling HSss; Hollandveen SS; Oude zeeklei SS)

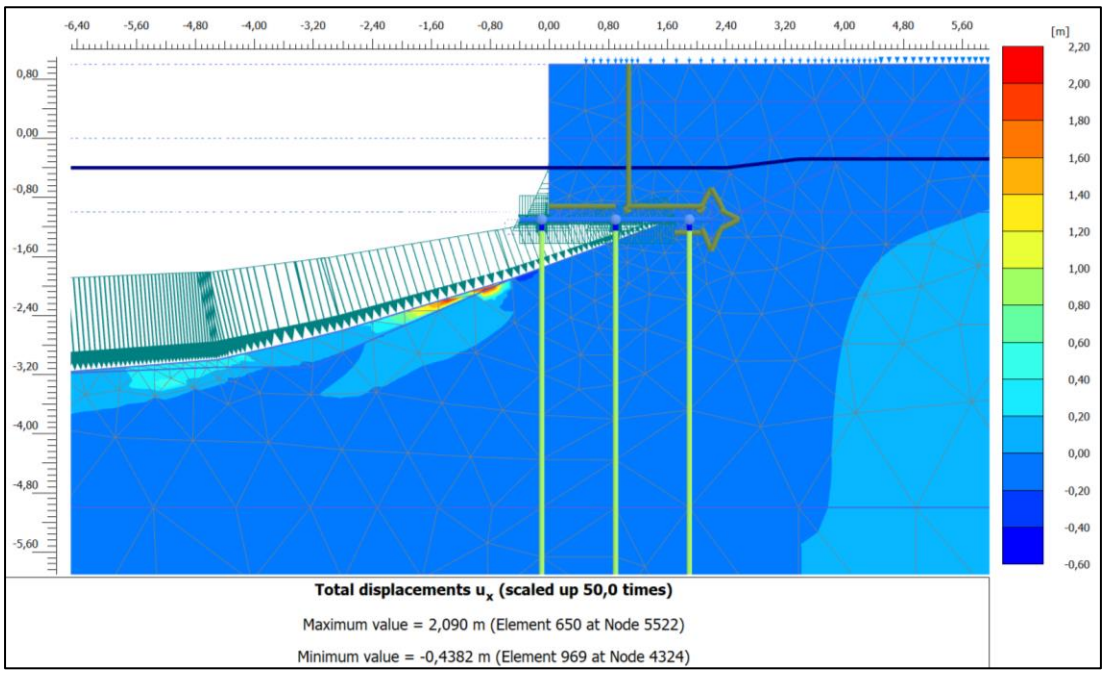

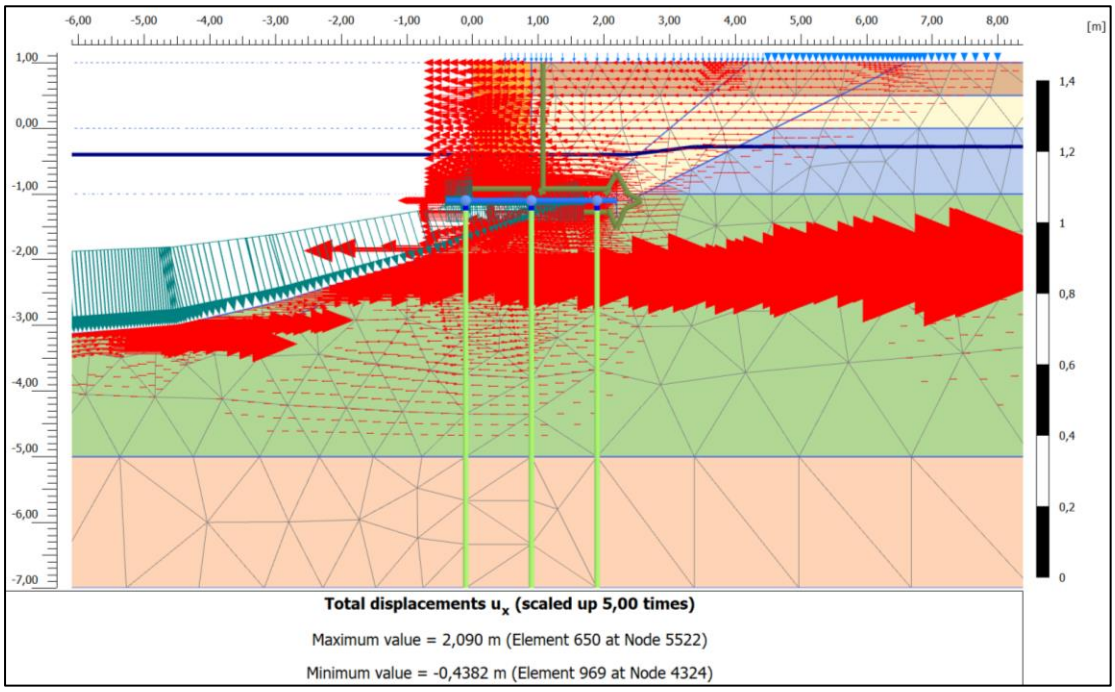

Simulation 7 with optimized parameter set (Geulopvulling HSss; Hollandveen SS; Oude zeeklei SS)

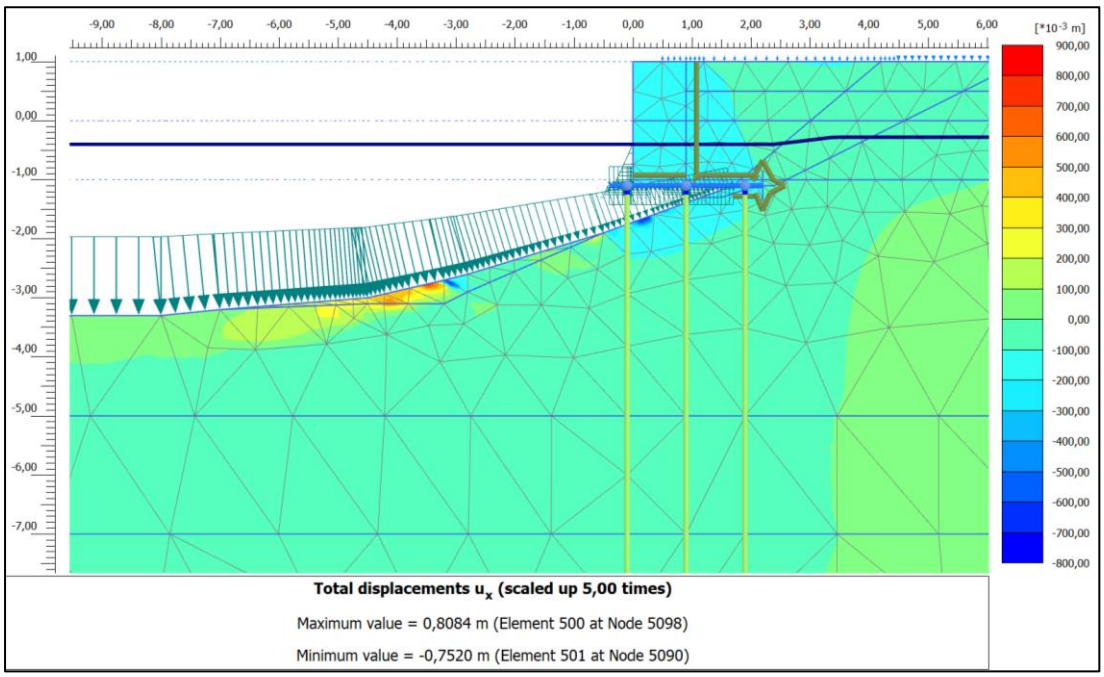

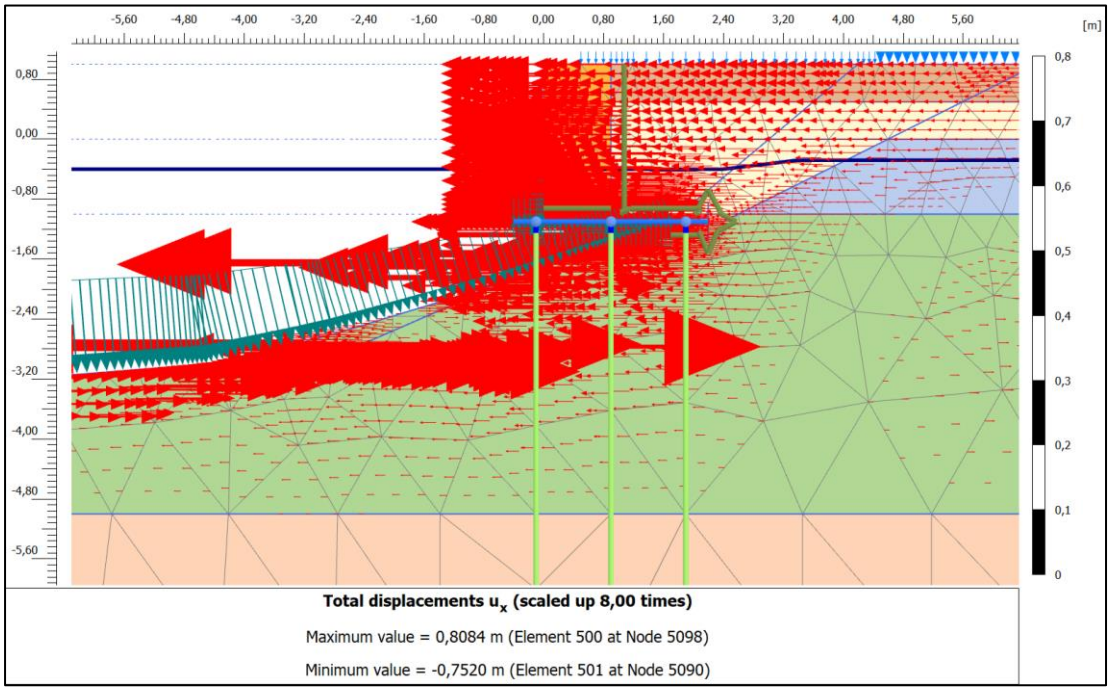

J. Archive Drawing Bilderdijkgracht